UNIVERSITÀ DEGLI STUDI DI PADOVA

Dipartimento di Fisica e Astronomia "Galileo Galilei"

Master Degree in Astrophysics and Cosmology

Final Dissertation

ASTROMETRIC SIGNATURES OF STARS WITH TESS PLANET CANDIDATES: CLOSE COMPANIONS AND FALSE ALARMS

Thesis supervisor

Prof. Domenico Nardiello

Thesis co-supervisor

Prof. Silvano Desidera

Candidate

Francesco Caregnato

Academic Year 2022/2023

Contents

Abstract

The quest to discover exoplanets, planets orbiting stars beyond our solar system, has been one of the most thrilling endeavors in contemporary astronomy. As astronomers employ advanced techniques and technologies to identify these distant worlds, the challenges posed by false positives have become a central focus of investigation. False positives in exoplanet detection, while presenting a formidable obstacle, also offer valuable insights into refining our methods and ensuring the accuracy of future discoveries.

This master thesis investigates the astrometric signatures associated with stars hosting planet candidates detected by the Transiting Exoplanet Survey Satellite (TESS). The study encompasses a brief description of the historical context of exoplanet detection, detection techniques such as radial velocity, transit, and astrometry, and an introduction to the Gaia and TESS space missions. Emphasis is placed on addressing the potential for false positives in exoplanet identification.

The research employs a comparative approach by cross-matching TESS catalogs with the recently released Gaia DR3 catalog and the Gaia-Hipparcos Proper Motion anomaly (PMa) catalog by Kervella et al. (2022). The properties of the candidate transiting exoplanets found by TESS, included in the so-called TESS Objects of Interest (TOI) catalog, are analyzed by using the Gaia DR3 catalog, and in particular, the information included in the Non-Single Star Catalogue (NSS) that is part of the Gaia release. The PMa catalog is introduced as a crucial component for evaluating proper motion anomalies.

The heart of the study involves a detailed analysis of TOIs, by using the tables obtained by cross-matching the TOIs catalog with the NSS catalog (TOI-NSS) and with the Kervella et al. (2022)'s catalog (TOI-PMa) The examination aims to uncover astrometric patterns and anomalies associated with the stellar hosts of TESS planet candidates. Notable cases, including TOI 503.01, TOI 1338.01, TOI 503.01 (HATS-26 b), WASP-2 b, TOI 148.01, TOI-185.01 (WASP-18 b), TOI 2543.01, TOI 144.01, TOI 179.01, TOI 200.01 (DS Tuc Ab), TOI 4399.01, and TOI 5394.01, are singled out for detailed scrutiny.

The research contributes to the refinement of exoplanet catalogs by offering insights into the astrometric signatures of stars hosting TESS planet candidates. The comparative analysis with Gaia DR3 and proper motion anomalies enhances our understanding of the complexities within stellar systems observed by TESS, providing a foundation for future investigations in the dynamic field of exoplanetary science.

Introduction

1.1 History of the detection of Exoplanets

For centuries scientists, philosophers, and science fiction writers suspected that extrasolar planets existed, but there was no way of knowing whether they were real, how common they were, or how similar they might be to the planets of the Solar System. Various detection claims made in the nineteenth century were rejected by astronomers. Some of the earliest claims of exoplanet detections involve the binary star 70 Ophiuchi. In 1855, William Stephen Jacob (1855) reported that there was a "planetary body" in the system due to orbital anomalies. He tried to use astrometric methods to detect an exoplanet, which was a new attempt at that time, although Friedrich Bessel had applied similar methods 10 years earlier to deduce the existence of Sirius B. In the 1890s, Thomas J. J. See (1896) claimed that the orbital anomalies proved the existence of a dark body with a 36-year period around one of the stars in the 70 Ophiuchi system. But, Forest Ray Moulton (1899) proved that a three-body system with those orbital parameters would be highly unstable. The claims by Jacob and See have both been shown to be erroneous. Discovery of a "third dark companion" was announced by Louis Berman (1932). This "dark body" around 70 Oph A was thought to have an 18-year period and a mass of 0.1 to 0.2 the Sun's mass. A claim of a planetary system was again made, this time by Reuyl and Holmberg (1943). The companion was estimated to have a mass between 0.008 and 0.012 $M_{\odot}$ and a 17-year period. This caused quite a sensation at the time but later observations have gradually discredited this claim. The negative results of past studies do not completely rule out the possibility of planets. In 2006 a McDonald Observatory team set limits to the presence of one or more planets around 70 Ophiuchi with masses between 0.46 and 12.8 Jupiter masses and average separations spanning between 0.05 and 5.2 AU.

During the 1950s and 1960s, Peter van de Kamp (1969) made another series of detection claims, this time for planets orbiting Barnard's Star. Later observations led him to conclude that there were two planets. However, numerous attempts were made to demonstrate this hypothesis (Gatewood and Eichhorn, 1973), but they led to the conclusion that the planets observed were the result of an incorrect method of data collection, based on photographic measurements. Recently, a planet has been found around Barnard's star, but not of the type assumed by van de Kamp. In 1952, more than 40 years before the first hot Jupiter was discovered, Otto Struve (1952) wrote that there is no compelling reason that planets could not be much closer to their parent star than is the case in the Solar System, and proposed that Doppler spectroscopy and the transit method could detect super-Jupiters in short orbits.

The first suspected scientific detection of exoplanets occurred in 1988/89 (Campbell et al., 1988) - (Latham et al., 1989) but, because of their large mass, they were classified as brown dwarfs. Shortly afterward, the first confirmation of detection came in 1992 (Wolszczan and Frail, 1992), with the discovery of several terrestrial-mass planets orbiting the pulsar PSR B1257+12. The first confirmation of an exoplanet orbiting a main-sequence star was made in 1995 (Mayor and Queloz, 1995), when a giant planet was found in a four-day orbit around the nearby star 51 Pegasi. The discovery of 51 Pegasi b, a "hot Jupiter" orbiting a Sun-like star, marked a watershed moment. Since then, thousands of similar planets have been discovered (Fig. 1.1).

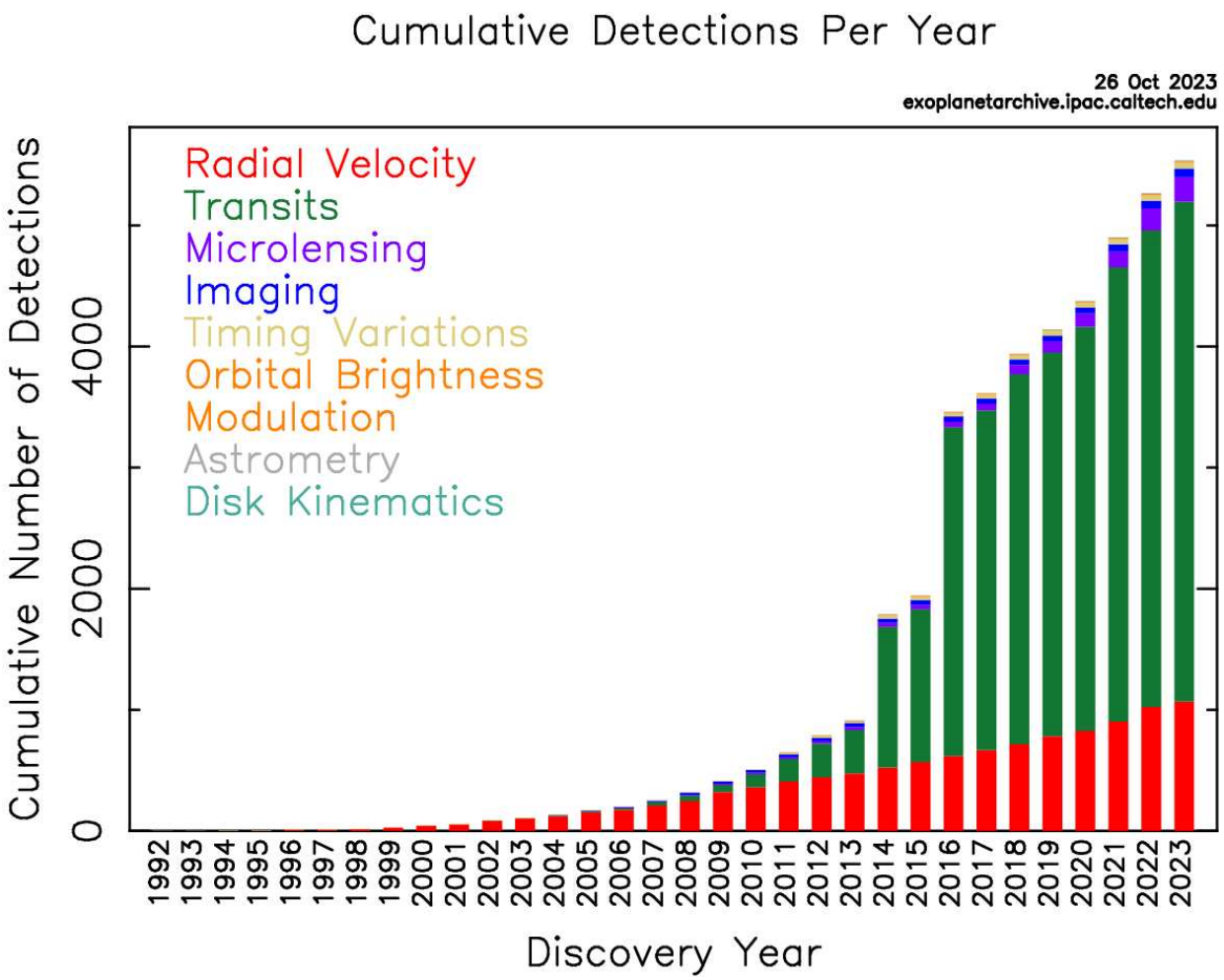

Figure 1.1: Plot of the cumulative planet detection per year

Size and mass play a crucial role in determining planet types. There are also varieties within the size/mass classifications (Table 1.1). There is a debate about the boundary between planets and brown dwarfs. Perryman (2018) suggests the threshold is 13 times Jupiter's mass, while others argue it is 20 times Jupiter's Mass. However, from a physical standpoint, objects with a mass less than 0.07-0.08 $M_{\odot}$ can not ignite hydrogen combustion in their core, making them planets. Anything between $13M_J$ and $0.07M_{\odot}$ is considered a brown dwarf. Each planet type varies in interior and exterior appearance depending on composition:

- Gas giants are planets with a similar size to Saturn or Jupiter, the largest planet in our solar system, or even bigger. However, there is more diversity within these categories. Hot Jupiters, for example, were one of the first types of planets discovered - gas giants that orbit very close to their stars ($P \leq 10$ days), causing their temperatures to rise above some thousand degrees.
- Neptunian planets are planets that share a similar size to Neptune or Uranus in our solar system. These planets are believed to have a combination of interior compositions, but all of them have hydrogen and helium-dominated outer atmospheres as well as rocky cores. In addition to this, we are also discovering mini-Neptunes, which are planets that are smaller than Neptune but larger than Earth. It is important to note that no planets of this size or type exist in our solar system.
- Super-Earths are typically terrestrial planets that may or may not have atmospheres. They are more massive than Earth but lighter than Neptune. Also, this kind of planets do not exist in our Solar System
- Terrestrial planets are small rocky planets that may have atmospheres, oceans, or signs of hab-

Planet classification		
Type	Mass Classification	Radius Classification
stellar companions	above $0.07M_{\odot}$	
brown dwarfs	$13M_J$ - $0.07M_{\odot}$	
Super jupiters	$10^3M_{\oplus}$ - 13 M_J	
Jupiters	$100M_{\oplus}$ - $10^3M_{\oplus}$	6 $R_{\oplus}$ - $22R_{\oplus}$
Neptunes		$4R_{\oplus}$-$6R_{\oplus}$
Mini neptunes	$10M_{\oplus}$ - $100M_{\oplus}$	2 $R_{\oplus}$ - $4R_{\oplus}$
SuperEarths	$2M_{\oplus}$ - $10M_{\oplus}$	$1.25R_{\oplus}$ - $2.0R_{\oplus}$
Earths	$1M_{\oplus}$ - $2M_{\oplus}$	$0.8R_{\oplus}$ - $1.25R_{\oplus}$
Sub earth	$< 1M_{\oplus}$	$< 0.8R_{\oplus}$

Table 1.1: Convention largely used to classify exoplanets: division by Mass and Radius

itability.

Exoplanets exhibit a remarkable range of sizes, from colossal gas giants exceeding Jupiter's dimensions to diminutive, rocky planets comparable in size to Earth or Mars. These celestial bodies can exist in extreme conditions, with temperatures hot enough to liquify metal or cold enough to freeze it solid. Some exoplanets are situated so close to their host stars that their orbital period is less than one day, while others orbit binary star systems e.g. Kepler 16b (Heath and Doyle, 2011). Additionally, there are exoplanets that are untethered to any star, wandering aimlessly through the cosmos in perpetual darkness, e.g. S Ori 52 (Zapatero Osorio et al., 2000). The Universe is diverse and there are no monothematic planetary systems. Our planetary system is coplanar, with eccentricities of planetary orbits close to zero, but many exoplanets have high eccentricities. There are some explanations for this phenomenon, like planet-planet scatter or Kozai-Lidov mechanism, but a global view is still not clear. The relationship radius-density and the relationship mass-density are to date widely accepted even if such correlation is not observed in the Solar System. (Fig. 1.2). Astronomers also have noted what seems to be a strange gap in planet sizes. It's been dubbed the "radius valley," or the radius gap, after Benjamin Fulton et al. (2017), lead author of a paper describing it. Data from NASA's Kepler spacecraft showed that planets of a certain size range (Fig. 1.3) are rare – those between 1.5 and 2 times the size (diameter) of Earth, which would place them among the super-Earths. It's possible that this represents a critical size in planet formation: Planets that reach this size quickly attract thick atmospheres of hydrogen and helium gas, and balloon up into gaseous planets, while planets smaller than this limit are not large enough to hold such an atmosphere and remain primarily rocky, terrestrial bodies. On the other hand, the smaller planets that orbit close to their stars could be the cores of Neptune-like worlds that had their atmospheres stripped away. Explaining the radius gap will require a far better understanding of how planetary systems form.

1.2 Detection Technique of exoplanets

Planets are much less bright than their parent star. For instance, the Sun is approximately one billion times brighter than the reflected light from any planet orbiting it. Detecting such a faint light source is challenging, especially when the light from the parent star causes glare that makes it difficult to distinguish the planet from the surrounding light. Therefore, astronomers have had to use indirect methods to detect extrasolar planets. So far, several different indirect methods have been a success (Fig. 1.4). In this section, we focus on the detection technique used in this work, while the other techniques will be briefly described.

1.2.1 Radial Velocity

Doppler spectroscopy, also known as the radial-velocity method, is a technique used to indirectly detect extrasolar planets, brown dwarfs and binary stars if are not eclipsing binary. It relies on observing the

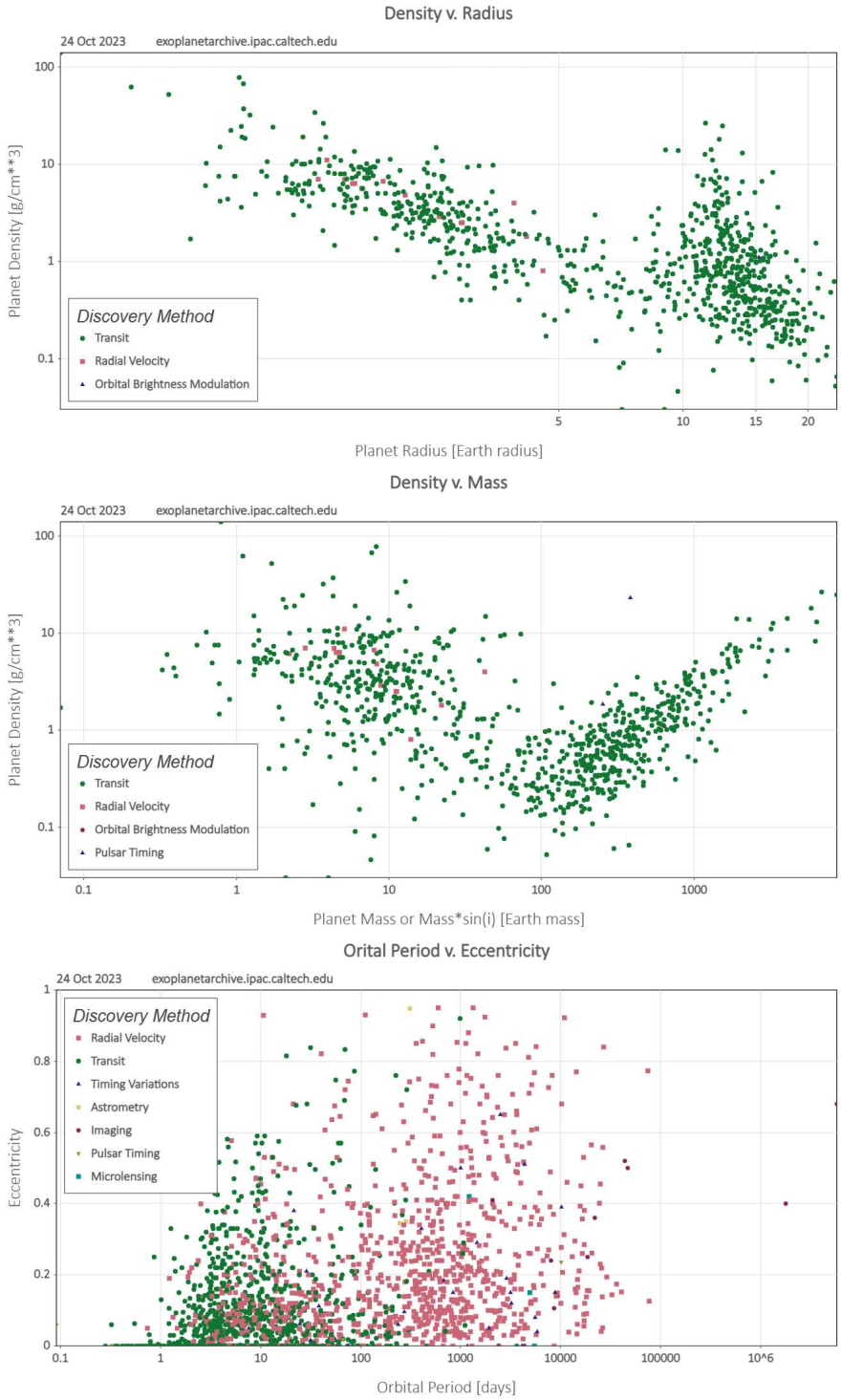

Figure 1.2: Upper plot: Density vs. Radius, in Earth Masses. central plot: Density vs. Mass, in Earth radii. Bottom plot: Eccentricity vs. Period.

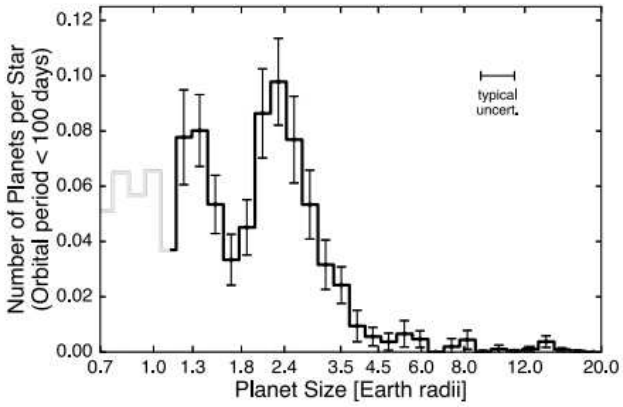

Figure 1.3: The radius gap: a drop of count of exoplanet around $1.8R_{\oplus}$.This effect is not due to a bias but an unsolved issue about planetary formation(Fulton et al., 2017).

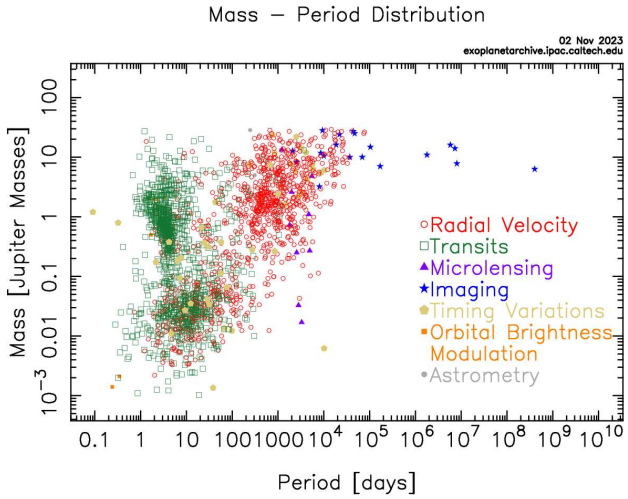

Figure 1.4: Distribution of exoplanet in function of Mass and Period and first detection method color-coded as reported in the plot

Doppler shifts in the spectrum of a star caused by variations in the star's radial velocity in response to the gravity of an orbiting planet.

The method measures the variations in the speed with which the star moves toward or away from Earth, which can be deduced from the displacement in the star's spectral lines due to the Doppler effect. By measuring these variations, the method confirms the presence of a planet using the binary mass function.

The speed of the star around the system's center of mass is much smaller than that of the planet, but velocity variations down to 3 m/s can be detected with modern spectrometers, such as the ESPRESSO Interferometer (Pepe et al., 2021) at the Very Large Telescope (VLT) at ESO's Paranal Observatory, the HARPS-N spectrometer at the TNG(Cosentino et al., 2012), the HARPS spectrometer (Mayor et al., 2003) at the ESO 3.6 meter telescope in La Silla Observatory, Chile, or the HIRES spectrometer(Vogt et al., 1994).

The radial-velocity method was the most productive technique used by planet hunters. It is distance-independent but requires high signal-to-noise ratio spectra to achieve high precision, and is generally used only for nearby stars, out to about 50 parsec from Earth, to find lower-mass planets. It is also not possible to simultaneously observe many target stars at a time with a single telescope. This method easily finds massive planets that are close to stars. Modern spectrographs can also easily detect Jupiter-mass planets orbiting 10 astronomical units away from the parent star. Earth-mass planets are currently detectable only in very small orbits around low-mass stars. For example, ESPRESSO has an accuracy of 10 cm/s, which is very close to the 9 cm/s RV variation produced by an Earth-like

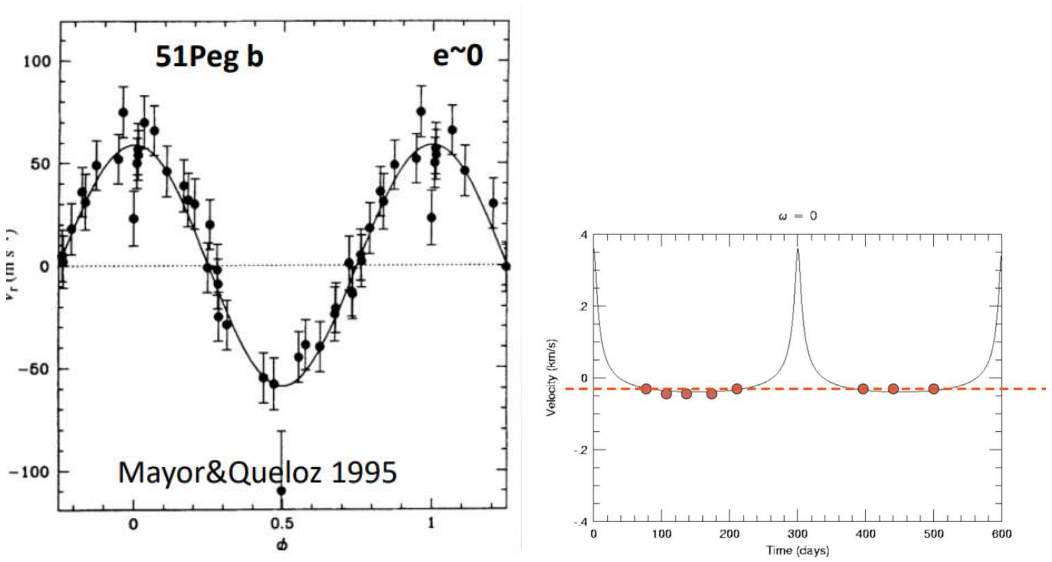

Figure 1.5: Example of Radial Velocity curve. Left: RV of 51 Pegasi-b. Right: Synthetic RV affected by high eccentricity.

planet orbiting around a sun-like star at a distance of 1 AU.

Planets are easier to detect around low-mass slowly rotating stars; these stars are more affected by gravitational tug from planets. Planets with orbits highly inclined with respect to the line of sight produce smaller visible wobbles and are thus more difficult to detect because the gravitational influence of the planet is smaller and less prominent. This means that only a fraction of the planet's orbital velocity contributes to the radial velocity variations observed from Earth. One of the advantages of the radial velocity method is that the eccentricity of the planet's orbit can be measured directly. One of the main disadvantages of the radial-velocity method is that it can only estimate a planet's minimum mass ($M_{true} * \sin i$). where M_{true} is the true mass of the planet and i is the inclination of the planet's orbit relative to the line of sight. The sine of the inclination angle ($\sin i$) introduces a projection effect, and only the component of the planet's velocity perpendicular to the line of sight contributes to the observable radial velocity. This implies that the measured radial velocity is always less than the true velocity of the planet, and hence, the derived mass is a lower limit.

The figure 1.5 (Left plot) illustrates the RV phased curve observed for 51 Peg star which is being orbited by 51 Peg b having a mass of 0.46 M_J. The right plot of Fig. 1.5 shows how eccentricity in the orbit will distort the curve and complicate the calculations. The star's velocity shows a periodic variance, suggesting an orbiting mass that is creating a gravitational pull on this star. Using Kepler's third law of planetary motion, the observed period of the planet's orbit around the star (equal to the period of the observed variations in the star's spectrum) can be used to determine the planet's distance from the star. From the semi-amplitude (ΔV) derive the mass (in degeneration with the inclination) using the following equation:

$$\Delta V = \frac{28.4 m_p \sin i}{P^{1/3} m_s^{2/3}} \tag{1.1}$$

Where m_p is the planetary mass (in Jovian masses), i is the inclination of the planet's orbit and m_s is the stellar mass (in solar masses). ΔV is in m/s. The radial-velocity method can be also used to confirm findings made by the transit method. When both methods are used in combination, the planet's true mass can be estimated as also the density of the planet. The Rossiter–McLaughlin effect (Fig. 1.6) is a spectroscopic phenomenon observed when either an eclipsing binary's secondary star or an extrasolar planet is seen to transit across the face of the primary or parent star. As the main star rotates on its axis, one quadrant of its photosphere will be seen to be coming towards the viewer, and the other visible quadrant to be moving away. These motions produce blueshifts and redshifts, respectively, in the star's spectrum, usually observed as a broadening of the spectral lines. When the

secondary star or planet transits the primary, it blocks part of the latter's disc, preventing some of the shifted light from reaching the observer. That causes the observed mean redshift of the primary star as a whole to vary from its normal value. As the transiting object moves across to the other side of the star's disc, the redshift anomaly will switch from being negative to being positive, or vice versa.

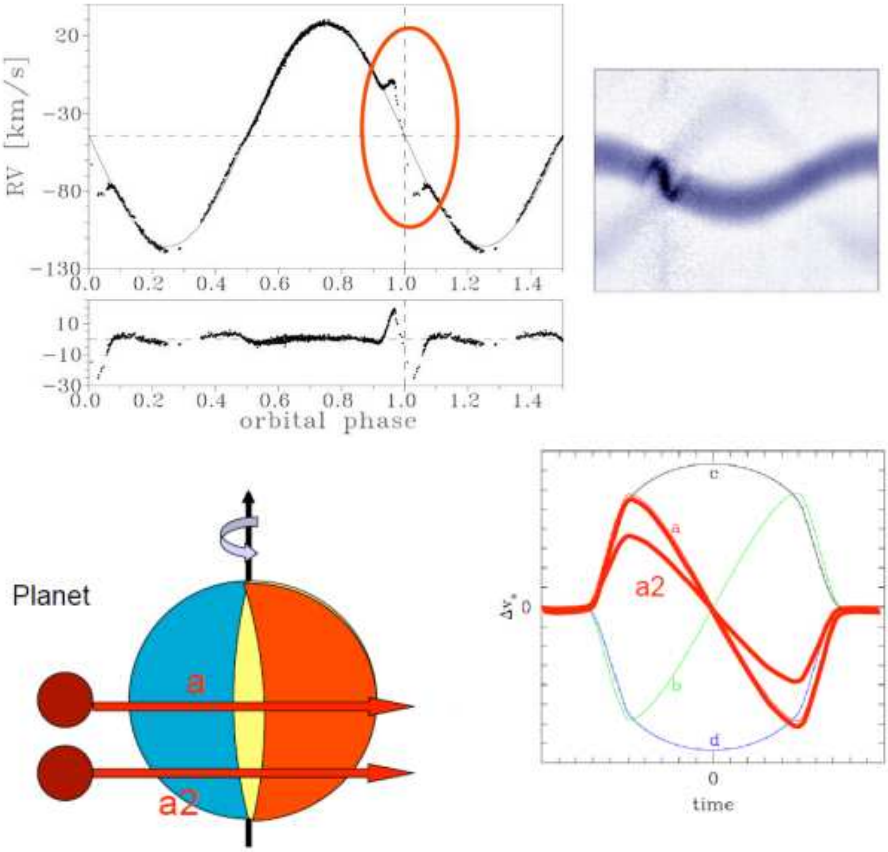

Figure 1.6: RV curve with Rossiter–McLaughlin effect and variation with the orbit inclination

Doppler spectrography can produce false signals, especially in multi-planet and multi-star systems. Magnetic fields and certain types of stellar activity can also give false signals. When the host star has multiple planets, false signals can also arise from insufficient data. Some of the false signals can be eliminated by analyzing the stability of the planetary system, conducting photometric analysis on the host star, and knowing its rotation period and stellar activity cycle periods.

If the planet's spectral lines can be distinguished from the star's spectral lines, the radial velocity of the planet itself can be found, which gives the inclination of the planet's orbit. This enables measurement of the planet's actual mass, rules out false positives, and provides data about the composition of the planet. However, such detection is only possible if the planet orbits a relatively bright star and reflects or emits a large amount of light (Richardson et al., 2007).

1.2.2 Transit

If a planet crosses (transits) in front of its parent star's disk, then the observed visual brightness of the star drops by a small amount, depending on the relative sizes of the star and the planet. A theoretical model of a transiting exoplanet light curve (Fig.1.7) predicts various characteristics of an observed planetary system, such as the transit depth (δ), transit duration (T), impact parameter (b), ingress/egress duration (τ), and period of the exoplanet (P). However, these observable are based on certain assumptions, such as the spherical shape of both the planet and star, the uniformity of the stellar disk, and the circularity of the orbit. Depending on the relative position of the observed transiting exoplanet during transit, the physical parameters of the light curve change.

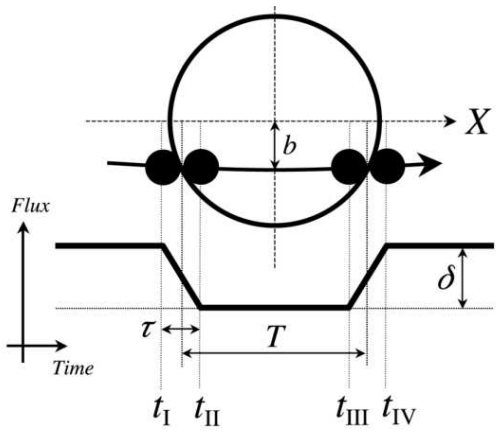

Figure 1.7: Transit Geometry

The transit depth of a transiting light curve describes the decrease in the normalized flux of the star during transit. This parameter indicates the size of the exoplanet relative to the star and it is proportional to $(\frac{R_p}{R_*})^2$. For instance, if an exoplanet transits a star of solar radius, a larger exoplanet radius would increase the transit depth, while a smaller exoplanet radius would decrease it.

The transit duration of an exoplanet is the time that a planet spends transiting a star. This observable changes depending on the speed of the planet in its orbit as it transits the star. The impact parameter is the distance between the center of the star and the plane of the transit. b is correlated with inclination: $bR_* = a\cos i$, where a is the semi-major axis of the planet's orbit.

By using these observable parameters, one can determine a number of different physical parameters such as semi-major axis, planet radius, and inclination through calculations. Combining this with radial velocity measurements of the star, the mass of the planet can also be determined.

Observing planetary transits has its drawbacks. One of the major disadvantages is that it can only be observed when the planet's orbit is perfectly aligned with the observer's point of view, inclination ~ 90 or few less. The probability of observing a planetary orbital plane in direct line of sight with a star is determined by the ratio of the diameter of the star to the 2x semi-major axis of the orbit. However, transit surveys can find more extrasolar planets than the radial-velocity method by scanning large areas of the sky that contain thousands or even hundreds of thousands of stars at once. Several surveys have taken this approach, such as the ground-based SuperWASP (Pollacco et al., 2006), KELT (Pepper et al., 2003) and HATNet (Bakos et al., 2004), as well as the space-based CoRoT (Baglin et al., 2006), Kepler (Borucki et al., 2010), K2 (Howell et al., 2014) and TESS missions (Ricker, 2015) and in the next future PLATO (Rauer et al., 2014). The most distant planets detected by Sagittarius Window Eclipsing Extrasolar Planet Search are located near the Galactic center (Sahu et al., 2006). However, it is difficult to conduct reliable follow-up observations of these stars with current technology.

The second disadvantage of this method is the high rate of false detection. Thus, a star with a single transit detection requires additional confirmation, typically from the radial-velocity method or orbital brightness modulation method. The false positive rate is very low in stars with two or more planet candidates, and such detection often can be validated without extensive follow-up observations. Some can also be confirmed through the transit timing variation method.

The transit method's main advantage is that the size of the planet can be determined from the light curve. When combined with the radial-velocity method (which determines the planet's mass), one can determine the density of the planet, and it allows us to know the physical structure of the planet (rocky or gaseous). The planets that have been studied by both methods are by far the best-characterized of all known exoplanets.

The transit method also makes it possible to study the atmosphere of the transiting planet. When the planet transits the star, light from the star passes through the upper atmosphere of the planet.

By studying the high-resolution stellar spectrum carefully, one can detect elements present in the planet's atmosphere. A planetary atmosphere, and planet for that matter, could also be detected by measuring the polarization of the starlight as it passes through or is reflected off the planet's atmosphere. Additionally, the secondary eclipse (when the planet's light is blocked by its star) allows direct measurement of the planet's radiation and helps to constrain the planet's orbital eccentricity. When the star's photometric intensity during the secondary eclipse is subtracted from its intensity before or after, only the signal caused by the planet remains. Then, it becomes possible to measure the planet's temperature and even to detect possible signs of cloud formations on it.

1.2.3 Astrometry

Astrometry is the oldest search method for extrasolar planets. It was initially popular because of its success in characterizing astrometric binary star systems. William Herschel made some statements about an unseen companion affecting the position of the star he cataloged as 70 Ophiuchi in the late 18th century (See, 1896). The first known astrometric calculation for an extrasolar planet was made by William Stephen Jacob (1855) for this star. Similar calculations were repeated by others for another half-century until finally refuted in the early 20th century (Reuyl and Holmberg, 1943). For two centuries, claims circulated of the discovery of unseen companions in orbit around nearby star systems, all reportedly found using this method. However, none of these claims survived scrutiny by other astronomers, and the technique fell into disrepute. Unfortunately, the changes in stellar position are so small, and atmospheric and systematic distortions so large, that even the best ground-based telescopes cannot produce precise enough measurements. Any claims of a planetary companion of less than 0.1 $M_{\odot}$ made before 1996 using this method are likely spurious.

The space-based observatory Gaia (Gaia Collaboration et al., 2016), launched in 2013, is expected to find thousands of planets via astrometry. Prior to the launch of Gaia, no planet detected by astrometry had been confirmed. One potential advantage of the astrometric method is that it is most sensitive to planets with large orbits. This makes it complementary to other methods that are most sensitive to planets with small orbits. However, very long observation times will be required, possibly years or even decades, as planets far enough from their star to allow detection via astrometry also take a long time to complete an orbit. Planets orbiting one of the stars in binary systems are more easily detectable, as they cause perturbations in the orbits of stars themselves. However, with this method, follow-up observations are needed to determine which star the planet orbits around.

Holl et al. (2023) discusses astrometric-orbit solutions for 1162 sources, which were determined with Gaia DR3. The solutions are grouped into three categories based on the mass of their companions. Seventeen solutions (nine validated) have companions with planetary-like masses ($M_c < 20M_J$), 52 solutions (29 validated) have companions with brown dwarf-like masses ($20M_J < M_c < 120M_J$), and 1093 solutions (160 validated) have companions with masses similar to low-mass stars ($M_c > 120M_J$).

1.2.4 Other Methods

Direct imaging

Planets are much fainter than stars and their light is often lost in the glare of their parent star. This makes it difficult to detect them directly. However, planets that are far enough from their host star to be resolved can be detected through their thermal emission. Young stars are the best targets for this technique since the planets around these stars emit more thermal radiation than exoplanets around older stars. It is also easier to obtain images of planets that are larger, hotter and farther from their parent star. Infrared imaging is often used to detect planets since they appear brighter in infrared than in visible light.

Direct imaging can only give rough estimates of a planet's mass. The planet's mass is derived from the star's age and the planet's temperature using evolutionary models. However, the mass can vary considerably as planets can form several million years after the star has formed. The planet's radius can be estimated based on its temperature, brightness, and distance from Earth.

Observations at multiple wavelengths may be needed to rule out the planet being a brown dwarf. Direct imaging can accurately measure the planet's orbit around the star. It works best for planets with face-on orbits rather than edge-on orbits. This is because a planet in a face-on orbit is visible throughout its orbit, while a planet with an edge-on orbit is only visible during its period of largest apparent separation from the parent star.

Coronagraphs are used to block the light from the star while leaving the planet visible.

One of the instruments used to perform direct imaging is the Spectro-Polarimetric High-contrast Exoplanet REsearch (SPHERE) (Beuzit et al., 2019). SPHERE is the extreme adaptive optics system and coronagraphic facility at the VLT. The primary science goal of SPHERE is imaging, low-resolution spectroscopic, and polarimetric characterization of extra-solar planetary systems. The instrument design is optimized to provide the highest image quality and contrast performance in a narrow field of view around bright targets that are observed in the visible or near-infrared. SPHERE is installed at the UT3 Nasmyth focus of the VLT. The first exoplanets whose orbital motion was confirmed by direct imaging are in the HR 8799 system (Fig. 1.8). This system (Marois et al., 2008) is a roughly 30 million-year-old main sequence star located at 39.6 parsec from Earth in the constellation of Pegasus. It has a mass of $1.47M_{\odot}$ a radius of $1.34R_{\odot}$ and 4.92 times sun luminosity. It is part of a system that also contains a debris disk and at least four massive planets.

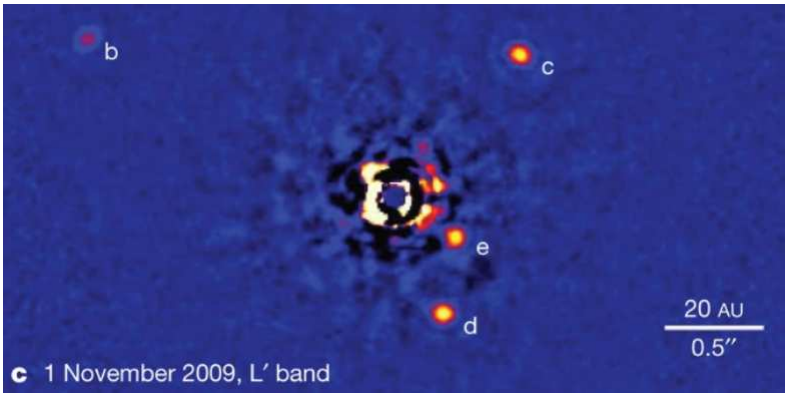

Figure 1.8: Planetary system of HR 8799. Formed by 4 planets, the first has a mass of $7M_J$ other three $10M_J$, the semi-major axis is respectively 16, 24, 38 and $68AU$

Microlensing

Gravitational microlensing (Gould and Loeb, 1992) is a phenomenon where the gravitational field of a star acts as a magnifying lens, making a distant star's light appear brighter. This can only happen when the two stars are almost perfectly aligned. These events are short-lived, lasting only for days or weeks, as all three celestial bodies - the two stars and Earth - are in motion relative to each other. Over the past few years, more than a thousand such events have been observed.

If the star causing the lensing has a planet, the planet's own gravity can also contribute to the lensing effect. However, this requires a very rare alignment, so a large number of distant stars need to be constantly monitored to detect planetary microlensing contributions at a reasonable rate. This method is most effective for detecting planets located between Earth and the center of the Galaxy because the Galactic center provides a large number of background stars.

Unlike most other methods, which have biases towards detecting planets with small or large orbits, the microlensing method is most sensitive to detecting planets that are at a distance of 1-10 astronomical units (AU) from Sun-like stars.

The disadvantage of the method is that the alignment that causes the lensing is a one-time event, which cannot be repeated. Additionally, the detected planets are typically several kiloparsecs away, making follow-up observations with other methods difficult. Only the planet's mass can be determined from microlensing, and even that is only within large errors. Other orbital properties, such as its period or

eccentricity, are challenging to determine using this method. Planets around low-mass stars are easier to detect using gravitational microlensing, as the effect of the planet's gravity is more prominent in relation to the star's gravity.

The main advantages of the gravitational microlensing method are that it can detect low-mass planets, planets in wide orbits comparable to those of Saturn and Uranus, and planets around very distant stars.

Time Variation

Pulsar time variation: Pulsars are neutron stars, the dense remnant of a star that has gone supernova. These stars emit radio waves extremely regularly as they rotate, which makes it possible to track their motion by observing the slight anomalies in the timing of their radio pulses. If a pulsar has a planet orbiting around it, the intrinsic rotation of the pulsar will cause it to move in its own small orbit. Calculations based on pulse-timing observations can reveal the parameters of the planet's orbit. This method was not originally designed for detecting planets, but it is so sensitive that it can detect planets that are far smaller than any other method can, down to less than a tenth the mass of Earth. It can also detect mutual gravitational perturbations between the various members of a planetary system, thereby revealing further information about those planets and their orbital parameters. In addition, it can easily detect planets that are relatively far away from the pulsar. However, there are two main drawbacks to the pulsar timing method: pulsars are relatively rare, and special circumstances are required for a planet to form, or survive, around a pulsar. Therefore, it is unlikely that a large number of planets will be found in this way (Perryman, 2011).

Pulsation time variation: Like pulsars, some other types of pulsating variable stars are regular enough that radial velocity could be determined purely photometrically from the Doppler shift of the pulsation frequency, without needing spectroscopy. This method is not as sensitive as the pulsar timing variation method, due to the periodic activity being longer and less regular. The ease of detecting planets around a variable star depends on the pulsation period of the star, the regularity of pulsations, the mass of the planet, and its distance from the host star (Perryman, 2011).

Transit time variation: The transit timing variation (TTV) method considers whether transits occur with strict periodicity or if there is a variation. When multiple transiting planets are detected, they can often be confirmed with the transit timing variation method. This is useful in planetary systems far from the Sun, where radial velocity methods cannot detect them due to the low signal-to-noise ratio. If a planet has been detected by the transit method, then variations in the timing of the transit provide an extremely sensitive method of detecting additional non-transiting planets in the system. It is easier to detect transit-timing variations if planets have relatively close orbits and when at least one of the planets is more massive, causing the orbital period of a less massive planet to be more perturbed (Perryman, 2011).

However, the main drawback of the transit timing method is that the specific physical properties of the planets, such as their size, composition, atmosphere, or surface features, are not directly observable using this method. Furthermore, multiple configurations of planetary systems or additional bodies can lead to similar transit timing variations. The degeneracy in solutions makes it challenging to determine the specific characteristics of individual planets based solely on transit timing data.

Transit duration variation: Transit duration variation (TDV) can help to determine the maximum mass of a planet, and in most cases, it can confirm if an object has planetary mass, but it does not put narrow constraints on its mass. Transit duration variation refers to changes in how long the transit takes. Duration variations may be caused by an exomoon, apsidal precession for eccentric planets due to another planet in the same system, or general relativity.

1.3 Space Missions adopted in this work

Most confirmed extrasolar planets have been found using space-based telescopes. Many of the detection methods can work more effectively with space-based telescopes that avoid atmospheric haze and turbulence. COROT (2007-2012) and Kepler were space missions dedicated for searching extrasolar planets using transits. COROT discovered about 30 new exoplanets [1]. Kepler (2009-2013) and K2 (2013-2018) have discovered over 2000 confirmed exoplanets [1]. Hubble Space Telescope and MOST have also found or confirmed a few planets [1]. The infrared Spitzer Space Telescope has been used to detect transits of extrasolar planets, as well as occultations of the planets by their host star and phase curves [1]. The Gaia mission, launched in December 2013, will use astrometry to determine the true masses of 1000 nearby exoplanets. TESS, launched in 2018, CHEOPS launched in 2019 and PLATO in 2026 are using the transit method to search exoplanets. In the following sections, I provide a detailed description of the two space missions that form the basis of this thesis.

1.3.1 Gaia mission

The Global Astrometric Interferometer for Astrophysics (GAIA) observatory, launched by the European Space Agency (ESA) in 2013, is designed for astrometry. The original acronym was abandoned with the change in the telescope design, which no longer involves interferometry. Instead, it is derived from Greek mythology, where Gaia is the personification of the Earth. The choice of the name reflects the mission's goal of mapping and understanding the Milky Way, essentially exploring and surveying our galactic home. Its main objective is to measure the positions, distances, and motions of stars with incredible precision. The standard deviation for bright stars is expected to be 6.7 micro-arcseconds or better in the parallax. For fainter stars, error levels increase, reaching 26.6 micro-arcseconds error in the parallax for 15th-magnitude stars, and several hundred micro-arcseconds for 20th-magnitude stars. The project aims to create the largest and most precise 3D space catalog ever made, consisting of about 2 billion astronomical objects, including stars, planets, comets, asteroids, and quasars. To study the precise position and motion of its target objects, the spacecraft monitored each of them about 70 times over the five years of the nominal mission (2014–2019) and continues to do so during its extension. The spacecraft has enough micro-propulsion fuel to operate until the second quarter of 2025. Gaia targets objects brighter than magnitude 20 in a broad photometric band that covers the extended visual range between near-UV and near-infrared. Additionally, Gaia is expected to detect thousands to tens of thousands of Jupiter-sized exoplanets beyond the Solar System by using the astrometry method, 500,000 quasars outside this Galaxy, and tens of thousands of known and new asteroids and comets within the Solar System.

The Gaia space mission has the following objectives:

- Determining the star's distance through the parallax to get an accurate measure of the intrinsic luminosity.
- Providing a more complete view of the stellar luminosity function, which is a statistical distribution of the intrinsic luminosities of stars, through the observation of the faintest objects
- Performing a detailed examination and re-examination of a great number of objects over a long period to gain a better understanding of the more rapid stages of stellar evolution
- Measuring a star's astrometric and kinematic properties to understand distant stellar populations.
- Studying many other areas of astrophysical research, including stellar evolution and physics, star formation, stellar variability, the distance scale, multiple stars, exoplanets, solar system bodies, unresolved galaxies and quasars, and fundamental physics.

[1] `https://exoplanetarchive.ipac.caltech.edu/cgi-bin/TblView/nph-tblView?app=ExoTbls&config=PS`

Binaries and multiple stars

Gaia(Gaia Collaboration et al., 2016) is an important mission that aims to enhance our knowledge of multiple stars. Its scanning direction provides an instantaneous spatial resolution similar to that of the Hubble Space Telescope, and it is surveying the entire sky. Gaia's instruments can aid in our understanding of multiple systems, enabling us to resolve many binaries. The astrometric wobbles of unresolved binaries can be used to identify multiple systems, while periodic changes in photometry can help to detect (eclipsing) binaries. The Gaia data will also provide an improved census of double-lined systems based on spectroscopy. With a large number of objects to study, Gaia will help to address fundamental questions of mass distributions and orbital eccentricities among binaries.

Exoplanets

Among the various scientific topics that Gaia can address, exoplanet research has been the most dynamic area in the past two decades(Gaia Collaboration et al., 2016). The field has expanded from hot, giant planets to smaller planets, to planets further away from their host star, and to multiple planetary systems. These advancements have been achieved both with space- and ground-based facilities. However, Gaia's astrometric capabilities remain unique, probing an area of exoplanetary systems' parameter space that has been poorly explored. It provides astrophysical parameters not obtainable by other means. One of Gaia's strengths in the exoplanet research field is the provision of an unbiased, volume-limited sample of Jupiter-mass planets in multiyear orbits around their host stars. These are logical prime targets for future searches of terrestrial-mass exoplanets in the habitable zone in an orbit protected by a giant planet further out. Additionally, Gaia's astrometric data allows for the measurement of actual masses (rather than lower limits) and provides detailed distributions of giant exoplanet properties (including the giant planet-brown dwarf transition regime) as a function of stellar-host properties with unprecedented resolution.

Data release

Several Gaia catalogs are released over the years each time with increasing amounts of information and better astrometry; the early releases also miss some stars, especially fainter stars located in dense star fields and members of close binary pairs. The first data release, Gaia DR1, based on 14 months of observation was released on 14 September 2016. The data release included:

- positions and magnitudes for 1.1 billion;
- positions, parallaxes and proper motions for more than 2 million stars based on a combination of Gaia and Tycho-2 data for those objects in both catalogs;
- light curves and characteristics for about 3,000 variable stars;
- positions and magnitudes for more than 2000 extragalactic sources used to define the celestial reference frame.

The second data release (DR2), which occurred on 25 April 2018, is based on 22 months of observations made between 25 July 2014 and 23 May 2016. It included:

- positions, parallaxes and proper motions for about 1.3 billion stars and positions of an additional 300 million stars in the magnitude range G = 3–20;
- red and blue photometric data for about 1.1 billion stars and single-color photometry for an additional 400 million stars;
- median radial velocities for about 7 million stars between magnitude 4 and 13.
- It also contained data for over 14,000 selected Solar System objects.

Gaia Data Release 3 is split into two installments: the early release called Gaia Early Data Release 3 (Gaia EDR3) and the full Gaia Data Release 3 (Gaia DR3). Gaia EDR3 was released on 3 December 2020. The full Gaia Data Release 3 (DR3) was published on 13 June 2022. The Gaia EDR3 included:

- position on the sky, parallax, and proper motion for around 1.468 billion sources, with a limiting magnitude of about G $\simeq$ 21 and a bright limit of about G $\simeq$ 3. The astrometric solution will be accompanied by some new quality indicators, like RUWE. The term RUWE stands for "Renormalized Unit Weight Error", designed to assess the goodness of fit between the observations of a star and the model predictions in the catalog.
- G magnitudes for around 1.806 billion sources.
- GBP (Blue Photometer Magnitude; This corresponds to the blue photometric band on Gaia, covering shorter wavelengths) and GRP (Red Photometer Magnitude; This corresponds to the red photometric band on Gaia, covering longer wavelength for around 1.542 billion and 1.555 billion sources, respectively.
- About 1.614 million celestial reference frame (Gaia-CRF3) sources.
- Simulated data from Gaia Object Generator (GOG) and Gaia Universe Model Snapshot (GUMS).

The full DR3, described in chapter 2.2, includes the EDR3 data plus:

- Solar System data;
- variability information;
- results for non-single stars, for quasars, and for extended objects;
- astrophysical parameters;
- special data set, the Gaia Andromeda Photometric Survey (GAPS).

1.3.2 TESS mission

Transiting Exoplanet Survey Satellite (TESS) (Ricker, 2015) is a space telescope for NASA's Explorer program, designed to search for exoplanets using the transit method in an area 400 times larger than that covered by the Kepler mission, almost all sky. The sole instrument on TESS is a package of four wide-field-of-view charge-coupled device (CCD) cameras. Each camera has a resolution of 21×21 $arcsec/pix$. The point-spread function (PSF) is usually 1-2 pixels in radius, this means that a single TESS pixel can include the flux from several objects in crowded fields. The TESS lenses have a combined field of view of $24° \times 96°$ (2300 deg^2, around 5% of the entire sky). TESS's all-sky survey would focus on nearby G-, K-, and M-type stars with apparent magnitudes brighter than magnitude 12. Approximately 500,000 stars, including 1,000 closest red dwarfs across the whole sky, form a high-priority sample. The mission is actually in the 6th year of its life.

The first two-year survey was broken up into 26 observation sectors, with an overlap of sectors (continuous viewing zone, CVZ) at the ecliptic poles to allow additional sensitivity toward smaller and longer-period exoplanets in that region of the celestial sphere. The spacecraft spent 27.4 days observing each sector, mapping the southern hemisphere of the sky in its first year of operation and the northern hemisphere in its second year. For every sector, the TESS spacecraft downlink about 200,000 two-minute cadence postage stamps, as well as full frame images binned on board at a 30-minute cadence. During the 2-years First Extended Mission, data collection was slightly changed:

- A new set of target stars has been selected
- The number of stars monitored at 2-minute cadence was increased from 15,000 to 20,000 per observing sector.
- Up to 1000 stars per sector have been monitored at a new fast 20-second cadence.
- The full-frame image cadence has been increased from every 30 minutes to every 10 minutes.
- Regions near the ecliptic have been partially covered.

During the second extended mission (5th and 6th year), the full-frame image cadence was further increased from every 10 minutes to every 200 seconds, the number of 2-minute cadence targets was reduced to $\sim$ 8000 per sector, and the number of 20-second cadence targets increased to $\sim$ 2000 per sector. The TESS input catalog (TIC) is used to help identify two-minute cadence target selection for the TESS mission and to calculate the physical and observational properties of planet candidates. It is for use by both the TESS science team and the public, and it is periodically updated, the current version is TIC-8.2 (see chapter 2.1).TIC (Stassun et al., 2018) contains all optically luminous and persistent objects in the sky, based on wide-field photometric point source catalogs. Objects not having significant persistent optical flux and those that move too fast for their celestial positions to be calculated with linear proper motions (such as planets, asteroids, TNOs, etc.) were excluded, for technical and logistical reasons.

1.3.3 False Positive

False positives in the transit photometry method arise in three common forms: blended eclipsing binary systems, grazing background eclipsing binary systems, and transits by planet-sized stars. Eclipsing binary systems usually produce deep eclipses that distinguish them from exoplanet transits, since planets are usually smaller than about $2R_J$, but eclipses are shallower for blended or grazing eclipsing binary systems.

Blended eclipsing binary systems consist of a normal eclipsing binary that contaminates the target star because of the low resolution of the instrument. The constant light of the third star dilutes the measured eclipse depth, so the light curve may resemble that of a transiting exoplanet. These cases often involve a large main sequence primary star in the eclipsing binary, which dominates the light. The secondary star in the eclipsing binary may be smaller and less luminous. Alternatively, the target star may be a giant star with the eclipsing binary containing a main sequence primary and secondary.

Grazing eclipsing binary systems are systems in which one object will just barely graze the limb of the other. In these cases, the maximum transit depth of the light curve will not be proportional to the ratio of the squares of the radii of the two stars, but will instead depend solely on the small fraction of the primary that is blocked by the secondary. The small measured dip in flux can mimic that of an exoplanet transit. Some of the false positive cases of this category can be easily found if the eclipsing binary system has a circular orbit, with the two companions having different masses. Due to the cyclic nature of the orbit, there would be two eclipsing events, one of the primary occulting the secondary and vice versa. If the two stars have significantly different masses, and this different radii and luminosities, then these two eclipses would have different depths. This repetition of a shallow and deep transit event can easily be detected and thus allow the system to be recognized as a grazing eclipsing binary system. However, if the two stellar companions are approximately the same mass, then these two eclipses would be indistinguishable, thus making it impossible to demonstrate that a grazing eclipsing binary system is being observed using only the transit photometry measurements. One of the methods to find eclipsing binaries (EBs) is to observe them using different filters. In different wavelength bands, the depths of the eclipses change, whereas for planets, this does not happen (Fig. 1.9).

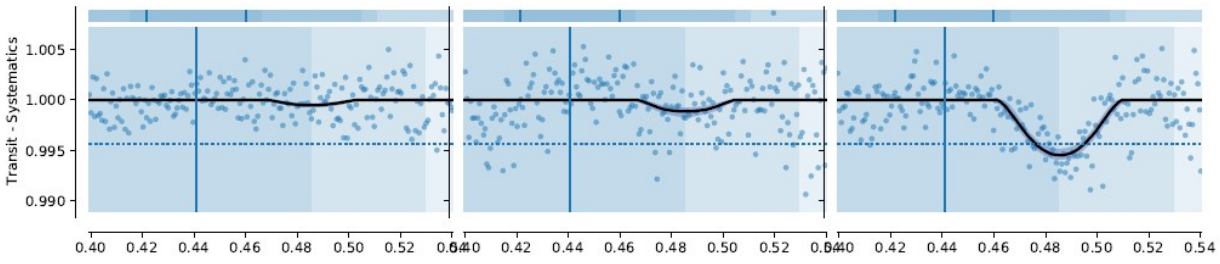

Figure 1.9: Multi-color photometry of TOI 4146.01, the tree filters are g, i and z_s. The change in the depths of the eclipses indicates that the transit is occurring around a star that is cooler than the main target

Finally, there are two types of stars that are approximately the same size as gas giant planets, white dwarfs and brown dwarfs. The light curve does not discriminate between masses as it only depends on the size of the transiting object. When possible, radial velocity measurements are used to verify that the transiting or eclipsing body is of planetary mass. Multi-band photometry can help to do this.

Flattening the lightcurve of a variable star in a non-perfect way can generate periodic signals that mimic transits, leading to the detection of false alarms.

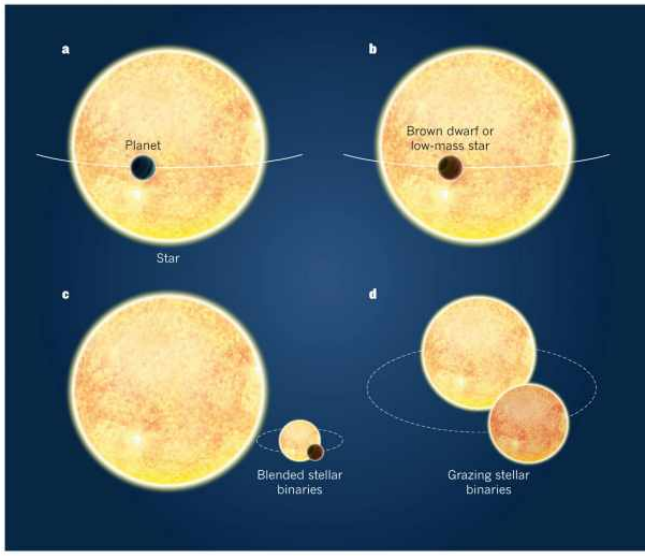

Figure 1.10: a, A gas-giant planet blocks a small amount of starlight as it passes in front of its host star. The resulting drop in light is similar to that produced by other systems, as follows: b, an orbiting brown-dwarf or low-mass star, both of which have radii similar to gas-giant planets; c, blended stellar binaries in a triple-star system that have deep eclipses strongly diluted by a bright neighboring star, mimicking the much shallower transits of a planet; d, grazing binary stars, in which the stars' disks overlap by only a tiny amount at each eclipse.

1.4 This work

This master thesis delves into the astrometric signatures associated with stars hosting planet candidates detected by TESS. This introductory section provides a historical perspective on the detection of exoplanets, highlighting the evolution of detection techniques, including radial velocity, transit, astrometry, and other methods. Noteworthy space missions, specifically Gaia and TESS, are introduced, and the concept of false positives in exoplanet detection is discussed.

The core of the work involves the analysis of various catalogs, emphasizing TESS, Gaia DR3, and the Proper Motion anomaly (PMa) catalog. The TESS catalogs, including the TIC and TOI catalogs, are explored, along with Gaia DR3 and its Non-Single Star (NSS) Catalogue. The PMa catalog, a key component for assessing proper motion anomalies, is introduced.

The thesis then delves into the detailed analysis of TESS Objects of Interest (TOI), examining the TOI-NSS and TOI-PM tables. The TOI analysis involves a meticulous exploration of astrometric data, uncovering patterns and anomalies associated with the stellar hosts of TESS planet candidates.

Highlighting specific cases of interest, the research spotlights objects like TOI 503.01, TOI 1338.01, TOI 503.01 (HATS-26 b), WASP-2 b, TOI 148.01, TOI 144.01, TOI 185.01 (WASP-18 b), TOI 2543.01, TOI 179.01, TOI 200.01 (DS Tuc Ab), TOI 4399.01, and TOI 5394.01. Each case is scrutinized for astrometric peculiarities, contributing to a comprehensive understanding of the complexities associated with these planetary systems.

The concluding section synthesizes the findings, offering insights into the astrometric signatures of stars hosting TESS planet candidates. The work not only contributes to emphasizing the useful tools

of the Gaia catalog in the contest of detecting False Positive but also provides a foundation for future investigations into the astrometric dynamics of stellar systems observed by TESS and Gaia.

Catalogs used in this work

2.1 TESS Catalogs

The two TESS catalogs used in this work are:

1. The TESS input catalog (TIC) is a catalog of bright sources in the sky that was used to select target stars for observation and evaluate transit signals.
2. The TOI catalog includes the TESS Objects of Interest (TOIs) vetted at the TESS Science Office (TSO) and deemed promising candidates for follow-up by the TESS Follow-up Observing Program (TFOP)

The following section describes in detail these catalogs.

2.1.1 TIC catalog

The TESS input catalog (TIC) (Stassun et al., 2018) is crucial for selecting the best targets for planetary transit searches and calculating the flux contamination in the TESS aperture for each target. It also provides reliable stellar radii for planetary radius calculations, which helps determine which targets receive mission-based photometric and spectroscopic follow-up.

The purpose of the TIC is to address four basic needs. They are:

1. To provide basic astronomical information for all sources in the TESS footprint. It is a catalog in which anyone can look up information about any object for which the TESS mission produces a light curve, barring moving or transient objects.
2. To enable the selection of primary transit-search (i.e., two-minute and fast cadence) targets for TESS. The incorporation of all luminous objects in the sky for the full TIC will allow a calculation of the flux contamination for all potential TESS targets. In practice, that involves a flux contamination value for every star in the Candidate Target List subset of the TIC.
3. To provide stellar parameter information for the TESS pipeline to evaluate exoplanet transit candidates. As TESS light curves are searched for transit candidates, data about the target star, such as effective temperature ($T_{\rm eff}$), surface gravity ($\log g$), mass ($M_\star$), radius ($R_\star$), and other parameters, are used to calculate the planet's properties.
4. To facilitate the identification of false positives, it is imperative that both the TESS pipeline and subsequent follow-up missions possess the capability to discern all established astrophysical sources within a specified angular radius of any object in the TIC. This identification should extend to a defined faintness limit, accompanied by comprehensive information about these sources. This comprehensive data empowers users to assess the likelihood of signals in a target's light curve originating from astrophysical sources other than the intended target itself.

2.1.2 TOI catalog

The data collected by TESS are processed into calibrated light curves by two data processing pipelines: the Science Processing Operations Center (SPOC) pipeline for the postage stamps and the Quick Look Pipeline (QLP) for the full-frame images (FFIs). These pipelines identify potential transiting planets by searching for periodic flux decreases, known as threshold-crossing events (TCEs).

The TESS Science Office (TSO) examines TCEs using the TESS light curve and other information to identify planet candidates that would benefit from follow-up observation. The light curves are first run through software that eliminates obvious non planetary signals; the remaining light curves are manually vetted to identify a set of TESS Objects of Interest (TOIs). These pipelines each calibrate the pixel data and use them to produce light curves in different ways.

The SPOC pipeline calibrates the pixel data, extracts photometry and centroids for each target star, and identifies and removes instrumental signatures. The pipeline then searches each light curve for TCEs, fits each TCE with a limb-darkened transit light-curve model, and performs diagnostic tests to assess the planetary nature of each TCE. The SPOC pipeline also calibrates the FFIs at the pixel level.

The QLP generates light curves from the FFIs, complementary to the SPOC pipeline, which produces light curves from the postage stamp data. The QLP separately performs its own calibration of the raw FFIs. For each sector, the QLP produces about half a million light curves. In addition, the QLP always uses all sectors of available data to create light curves i.e., the QLP runs over multiple sectors of data together.

To search for transits, both the SPOC and QLP pipeline phase-fold processed light curves with a large number of trial periods to search for repeating transit-like drops in brightness. Any drop in brightness that passes a specified threshold requirement is called a TCE. Each TCE has an associated data validation (DV) report that provides a detrended and phase-folded light curve in addition to auxiliary data products (Guerrero et al., 2021).

Figures 2.1 and 2.2 show the report generated by the two pipelines.

The SPOC DV (fig. 2.1) summary report comprises four rows with different information. In the first row, the TESS detrended light curve is plotted with transits marked by blue triangles. The sector boundaries are indicated by red vertical dashed lines, and the green vertical dashed lines mark momentum dumps. The second row on the left shows the TESS light curve folded on the planet candidate's orbital period. The black points represent all data points, the cyan points show data binned at one-fifth of the fitted transit duration, and the red line is a model fit to the transit. The second row on the right displays the best candidate for a secondary transit found in the phase-folded light curve. The third row on the left is a zoom-in on the phase-folded light curve around the transit. The third row on the right shows the whitened transit fit indicated by the red line. The binned residuals from the fit are displayed in green, and the out-of-phase residuals from the fit are shown in magenta. In the fourth row on the left, the phase-folded odd transits are compared with the phase-folded even transits. The red dashed lines indicate transit depths, and the title line reports the difference's significance between the odd and even transits. The fourth row in the middle is a centroid offset plot showing the R.A. and decl. offsets of a transit source with respect to the position of the target star. The centroid offsets for each sector are shown with green crosses, and the mean centroid offset over all sectors is shown with a magenta cross. The location of the target star is marked by a red star, and the 3σ radius of uncertainty for the transit source offset is shown by a blue circle. In the fourth row on the right, the fitted planet parameters and DV diagnostic test results are displayed.

The QLP DV summary report plots (fig. 2.2). The top row shows the detrended full light curve with all available sectors stitched together. Transits are marked by red vertical lines. The middle row on the left shows the phase-folded light curve. The gray points are all data points, and the blue points are binned relative to the transit window size to guide the eye. The middle row on the right displays the phase-folded light curve at phase 0.5 for a secondary eclipse test. The bottom row shows even

and odd transits. The model fit is shown in orange, and the depths of even transits are marked by darker dashed lines while odd transits are marked by lighter dashed lines. A significant difference in the depths $> 5\sigma$ would suggest that the TCE is an EB at twice the period. The right-hand column displays planet and stellar parameters.

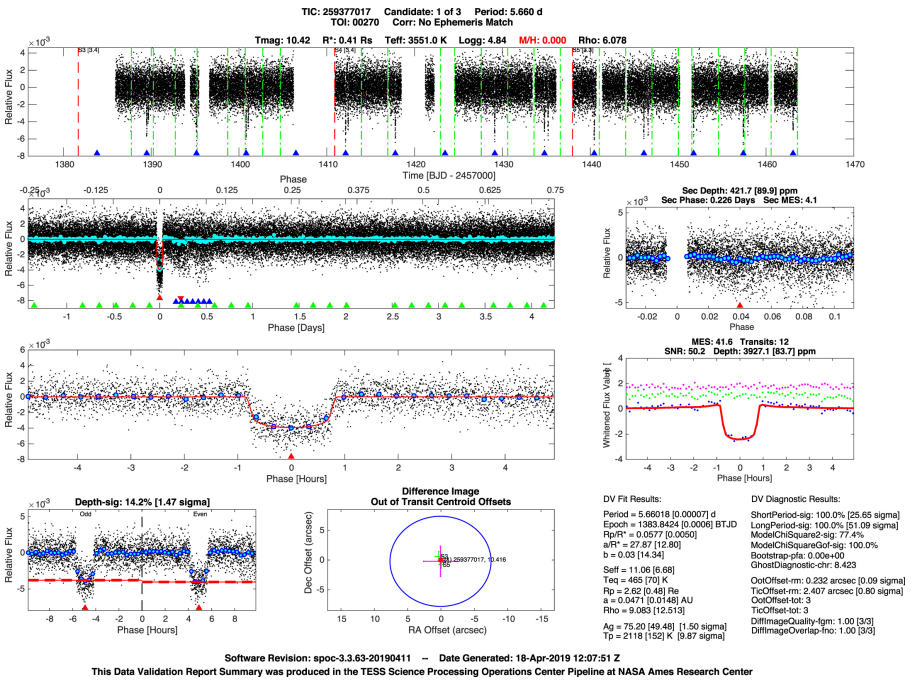

Figure 2.1: The SPOC DV summary report plots for TOI 270 b.

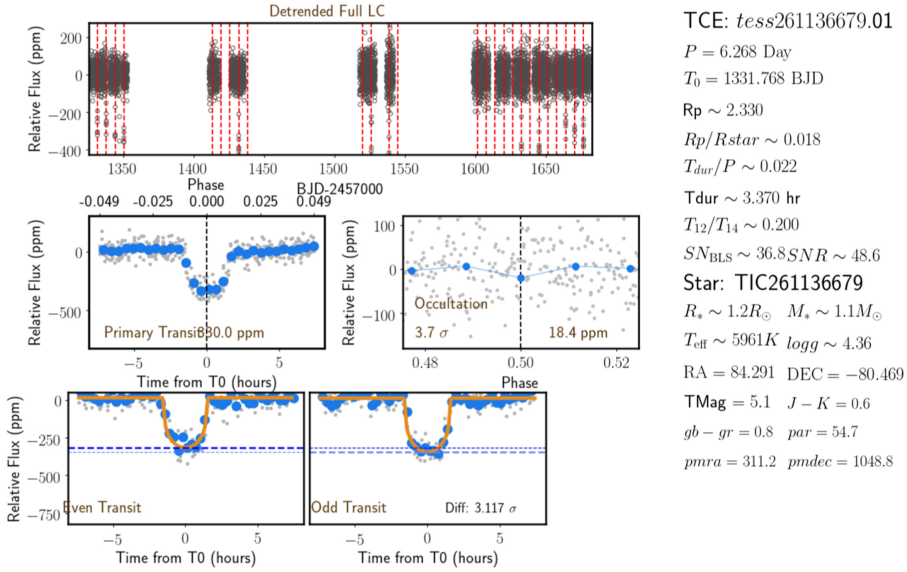

Figure 2.2: The QLP DV summary report plots for π Men c.

The online TOI catalog at ExoFOP-TESS is continuously updated to provide the most recent information to the community:

1. The TOIs that appear in several sectors accumulate more observations, which improve the determinations of period, epoch, and other parameters. The TOI catalog is therefore updated with parameters from the longest baseline of data for each TOI, with a preference for SPOC postage stamp data, largely due to its 2-minute cadence and review process as the pipeline of record.

2. The TOIs on the ExoFOP-TESS platform have updated TESS Follow-Up Observing Program

(TFOP) working group priorities as each working group makes progress with follow-up observations.

3. When TFOP identifies TOIs as false positives, their initial disposition in the TOI catalog remains unchanged (to preserve the candidate's history), but a separate TFOP working group disposition is updated on ExoFOP-TESS. The TFOP working group disposition (see table 2.1) is updated in the TOI catalog as well.

Disposition of the TOI	
TESS Disposition	TFOPWG Disposition
• CP=confirmed planet • KP=known planet • PC=planetary candidate • EB=eclipsing Binary • O=Other • IS= Instrument Systematics	• APC=ambiguous planetary candidate • CP=confirmed planet • FA=false alarm • FP=false positive • KP=known planet • PC=planetary candidate

Table 2.1: Table of Disposition find in TOI Catalog

2.2 Gaia DR3

Gaia DR3 (Gaia Collaboration et al., 2023a) is the third data release of the Gaia mission by the European Space Agency, containing a range of new data products. The most notable additions include an expanded radial velocity measurement and a comprehensive astrophysical characterization of the Gaia sources. The Gaia DR3 catalog is the result of processing raw data collected during the first 34 months of the mission, by the Gaia Data Processing and Analysis Consortium.

The release includes more than 33 million objects with new determinations of their mean radial velocities based on data collected by Gaia. For most sources with radial velocities, they provide the G_{RVS} magnitudes, and for a subset of these sources, a line-broadening parameter is given. Medium Gaia spectra are also made available to the community. In addition, the Gaia DR3 catalog includes astrophysical parameters and source class probabilities for about 470 million and 1500 million sources, respectively, including stars, galaxies, and quasars. Orbital elements and trend parameters are provided for about 800,000 astrometric, spectroscopic, and eclipsing binary stars, and there are more than 150,000 Solar System objects with preliminary orbital solutions and observations from individual epochs.

Reflectance spectra derived from epoch BP/RP spectral data are published for about 60,000 asteroids. Finally, an additional data set is provided, namely the Gaia Andromeda Photometric Survey (Evans et al., 2023), which consists of a photometric time series for all sources located in a 5.5-degree radius field centered on the Andromeda Galaxy.

Overall, Gaia DR3 contained astrometry and broadband photometry for a total of 1.8 billion objects, based on 34 months of satellite operations. Radial velocities for 7 million sources were taken from the second data release, Gaia DR2, with a small number of spurious radial velocities removed. The astrophysical information provided by Gaia DR3 is expected to unlock the full potential of Gaia's measurements (Gaia Collaboration et al., 2023b).

2.2.1 Non Single Star (NSS) Catalogue

The Gaia DR3 catalog is a significant milestone in astronomy as it contains around 800,000 solutions for orbital elements or trend parameters of astrometric, spectroscopic, and eclipsing binaries, and their various combinations. With its rich data, Gaia DR3 is expected to provide valuable insights into the analysis of stellar multiplicity and dynamical masses. The precursor to Gaia, HIPPARCOS (199,

1997) had already discovered and measured double stars, including unresolved astrometric binaries, enabling the determination of stellar masses, but only for a limited number of sources.

The new Gaia DR3 data products include also variability, radial velocities, and astrophysical parameters determined using either high-resolution (RVS) or low-resolution data (BP-RP photometers) for a vast fraction of the catalog. The DR3 analysis also includes the first analysis of unresolved binary star contents, covering typical binary classes (astrometric, spectroscopic, photometric) and presented in several tables, such as two-body orbits, astrometric or spectroscopic accelerations, and variable binaries. These tables contain the orbital or trend parameters of the binaries that have been discovered, and it offers the possibility of deriving the physical properties of individual components. Moreover, this should improve measurements of these systems in the main catalog, with better astrometric parameters or systemic radial velocity.

It is important to note that only a small portion of the binary content of the main catalog has been analyzed for DR3. Although the Gaia data analysis has made it possible to obtain a much larger multi-type catalog of binaries than previously compiled, it must be emphasized that it was a challenging task to achieve over the centuries[1]. For Gaia DR3, the handling of resolved binaries was not yet possible, so only unresolved binaries have been considered in this data release. The various types of solutions, shown in the table 2.2, that have been produced for the three methods (astrometric, photometric, and spectroscopic) are distributed in four main different tables: `nss_two_body_orbit` when the full orbital motion is known, `nss_acceleration_astro` and `nss_non_linear_spectro` when a trend is known only, and `nss_vim_fl` for variable fixed binaries. The following list summarizes the main features:

- `nss_two_body_orbit` contains non-single-star orbital models for sources compatible with an orbital two-body solution. This covers astrometric binaries, spectroscopic binaries, eclipsing binaries and certain combinations thereof.
- `nss_acceleration_astro` contains non-single-star astrometric models for sources having a non-linear proper motion which is compatible with an acceleration solution.
- `nss_non_linear_spectro` contains non-single-star orbital models for spectroscopic binaries compatible with a trend.
- `nss_vim_fl` contains non-single-star models for sources compatible with a Variability Induced Mover (VIM) solution.

solution type	table name	binary type
EclipsingBinary	nss_two_body_orbit	eclipsing
EclipsingSpectro	nss_two_body_orbit	eclipsing + spectroscopic
SB1C	nss_two_body_orbit	spectroscopic
SB2C	nss_two_body_orbit	spectroscopic
SB1	nss_two_body_orbit	spectroscopic
SB2	nss_two_body_orbit	spectroscopic
AstroSpectroSB1	nss_two_body_orbit	astrometric + spectroscopic
SecondDegreeTrendSB1	nss_non_linear_spectro	spectroscopic
FirstDegreeTrendSB1	nss_non_linear_spectro	spectroscopic
Orbital	nss_two_body_orbit	astrometric
OrbitalAlternative[Validated]	nss_two_body_orbit	astrometric
OrbitalTargetedSearch[Validated]	nss_two_body_orbit	astrometric
Acceleration9	nss_acceleration_astro	astrometric
Acceleration7	nss_acceleration_astro	astrometric
VIMF	nss_vim_fl	astrometric

Table 2.2: Definition of `nss_solution_type` in the associated NSS table.

Astrometric binaries

The motion of an unresolved binary can be described with several models, depending on its orbital period. When the period is much longer than the mission time interval, the trajectory appears like a parabolic arc. In this case, adding a constant acceleration to the single-star model is sufficient, which is what the "constant acceleration" model (also known as Acceleration7) does.

For periods that are slightly shorter than the mission time interval, the trajectory of the photocentre is still an arc, but it is necessary to include the time derivative of the acceleration. This model is then called the "variable acceleration model" (also known as Acceleration9).

When the period does not exceed the mission time interval, it is possible to calculate the orbit parameters by fitting an "orbital model".

For astrometric epoch data of low signal-to-noise ratio (SNR) orbits, such as planetary-mass or brown-dwarf companions, as well as near-equal mass binaries the solutions produced by the development unit responsible for fitting Keplerian parameters were not always well modeled in terms of acceleration or binary orbital fits of the non-single stars pipeline. This resulted in a so-called "stochastic" solution. In this stochastic solution sample, another orbital fit (OrbitalAlternative) was produced.

For Gaia DR3, an independent and targeted search was performed for significant astrometric orbital signals for a set of sources, which included host stars with known exoplanets, brown dwarfs, and stellar companions. The sources identified in this search are found with the `OrbitalTargetedSearch` pipeline[1].

Spettroscopic binaries

The RVS instrument provides spectra for the brightest stars that help to derive physical parameters and radial velocities for stars exhibiting a normal single spectrum. The RVS spectroscopic processing pipeline converts the instrumental spectra obtained at each RVS transit to proper physical spectra. The radial velocity is measured by cross-correlating the observed reduced spectra with a theoretical/synthetic spectrum computed with various stellar atmosphere models. The best-tested model provides the best radial velocity. The STA (Single Transit Analysis) pipeline performs the measurements of the single spectra. The MTA (Multiple Transit Analysis) analyses the list of good epoch radial velocities (RV) corresponding to a particular star to detect and separate variable RV sets from constant RV sets. The median of the epoch RVs of constant stars is computed and appears in the catalog. Stars with variable RVs are further considered by the pipeline and are forwarded to the NSS spectroscopic binary processing (SB1 and SB1C).

Objects presenting confirmed composite spectra are deviated from the subsequent main spectroscopic processing after the measurements of both RVs and both projected rotational velocities. This is done transit per transit. The list of objects being spectroscopically double (SB2 and SB2C) is transmitted to the NSS processing along with the two radial velocities and the two projected broadening velocities.

Sometimes, the radial velocity evolution as a function of time just exhibits a trend. This could be a transient behavior observed by chance or may correspond to a small piece of slow motion. It could also correspond to an orbital motion with a period well longer than the span of time of the observations by the satellite. The span of time is 34 months for the Gaia DR3, but it could be slightly shorter for some objects because it combines with the gaps in the scanning law. The present trend modeling is restricted to one-degree and two-degree polynomials (`FirstDegreeTrendSB1, SecondDegreeTrendSB1`) with time as the independent variable[1].

Photometric binaries

One outcome of this work for Gaia DR3 has been the identification of $\sim 2.2 \times 10^6$ eclipsing binary (EB) and ellipsoidal systems for which a number of parameters characterizing their light curves (LCs) have been calculated. These include the photometric period, the times of mid-eclipse, as well as eclipse durations and depths. A fraction of sources studied by the upstream pipelines have been

identified to fit in more than one orbital model. The aim of the combined solutions pipeline is to find the solutions that are common and to produce an updated solution in order to improve the precision. Spectroscopic binaries (all models) and astrometric binaries with orbital model (`Orbital and OrbitalAlternative`) are combined in `AstroSpectroSB1` binaries. SB1 spectroscopic binaries and eclipsing binaries are combined in `EclipsingSpectro` binaries[1].

2.3 PMa Catalog

The detection of companions from their influence on the Proper Motion (PM) of a star is based on the comparison of long-term and short-term PMs of the star. For a single star, the long-term PM determined from the positions measured at the HIPPARCOS and EDR3 epochs is the same as the short-term PM measured by each mission over a few years. However, for a binary star, the short-term PM includes the tangential component of its orbital velocity. This velocity changes over time as the star orbits its companion, causing a deviation between the short-term and long-term PMs of the star. This deviation is known as the Proper Motion Anomaly (PMa), which is an efficient and sensitive indicator to detect non-single stars, as it is a proxy for the orbital velocity of the system's photocenter around its center of mass.

Thanks to the long-time baseline between the HIPPARCOS and Gaia epochs, the PMa can now be measured with high accuracy, making it possible to detect companions with substellar mass around nearby stars (Kervella et al., 2022). In the case of an isolated, single star with no intrinsic morphological change, the motion of its photocenter is uniform and rectilinear, and the PM vector is constant in direction and norm. However, in the case of a binary system, the presence of a secondary mass causes the barycenter to shift away from the primary star, and the photocenter of the system is displaced due to the photometric contribution from the secondary.

For an ideal, unresolved binary system consisting of two identical stars with equal masses and luminosities, the positions of the barycenter and the photocenter remain the same, and no time-dependent variation of the PM vectors is detectable. However, in the general case where the luminosity ratio of the low-mass companion to that of its parent star is much smaller than the ratio of their masses, the center of mass is shifted relative to the photocenter. As both stars revolve around their center of mass, the photocenter, which is close to the geometrical center of the primary when the ratio of their masses is much smaller than 1, follows a "virtual" orbit around the barycenter (Kervella et al., 2019b).

In Figure 2.3 identifies $\mu_{\rm HG}$ as the projected velocity vector of the center of mass, while $\mu_{\rm Hip}$ and $\mu_{\rm G3}$ represent the projected velocity vector of the photocenter of the system at the HIPPARCOS and Gaia DR3 epochs, respectively (Kervella et al., 2019a). The PMa vector $\Delta\mu_{Hip/G3}$ is defined as the result of the subtraction of the long-term PM vector $\mu_{\rm HG}$ from the PM vectors $\mu_{Hip/G3}$ of the two catalogs:

$$\Delta\mu_{Hip/G3} = \mu_{Hip/G3} - \mu_{HG} \tag{2.1}$$

For nearby stars (a few tens of parsec) the PMA has a sensitivity for planet-like companions, as shown by the detection of various systems with RV planets or with planets detected in direct imaging Bonavita et al. (2022). Nevertheless, most of the TESS targets are farther away and therefore the sensitivity is for companions of greater mass.

The data used in this work taken by this catalog are:

- the SNR(Signal to Noise Ratio) of PMa, used to find stars with high PMa
- the correspondent mass of a companion for some separations (3,5,10,30 au), used to check if the PMa is due to the object found by TESS/Gaia

[1] `https://gea.esac.esa.int/archive/documentation/GDR3/Data_analysis/chap_cu4nss/`

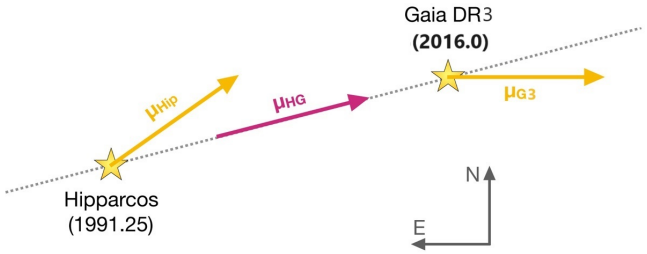

Figure 2.3: Principle of the search for a proper motion anomaly. $\mu_{\rm Hip}$ designates the HIPPARCOS proper motion vector (epoch 1991.25), $\mu_{\rm HG}$ the mean proper motion vector between the HIPPARCOS and Gaia DR3 positions, and $\mu_{\rm G3}$ is the Gaia DR3 proper motion vector (epoch 2016.0).

Data Analysis

3.1 Table TOI-NSS

I downloaded the full table of TOIs from exoFOP[1], which contained 6875 entries. In order to match this table with the TIC (TESS Input Catalog v8.2) (Stassun et al., 2018), I used the right ascension (RA) and declination (Dec) and searched for the best match within a radius of 100 arcseconds. This radius is chose to search all star in the TOI catalog with high proper motion. The (RA, DEC) coordinates in the TIC catalog, when matched with TOPCAT, are in J2000, meaning the stars are referenced to the equinox of the year 2000. Therefore, stars with significant proper motions may have shifted by a few arcseconds since then. After removing all false matches and keeping only the stars with the same TIC ID in both catalogs, I ended up with a new table containing the 6875 rows of the TOI.

I matched the previously obtained table with the Gaia DR3 catalog. Similar to the TOI-TIC match, I searched for all matches within a 100 arcsecond radius from the target position in RA and Dec. I removed all sources that did not have the same Gaia ID in the matched catalog. This resulted in a table with 6364 rows of all TOI sources with correspondence in the Gaia catalog. The approximately 500 lost stars were due to the fact that the Gaia ID I confronted was DR2 in the TIC catalog, while in the Gaia catalog it was DR3. Hence, the same stars may have different IDs. Figure 3.1 shows the position in the CMD of the TOIs (in red) with respect to a sample of star randomly extracted from the Gaia DR3 catalog (in gray)
Figure 3.2 shows the distribution of the Gmag (left panel) and of the distance (right panel) of the TOIs. The mean magnitude is 4.416 ± 2.16 G_{mag} while the mean distance is 470.699 ± 584.353 pc.

Finally, I downloaded the NSS catalogs from the Gaia archive to find all stars with the same Gaia ID as in our TESS-Gaia table. The new obtained table (3.1) contained 322 rows with TESS and TFOPWG Disposition, the NSS solution from Gaia, and the orbital period calculated both in Gaia and TESS. Figure 3.3 shows the positions in the CMD of the objects in this last table with respect to stars taken from the TESS-Gaia table. Figure 3.4 shows the Gmag (left panel) and distance (right panel) distributions of the TOI-NSS stars. The mean magnitude is 3.801 ± 1.44 G_{mag} while the mean distance is 387.291 ± 430.839 pc.

[1] last update to 25/10/2023

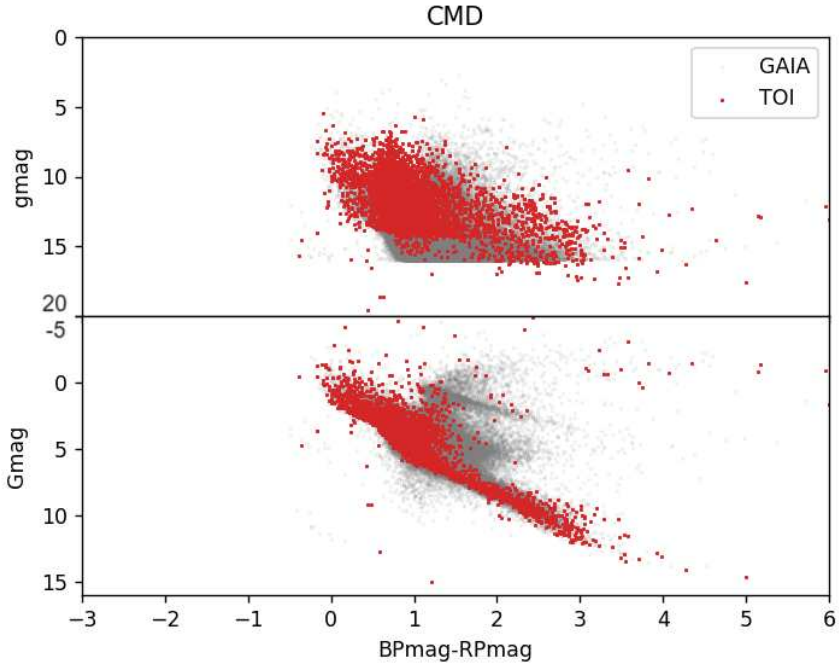

Figure 3.1: Color-Magnitude Diagram of TOIs (in red) and randomly chosen stars in the Gaia DR3 catalog (in grey)

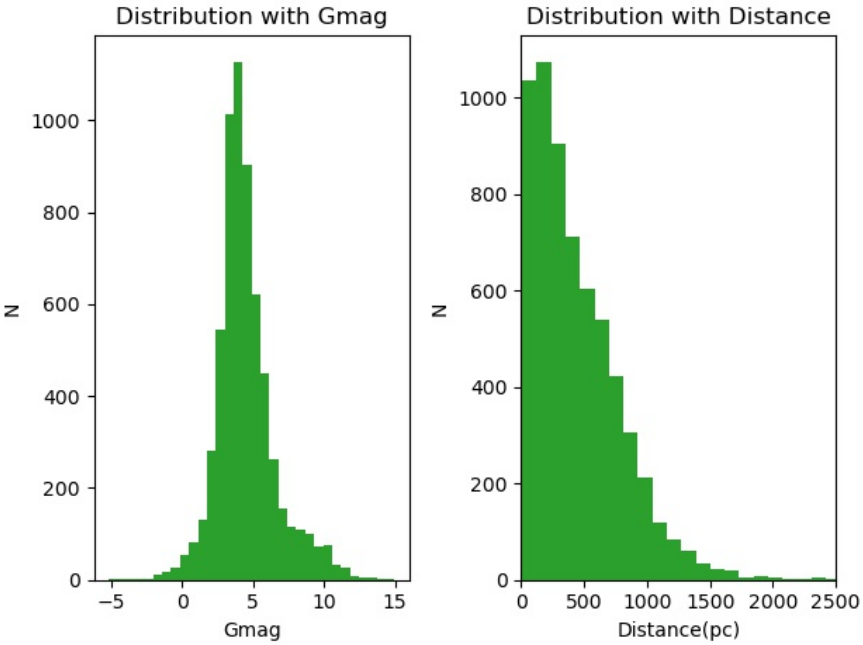

Figure 3.2: Left plot: Distribution of TOI star in function of Gaia Magnitude. Right plot: Distribution of TOI star in function of Distance

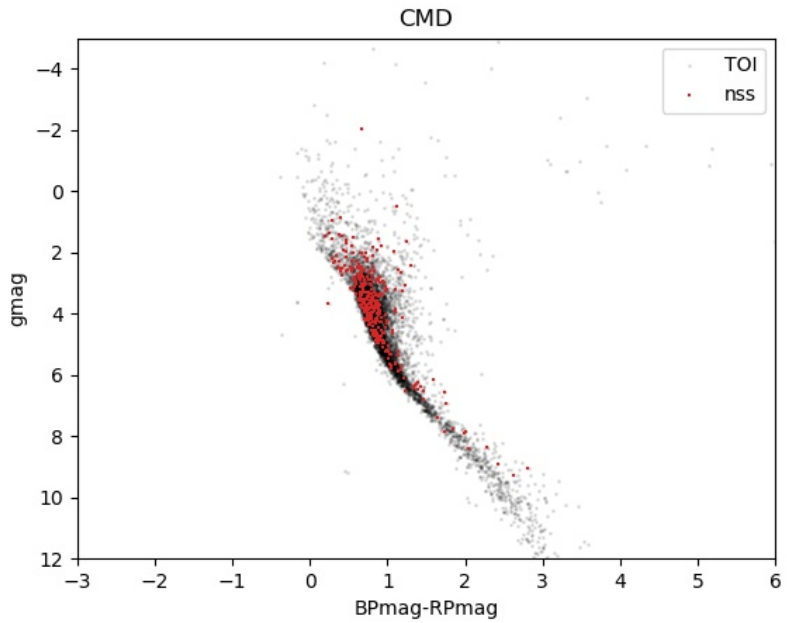

Figure 3.3: Color-Magnitude Diagram of TOIs star (in black) and Gaia non-single stars (in red)

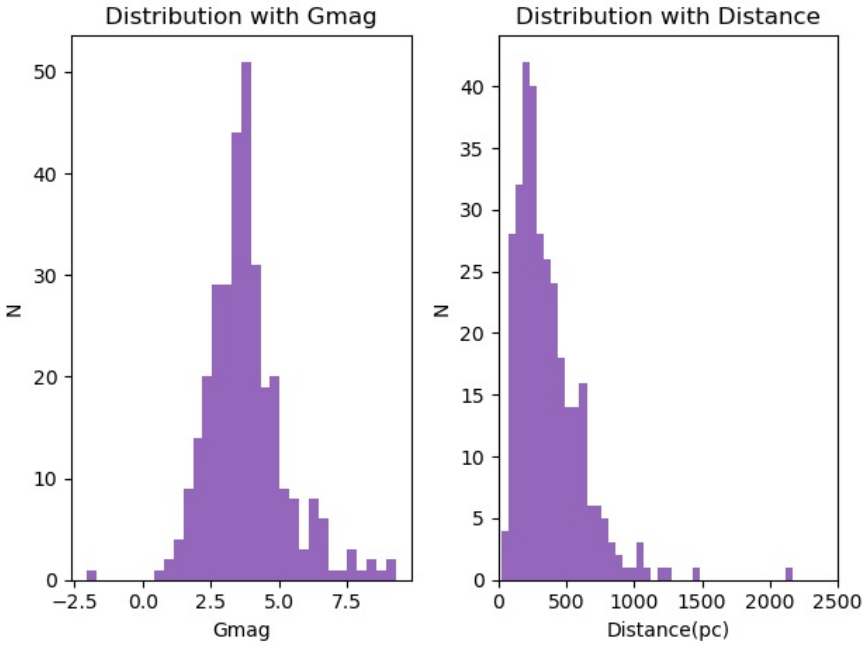

Figure 3.4: Left panel: Distribution of the Gaia magnitudes of the object in the TOI-NSS catalog. Right panel: Distribution of the distances of the stars in the TOI-NSS catalog

TESS Disposition	TFOPWG Disposition	nss_solution_type	TIC
CP	CP	SB1	186812530, 260128333
EB	APC	Acceleration9	255704097
		SB1	1449640, 102195674
	FP	Acceleration7	11
		Acceleration7, FirstDegreeTrendSB1	341729521
		Acceleration7, SB1	320525204, 1400770435
		Acceleration9	367102581, 453464017
		AstroSpectroSB1	300810086, 309402106, 131419878
		Orbital	219164808
		OrbitalTargetedSearch	144440290, 219205407
		SB1	18
		SB2	128463355, 97158538, 279212407
		SB2C	289988797, 258557847
		SecondDegreeTrendSB1	143526444
IS	FA	AstroSpectroSB1	49687222
KP	KP	OrbitalTargetedSearch	315002523, 374530847
		SB1	100100827
O	FP	Orbital	164150539
		OrbitalTargetedSearch	290348382
PC	APC	Acceleration7	7
		Acceleration9	434105231 165885558
		Acceleration9, FirstDegreeTrendSB1	116483734
		Acceleration9, SB1	270507305
		Acceleration9, SecondDegreeTrendSB1	128790976
		AstroSpectroSB1	373844472 136274063 281100535
		Orbital	10
		SB1	54
		SB2	134404603 44797824
	CP	SB1	393940766 270604417
	FA	Acceleration7	459903429 459952217
	FP	Acceleration7	12
		Acceleration9	6
		Acceleration9, FirstDegreeTrendSB1	136971594
		AstroSpectroSB1	5
		FirstDegreeTrendSB1	260849386
		Orbital	6
		OrbitalTargetedSearch	118021229
		OrbitalTargetedSearchValidated	70887357
		SB1	33
		SB2	147576037 41330864
		Acceleration7	21
	PC	Acceleration7, SecondDegreeTrendSB1	269558487
		Acceleration9	9
		Acceleration9, SB1	87090944 219697927
		Acceleration9, SecondDegreeTrendSB1	239198720
		AstroSpectroSB1	9
		FirstDegreeTrendSB1	77527511 155044736
		Orbital	2
		OrbitalTargetedSearch	167418903 260130483
		OrbitalTargetedSearchValidated	47316976 201292545 183593642
		SB1	50
		SB2	419419534 384744828
		SB2C	453105377
		SecondDegreeTrendSB1	14091704 160487753 374200604

Table 3.1: Number of TIC ID groups by TESS Disposition, TFOPWG Disposition, and non-single star solution from Gaia. The ID of the individual object is displayed only if the number of objects per group is < 3. Otherwise, it is reported the total number of objects in the group. See 2.1 for the definition of acronyms

3.2 Table TOI-PMa

By using the table of proper motion anomalies created by Kervella et al. (2022), I searched all objects with the same Gaia ID of the table TOI-Gaia. The table by Kervella et al. (2022) gives also the mass of the probable companion responsible for the PMa assuming an orbit of 3,5,10 or 30 au. They assume that the companion's orbit is circular, so it can be used as a lower limit. In this analysis, I considered a TOI as an object with probable additional companions if it has a snrPMa > 3.0. The final table obtained (3.2) has 66 entries.

Gaia	TOI	TESS	TFOPWG	Stellar Mass	Period	PMaRA	PMaDE	snrPMa	RUWE
4621607053580909568	128.01	PC	PC	1.13	4.9404783	0.046	-0.178	3.87	0.935
4623036865373793408	144.01	CP	CP	1.1	6.267832	0.165	-0.586	7.94	0.814
6531037981670835584	222.01	EB	FP	1.02	0.0	0.119	0.141	3.26	1.779
4728513943538448512	179.01	PC	CP	0.85	4.1374379166706	-0.407	-0.032	11.39	0.994
6387058411482257536	200.01	CP	CP	0.94	8.1382243427785	-0.008	0.164	4.65	0.913
4767547667180525696	201.01	CP	CP	1.31	52.978141944942	-0.179	-0.235	5.85	1.098
4767547667180525696	201.02	PC	PC	1.31	5.8492655	-0.179	-0.235	5.85	1.098
4784439709132505344	271.01	PC	APC	1.15	2.4759733064038	13.096	10.812	75.81	8.466
4917040330405933824	381.01	EB	FP	1.13	4.89577	-0.088	0.059	3.16	1.046
5167486711022397696	394.01	EB	APC	1.254	0.39149	4.044	-9.515	85.71	3.181
5068777809824976256	402.01	CP	CP	0.88	4.7559736792878	-0.774	-0.451	21.79	0.891
5068777809824976256	402.02	CP	CP	0.88	17.180721359013	-0.774	-0.451	21.79	0.891
5153091836072107136	455.01	CP	CP	0.249439	5.3587759524822	-7.046	8.977	18.84	1.073
5508330367833229824	510.01	PC	APC	1.07	1.3523942	5.783	1.905	95.23	2.432
3825847092208384640	635.01	PC	FA	1.05	0.493379	-0.357	-0.047	6.85	1.031
3574891599052022144	680.01	PC	APC	1.102	0.43356904747084	0.096	2.028	19.42	3.711
5412250540681250560	731.01	CP	CP	0.454797	0.3219233	-0.09	0.465	3.81	0.972
3341977210515243648	896.01	PC	FA	1.39	3.52985	1.374	-4.036	21.63	1.395
5806162435437141888	909.01	EB	FP	1.13	3.9043855	-0.078	-0.113	3.93	1.036
3144707232307362688	1012.01	PC	APC	2.251	0.884182	0.205	0.802	5.51	3.694
6422184406377527936	1114.01	PC	APC	0.0	2.4887726	0.164	0.195	3.74	1.577
6356417496318028800	1099.01	PC	PC	0.78	6.441006	-0.323	0.375	11.97	1.156
1625373404725030528	1131.01	PC	PC	0.985	0.5860337	1.458	0.546	5.52	12.514
2086512227851023872	1144.01	KP	KP	0.77	4.8878053328095	-0.223	-0.02	4.33	0.948
6685705320278556544	1124.01	PC	APC	1.42	3.5187707	15.929	8.825	53.41	11.766
2033123654092592384	1151.01	KP	KP	2.282	3.4741010863105	-0.114	-0.193	6.24	0.946
5337558310677264768	1204.01	PC	PC	1.1	1.3812379548661	0.684	0.495	20.05	0.979
1959980910760446720	1323.01	EB	FP	2.273	2.03905	0.185	0.023	4.82	1.018
1985325925092948096	1398.01	PC	APC	2.45	6.5560894	-0.121	-0.095	3.12	1.409
1436764902379398144	1418.01	V	FA	2.106	0.6763235099057	0.258	-1.028	27.93	0.921
545560867790611072	1573.01	KP	KP	1.1	21.2169065	0.087	0.078	3.16	0.901
398891857800597120	1552.01	PC	FP	2.32	7.57193	0.407	-0.743	15.34	0.993
3456154930349411200	1665.01	PC	FP	0.0	1.76406	0.134	0.387	8.07	0.944
475384301928844288	1684.01	PC	PC	0.0	1.1549928	-0.772	-10.212	203.17	1.58
1036060018624478464	1719.01	PC	PC	1.14	2.7552506	1.62	0.36	7.77	10.378
3938542739088394240	1831.01	PC	APC	1.488	0.55532443820971	-0.257	0.176	4.95	0.965
1458687549330917376	1837.01	PC	APC	1.092	5.8182238767198	1.505	0.264	11.38	7.368
644224345413418880	1898.01	PC	PC	1.24	45.5221234	0.13	-0.116	3.83	0.949
6102575170962644480	1946.01	EB	FP	1.54	10.8458712	-3.352	-0.195	18.32	5.879
6089980982526907648	1976.01	PC	APC	0.0	7.6943096	0.521	0.391	3.27	5.229
5312673922948554880	1986.01	EB	APC	0.0	7.5043829155643	0.465	1.381	4.35	6.768
2791782794564103808	2009.01	PC	PC	0.76	1071.0898448029	0.159	0.03	3.02	1.211
1271484768305363584	2017.01	PC	FP	0.0	5.4983034131714	-0.407	0.404	3.93	7.115
1628229527914028544	2069.01	PC	PC	0.9	5.9214228765562	-0.104	0.008	3.27	0.944
1330060219481975424	2118.01	PC	FP	1.283	2.34483	0.047	-2.792	29.17	4.373
1428824435562332672	2082.01	PC	PC	1.11	30.200336	-0.119	-0.034	3.17	0.871
1936088042049360896	2434.01	PC	APC	2.397	1.3808137669467	0.056	0.146	3.19	1.375
3511580658668406528	4175.01	PC	PC	0.0	2.1632835	-0.61	0.013	9.88	1.342
3282743461108145024	4314.01	PC	FA	1.851	73.580981995885	-1.231	-1.435	27.79	2.235
6632318361397624960	4399.01	PC	CP	1.1	7.7121208408771	0.141	-0.174	5.82	1.07
1827242816201846144	4470.01	KP	KP	0.84	2.2185748039122	-0.081	0.066	3.94	0.951
3402980516507429888	4603.01	PC	CP	1.176	7.2454963	0.308	0.179	5.6	0.999
5822482108594169472	4568.01	PC	PC	1.07	14.0063765	-1.081	0.784	12.16	6.303
666427539629086976	5140.01	PC	PC	1.13	15.611363326614	-0.114	0.053	3.05	0.976
3418915433588729856	5079.01	PC	FP	0.86	1.4923632	0.341	-0.131	3.58	0.977
108165903787108352	5099.01	PC	PC	1.45	14.450540107369	0.174	0.114	3.23	0.933
3913486896315719424	5521.01	PC	PC	1.274	18.514853794763	-0.282	-0.654	8.93	1.676
1667489892685370624	5383.01	PC	PC	1.45	2.8114961	-0.092	0.235	3.5	2.531
623779716969345920	5394.01	PC	PC	1.1	15.1935123	0.06	-0.193	3.29	1.855
1814257343328666624	5811.01	PC	PC	0.0	6.2571822	3.499	0.072	37.67	1.842
1887706880428475520	5962.01	PC	FP	0.934	1.9261183169147	0.116	0.25	3.11	0.977
2286390900469275136	6246.01	PC	PC	1.795	6.7786403337287	-0.144	0.973	25.03	1.076
5746169949987879680	6260.01	PC	PC	1.812	2.3898191	-0.011	-12.172	77.69	4.512
5452634262730082176	6709.01	PC	PC	0.78	2.3477335829256	0.103	-0.157	3.54	0.959
4767020077694168576	6691.01	PC	PC	1.4	0.0	0.122	-0.119	4.01	1.263
3494677900774838144	6713.01	PC	PC	0.81	2.1538048644427	0.15	-0.022	3.55	0.981

Table 3.2: Table of all TOI objects with a correspondence in the PMa catalog by Krevella et al. (2022)

3.3 TOIs Analysis

In this section, I analyze the objects that have been obtained in the previous tables. The equations used in this work are an approximation for the cases where the mass of the primary star is much bigger than the mass of the companion. I calculated, when possible, the mass using the following formula. :

$$M_{planet} = \frac{k}{203} \cdot (P_{Gaia})^{\frac{1}{3}} (M_*)^{\frac{2}{3}} \sqrt{1 - e^2} \tag{3.1}$$

where k $[m/s]$ is the semi-amplitude of the radial velocity curve related to the first component (the primary star). The first component is either the only visible one (concerns SB1, SB1C solutions) or is expected to be any of the two stars (concerns SB2, SB2C solutions). $P_{Gaia}[days]$ is the period of the companion and e is the eccentricity of the orbit, both measured by Gaia. $M_*[M_\odot]$ is the mass of the star, retrieved from the TIC catalog. The associated errors have been calculated with the error propagation formula:

$$\sigma_{M_{planet}} = \sqrt{\left(\frac{\partial M_{planet}}{\partial P_{Gaia}}\sigma_{P_{Gaia}}\right)^2 + \left(\frac{\partial M_{planet}}{\partial k}\sigma_k\right)^2 + \left(\frac{\partial M_{planet}}{\partial M_*}\sigma_{M_*}\right)^2 + \left(\frac{\partial M_{planet}}{\partial e}\sigma_e\right)^2} \tag{3.2}$$

To calculate the semi-major axis (a) I use Kepler's third low:

$$a^3 = \frac{P^2 G M_*}{4\pi^2} \tag{3.3}$$

where P is the period found by TESS (or Gaia), G is the gravitational constant and M_* is the mass of the star, retrieved from the TIC catalog. The associated error is:

$$\sigma_a = \sqrt{\left(\frac{\partial M_{planet}}{\partial P}\sigma_P\right)^2 + \left(\frac{\partial M_{planet}}{\partial M_*}\sigma_{M_*}\right)^2} \tag{3.4}$$

If I have both planetary mass and Radius, the density ($\frac{M}{4/3\pi R^3}$) is derived. For each object, I report the information retrieved from the literature and those obtained from TOI and Gaia catalogs such as Stellar and Planet Parameters.

Period Analysis

If I compare the period measured by TESS and Gaia it can be seen that most of the points lie along 2:1, 1:1 and 1:2 ratios between periods (Fig. 3.5). All the objects found with this relation have the spectroscopic binary model as `nss_solution_type`. 131 objects out of 322 are following these relationships:

- 115 objects have the same period observed in the Gaia and TESS catalogs
- 12 objects have a Gaia period that is twice the TESS period.
- 4 objects have a Gaia period that is half of the TESS period.

Selecting all the candidates that have either Planet Candidate (PC) or Ambiguous Planet Candidate (APC) status in TFOPWG Disposition (Table 3.3) I found 84 candidates. For these objects, it is evident that every computed candidate mass exceeds the lower bound of BD. Of the remaining 47 TOIs, 44 are FPs, with mass above 0.07 $M_\odot$ and 3 are CPs:

- 148.01 is a stellar companion of 86.72 M_J
- 185.01, alias WASP-18b, is a known planet of 10.49 M_J
- 503.01 is a brown dwarf of 52.49 M_J

TOI	TESS P [days]	Semi-major axis [AU]	Gaia P [days]	Semi-major axis [AU]	planet mass [M_jup]	planet mass error	companion mass [M_jup]	companion mass error
121.01	14.76367	0.123	14.78109	0.123	111.73	10.5	111.77	10.5
162.01	7.76469	0.076	7.76531	0.076	128.02	16.58	128.03	16.58
446.01	3.5018	0.049	3.50176	0.049	153.0	18.85	153.0	18.85
459.01	4.42913	0.058	4.42917	0.058	516.42	56.69	516.42	56.69
668.01	4.37873	0.056	4.37836	0.056	160.45	16.4	160.44	16.4
759.01	4.21357	0.055	4.21329	0.055	106.44	15.01	106.44	15.01
764.01	5.63167	0.07	5.63079	0.07	243.69	30.39	243.68	30.39
901.01	3.23084	0.046	3.231	0.046	417.66	41.77	417.66	41.77
924.01	12.12739	0.104	12.12195	0.104	258.71	26.34	258.67	26.33
948.01	12.7009	0.108	12.71088	0.108	375.07	31.52	375.17	31.53
1059.01	9.44965	0.084	9.44988	0.084	203.05	16.49	203.06	16.49
1115.01	4.45199	0.06	4.45273	0.06	500.11	65.04	500.14	65.04
1119.01	10.95663	0.106	10.95889	0.106	491.81	53.44	491.85	53.44
1153.01	6.03608	0.077	6.03613	0.077	556.97	69.49	556.98	69.49
1371.01	5.00956	0.065	5.00973	0.065	172.86	19.94	172.86	19.94
1455.01	3.62314	0.051	3.62345	0.051	143.37	17.13	143.38	17.14
1461.01	3.56868	0.047	3.56774	0.047	162.35	16.93	162.33	16.92
1553.01	5.93821	0.073	5.93844	0.073	345.09	42.39	345.1	42.39
1608.01	2.47273	0.037	2.47284	0.037	80.3	7.27	80.3	7.27
1822.01	9.61366	0.088	9.60871	0.088	94.54	9.33	94.52	9.33
1951.01	4.8294	0.062	4.82955	0.062	131.32	17.25	131.32	17.25
1974.01	5.43822	0.06	5.43772	0.06	359.53	30.04	359.52	30.04
2038.01	3.73212	0.052	3.73216	0.052	119.89	18.34	119.89	18.34
2157.01	8.4249	0.082	8.42351	0.082	137.02	12.34	137.02	12.34
2159.01	10.05097	0.093	10.05146	0.093	114.86	10.75	114.87	10.75
2349.01	11.57385	0.101	11.56211	0.101	149.06	16.44	149.01	16.43
2366.01	17.18699	0.136	17.17497	0.136	300.02	27.92	299.95	27.91
2469.01	2.37675	0.04	2.37813	0.04	164.15	23.23	164.18	23.24
2492.01	10.10114	0.101	10.09911	0.101	162.3	41.35	162.29	41.34
2533.01	6.68579	0.073	6.69241	0.073	74.67	13.19	74.69	13.2
2598.01	5.73436	0.055	5.73382	0.055	342.0	28.97	341.99	28.97
2606.01	1.45092	0.028	1.4508	0.028	123.14	21.23	123.14	21.23
2819.01	4.39055	0.055	4.39132	0.055	451.45	43.08	451.48	43.09
3006.01	8.61346	0.092	8.61119	0.092	636.07	74.53	636.01	74.53
3010.01	9.55377	0.09	9.54298	0.089	190.29	24.92	190.22	24.91
3148.01	4.28144		4.28108					
3155.01	4.64922	0.052	4.64947	0.052	87.07	7.72	87.07	7.72
3241.01	6.83809	0.072	6.83559	0.072	155.85	15.15	155.83	15.15
3260.01	11.45201	0.105	11.45074	0.105	282.75	32.19	282.74	32.19
3298.01	3.05379	0.043	3.05342	0.043	324.03	34.5	324.02	34.5
3389.01	1.68015	0.029	1.64171	0.029	277.51	26.83	275.38	26.63
3501.01	15.35025	0.125	15.34617	0.125	181.03	16.47	181.02	16.47
3502.01	3.44629	0.055	3.44688	0.055	263.03	43.53	263.05	43.53
3542.01	4.20219	0.057	4.20558	0.057	130.14	16.8	130.18	16.81
3756.01	4.42367	0.055	4.42384	0.055	487.49	45.75	487.49	45.75
3904.01	10.16148	0.098	10.15982	0.098	442.61	44.11	442.58	44.11
4338.01	7.49978	0.072	7.49949	0.072	253.98	22.48	253.98	22.48
4400.01	7.06731	0.072	7.06131	0.072	135.57	17.05	135.53	17.04
4462.01	4.9133	0.058	4.91455	0.058	85.08	8.33	85.09	8.33
4657.01	8.11295	0.084	8.11076	0.084	476.62	47.54	476.58	47.53
4792.01	8.44817	0.082	8.44816	0.082	341.28	27.99	341.28	27.99
4807.01	17.68686	0.119	17.68939	0.119	231.42	35.53	231.44	35.53
4973.01	7.94863	0.079	7.94833	0.079	233.05	19.94	233.04	19.94
5103.01	4.98987	0.061	4.98999	0.061	564.0	58.31	564.0	58.31
5149.01	27.3715	0.182	27.3883	0.182	123.96	17.15	123.99	17.16
5156.01	22.85229	0.161	22.85312	0.161	189.12	18.26	189.12	18.26
5197.01	20.57734	0.139	20.57286	0.139	319.87	27.23	319.84	27.23
5200.01	17.4373	0.145	17.43558	0.145	438.92	47.26	438.91	47.26
5307.01	5.29763	0.051	5.29846	0.051	411.54	36.16	411.56	36.16
5372.01	11.62708	0.102	11.63028	0.102	568.7	78.84	568.76	78.84
5379.01	12.74265	0.116	12.74426	0.116	417.62	44.28	417.64	44.28
5394.01	15.19351	0.124	15.19502	0.124	341.06	28.11	341.07	28.11
5427.01	5.23742	0.061	5.2345	0.061	69.84	11.02	69.83	11.02
5475.01	10.0532	0.101	10.05227	0.101	640.51	75.93	640.49	75.93
5547.01	19.6305	0.141	19.63351	0.141	312.35	41.2	312.37	41.2
5677.01	3.84802	0.051	3.84803	0.051	267.98	26.06	267.98	26.06
5761.01	19.54221	0.137	19.54594	0.137	434.08	37.74	434.11	37.74
5860.01	5.24989	0.061	5.2484	0.061	242.29	49.91	242.27	49.91
5882.01	7.14877	0.073	7.15108	0.073	22.62	3.33	22.62	3.33
6111.01	5.83403	0.064	5.83283	0.064	519.14	48.15	519.1	48.15
6117.01	9.86631	0.095	9.86148	0.095	78.32	12.73	78.31	12.73
6133.01	3.65343	0.05	3.65272	0.05	171.27	19.83	171.26	19.82
6207.01	9.77124	0.087	9.76641	0.087	120.63	13.66	120.61	13.66
6218.01	5.15702	0.052	5.15542	0.052	63.97	7.31	63.97	7.31
6568.01	17.43681	0.142	17.43205	0.142	125.69	15.11	125.68	15.11
6611.01	6.55687	0.072	6.56902	0.072	113.22	15.59	113.29	15.6
865.01	0.74558	0.016	1.49117	0.025	461.24	38.43	581.12	48.42
2544.01	10.53058	0.098	21.05714	0.155	344.39	30.92	433.87	38.95
3191.01	4.43679	0.058	8.87867	0.092	611.44	69.47	770.51	87.55
3243.01	2.05191		4.05546					
4383.01	3.04213	0.046	6.08399	0.072	786.37	87.1	990.75	109.73
1698.01	17.04198		8.52111					
2482.01	14.93156		7.668					
4978.01	4.71903	0.06	2.20144	0.036	250.54	34.12	194.31	26.46

Table 3.3: Table of PC/APC with period ratio between Gaia and TESS equal to 1,2 or 0.5. The highlighted row are objects in the BD regime

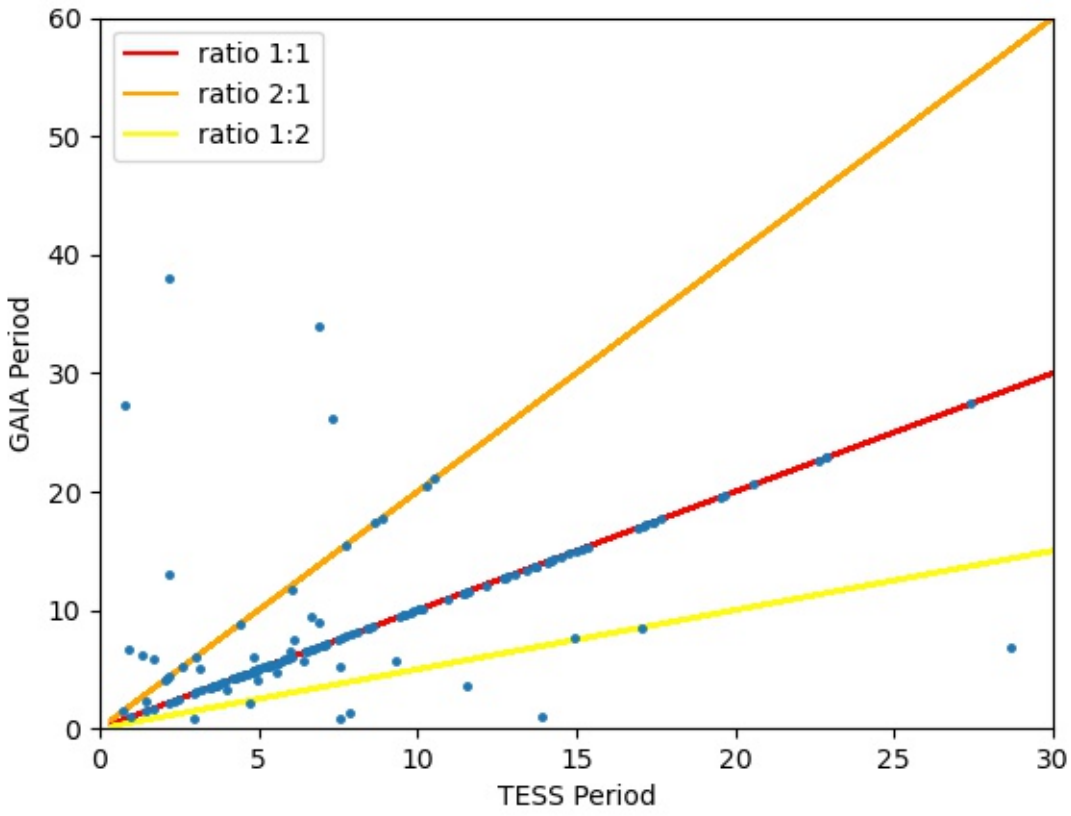

Figure 3.5: Relation Gaia-TESS period: the red line represents an equal period between Gaia/TESS, the yellow line Gaia/TESS=0.5 and the orange line Gaia/TESS=2

3.3.1 Acceleration Analysis

If I search in the TOI-NSS table I find 84 candidates with Acceleration7 or Acceleration8 in the `nss_solution_type`(Tab. 3.4. For these candidates:

- 37 have FP as TFOPWG disposition
- 47 have PC/APC as TFOPWG disposition

The acceleration projected on the sky, Γ, can be calculated with the formula:

$$\Gamma = \frac{\sqrt{g_\alpha^2 + g_\delta^2}}{\varpi} \tag{3.5}$$

When g_α and g_δ are the equatorial coordinates of the acceleration in mas/yr^2 and ϖ is the parallax in mas, Γ is in AU/yr^2. If it is assumed that the distance between the components is approximately equal to the semi-major axis of the orbit of one component around the other, then Γ is approximately:

$$\Gamma \sim 4\pi^2 \frac{M_1^{1/3}}{P_{yr}^{3/4}} \left(\frac{q}{1+q}\right)^{2/3} \tag{3.6}$$

where P is the period, M_1 is the mass of the brightest component and q is the ratio between the mass of the other component and M_1. For these objects, it is not possible to retrieve the mass because the TESS period can not be compared with the acceleration parameter measured by Gaia.

TOI	TESS Disposition	TFOPWG Disposition	period	Period (days)	accel_ra	accel_dec	parallax
164.01	EB	FP	NaN	7.318980	3.231008	-2.191525	2.975472
171.01	PC	PC	NaN	1.238603	-0.807715	-1.674655	3.884384
171.02	PC	FP	NaN	1.813577	-0.807715	-1.674655	3.884384
217.01	EB	FP	NaN	3.138604	-4.064068	0.821398	7.026729
271.01	PC	APC	NaN	2.475973	-5.975081	-0.991836	9.864051
311.01	PC	APC	NaN	0.796299	-0.393836	3.560524	4.423568
363.01	PC	APC	NaN	8.223880	-2.449176	-0.316790	2.168709
510.01	PC	APC	NaN	1.352394	1.159849	-1.360234	10.733507
827.01	PC	APC	978.014792	1.228244	-1.193757	0.145179	2.890943
855.01	PC	PC	NaN	1.830116	-1.287662	-1.935725	3.180801
877.01	EB	APC	NaN	6.014943	-1.064472	0.956368	2.020099
918.01	PC	FP	NaN	1.114007	2.588308	0.623317	1.818923
928.01	EB	FP	NaN	30.579080	1.593716	0.217595	3.252793
997.01	EB	FP	NaN	8.413486	0.707935	0.411630	8.824320
1120.01	EB	FP	NaN	1.662260	2.828427	-0.272567	2.180900
1124.01	PC	APC	NaN	3.518771	3.746569	-7.601665	13.051148
1140.01	EB	FP	13.743000	13.742953	-0.625777	1.213492	8.223231
1175.01	EB	FP	NaN	7.502271	0.496684	-0.948017	4.647891
1254.01	PC	PC	NaN	1.018011	-0.323164	-1.226145	5.033186
1309.01	PC	FP	NaN	1.498610	1.788142	0.896772	1.431731
1344.01	EB	FP	13.743000	13.743177	-0.625777	1.213492	8.223231
1348.01	PC	FP	NaN	2.140560	2.560593	2.095179	9.741100
1360.01	PC	FP	NaN	0.709020	0.792930	-0.699821	1.872342
1367.01	EB	FP	NaN	2.088113	-0.067294	-0.862273	5.061155
1368.01	PC	FP	NaN	1.255620	5.345464	1.106222	6.272848
1378.01	PC	APC	NaN	5.778532	-0.592369	1.041451	1.731688
1392.01	PC	FP	NaN	2.868760	-0.066322	0.977684	1.669003
1412.01	PC	APC	NaN	4.731977	8.572850	-3.543585	12.350262
1429.01	PC	FP	NaN	0.641256	-1.782501	-0.342830	2.312686
1520.01	PC	PC	NaN	6.146173	1.077363	0.872330	5.097327
1522.01	EB	FP	NaN	2.979859	-2.424161	-6.506494	3.667284
1546.01	PC	PC	NaN	1.133450	3.457529	-6.448050	4.210759
1556.01	EB	FP	NaN	1.441270	0.080028	0.966630	3.179844
1570.01	PC	FP	NaN	1.746260	-2.473704	2.881548	3.368740
1587.01	EB	FP	NaN	12.534303	-1.234026	0.800420	1.808210
1671.01	PC	FA	NaN	8.136640	0.370156	0.986148	4.611795
1677.01	PC	PC	1231.093370	0.643581	6.938013	-0.598846	5.486831
1684.01	PC	PC	NaN	1.154993	1.694328	-0.132165	11.475292
1946.01	EB	FP	NaN	10.845871	1.476293	-3.799012	3.948047
1993.01	EB	FP	NaN	3.941690	-0.378532	-2.836360	3.164431
2027.01	PC	FP	NaN	1.463290	-1.642547	-2.333121	3.791546
2042.01	PC	FP	NaN	2.418720	-3.260000	0.902019	1.931952
2118.01	PC	FP	NaN	2.344830	1.888571	0.391493	5.157877
2315.01	PC	APC	NaN	1.440823	1.027969	-0.440173	3.339743
2352.01	PC	PC	NaN	1.680446	1.415193	-0.488174	4.343733
2354.01	EB	FP	NaN	0.510990	-1.462254	1.021885	1.860910
2444.01	PC	APC	NaN	1.647389	2.467092	-0.737983	5.580942
2496.01	PC	PC	NaN	1.574683	0.299528	1.986223	5.087983
2510.01	EB	FP	NaN	1.978515	-0.830137	-3.670951	4.893645
2551.01	PC	PC	NaN	5.436841	-1.608122	-0.384912	1.298417
2708.01	PC	FP	NaN	2.354017	-0.084971	1.143660	1.144472
2922.01	PC	PC	NaN	1.360522	-0.065261	0.956439	2.688274
3056.01	PC	PC	NaN	1.809291	0.194083	-0.999969	0.825283
3279.01	PC	PC	NaN	0.419136	0.676947	-1.050105	1.636579
3302.01	PC	PC	NaN	1.557025	-1.106246	2.610657	1.640838
3357.01	PC	FP	NaN	2.653578	-0.733155	1.129173	1.615045
3375.01	PC	FP	NaN	1.236832	1.982931	-1.409769	1.397955
3792.01	PC	PC	NaN	0.772907	-1.304443	2.853966	1.359668
3844.01	PC	APC	NaN	0.896271	1.330802	-3.569912	1.808598
3880.01	PC	PC	NaN	2.161482	-2.036909	-2.786593	3.361844
3979.01	PC	FP	NaN	2.041659	0.694809	0.444136	1.147361
4037.01	PC	FP	NaN	4.725713	-0.164705	-0.113377	1.533574
4238.01	PC	PC	NaN	1.273224	2.506916	-0.391512	2.601758
4314.01	PC	FA	NaN	73.580982	2.136795	0.779655	6.482197
4346.01	PC	FP	NaN	3.907712	-0.908072	-0.583037	7.585817
4432.01	PC	PC	NaN	3.041339	1.456932	6.365259	4.691168
4505.01	PC	PC	NaN	19.473548	-0.583226	0.795611	2.326096
4555.01	PC	PC	NaN	522.627268	1.897130	-0.344681	10.354535
4614.01	PC	PC	NaN	13.833889	16.175387	-2.494228	9.881556
4879.01	PC	PC	NaN	5.376311	-0.655845	1.452843	1.136859
4967.01	PC	PC	NaN	0.597937	-1.274714	1.207691	1.094260
5013.01	PC	PC	NaN	8.989491	0.689005	0.960422	0.771598
5364.01	PC	PC	NaN	1.446688	2.343290	-1.795659	1.568469
5443.01	PC	PC	NaN	1.675766	1.720637	-0.514520	1.220435
5485.01	PC	PC	NaN	2.584530	0.995979	-1.010592	1.360148
5544.01	PC	PC	NaN	4.205074	0.797022	-2.813001	8.907729
5563.01	PC	PC	NaN	NaN	-0.321792	0.321646	4.705142
5702.01	PC	PC	NaN	3.129132	-0.367056	-1.156042	4.451911
5784.01	PC	FP	NaN	8.680019	-0.274801	3.459068	3.109081
6053.01	PC	APC	NaN	2.211828	3.749760	0.834949	3.086930
6066.01	PC	PC	1143.984296	1.826760	0.398656	2.662857	6.325025
6077.01	PC	PC	NaN	2.211110	-1.492612	-0.190187	7.938310
6142.01	PC	PC	NaN	4.956481	-1.092990	0.133465	1.885846
6226.01	PC	PC	NaN	3.885729	0.107705	1.127023	1.005362

Table 3.4: TOI with Acceleration7 or Acceleration8 in the `nss_solution_type`

Interesting Object

I present in this chapter a selection of targets of special interest, divided by system configuration (Circumprimary or Circumbinary target) and companion's mass i.e planets, BD, or stellar objects.

4.1 Circumbinary

4.1.1 TOI 1338.01

TOI 1338.01 is a Confirmed Planet (CP) in both TESS and TFOPWG disposition. The discovery of a circumbinary planet (CBP) around the TOI 1338 binary system was first reported by Kostov et al. (2020). TESS and Gaia have found different periods because their data samples are different and measure different phenomena. Gaia measured the period of the stellar companion, which is 14.630 ± 0.006 days. On the other hand, TESS has discovered a planet that orbits around the inner binary system with a period of 95.2 ± 0.033 days.

TOI-1338.01 orbits around its host stars in 95.20 ± 0.03 days. The primary star has a mass of $1.02 \pm 0.12 M_{\odot}$, a radius of $1.52 \pm 0.070 R_{\odot}$, an effective temperature of 5723.2 ± 57.0 K, and a metallicity of -0.4 ± 0.09 dex. The primary stellar parameters are summarized in Table 4.1. The stellar companion has a mass of $0.275 \pm 0.025 M_{\odot}$ and orbits the primary star in 14.630 ± 0.006 days with an eccentricity of 0.185 ± 0.036.

The planet has a radius of $0.70 \pm 0.07 R_J$ and a semi-major axis of 0.4447 ± 0.0007 AU. For further information about the planetary and stellar companion, see to Table 4.2.

Parameter	This Work	Kostov et al. (2020)
Mass $[M_{\odot}]$	1.02 ± 0.12	$1.038^{+0.068}_{-0.069}$
Radius $[R_{\odot}]$	1.52 ± 0.070	$1.299^{+0.024}_{-0.026}$
$T_{\rm eff}[K]$	5723.2 ± 57.0	$5990.7^{+98.1}_{-91.5}$
Metallicity $[Fe/H]dex$	-0.4 ± 0.09	0.01 ± 0.05
Log(g)	3.6 ± 0.08	4.0 ± 0.08
Distance $[pc]$	399.017 ± 3.1375	405 ± 3

Table 4.1: Stellar parameters for TOI 1338A. The measures were taken from the TIC catalog.

Parameter	This Work	Kostov et al. (2020)
Stellar Companion Parameters		
mass $[M_\odot]$	0.275 ± 0.025	$0.297^{+0.011}_{-0.012}$
semi-major axis $[AU]$	0.1276 ± 0.0048	$0.1288^{+0.0024}_{-0.0025}$
eccentricity	0.185 ± 0.036	0.15601 ± 0.00015
K = RV semi-amplitude$[m/s]$	23969.0 ± 963.0	$21624.8^{+3.4}_{-3.2}$
period Gaia$[days]$	14.630 ± 0.006	$14.608561^{+0.000013}_{-0.000012}$
Planet parameters		
radius $[R_J]$	0.70 ± 0.07	0.597 ± 0.010
semi-major axis $[AU]$	0.4447 ± 0.0007	$0.4491^{+0.0084}_{-0.0088}$
period TESS$[days]$	95.20 ± 0.033	$95.141^{+0.031}_{-0.035}$

Table 4.2: Parameters for TOI 1338.01 and TOI 1338B.

4.2 Transiting planets with additional outer companions from PMA

4.2.1 TOI 179.01

The planet TOI 179b has been classified as a Planet Candidate (PC) in TESS disposition and a Confirmed Planet (CP) in TFOPWG. The paper work by Desidera et al. (2023) announces the confirmation of a transiting compact Neptune-mass planet and a low-mass companion in outer orbit. Intensive radial velocity monitoring performed with HARPS and deep high-contrast imaging observations obtained with SPHERE and NACO at VLT were used to confirm the transiting planet. In this work, this system was found in the PMa catalog. This catalog predicts a mass of $7.99 M_J$ at a projected distance of $3au$ for the companion in outer orbit. This is not in agreement with the $83^{+4}_{-6} M_J$ found by Desidera et al. (2023) in an orbit of $3.3au$ (Table 4.5). This is due to the fact that the true separation of the binary is larger than 3 AU and is not a circular orbit. The host star has a mass of $0.85 \pm 0.10 M_\odot$, a radius of $0.80 \pm 0.048 R_\odot$, an effective temperature of 5058 ± 181 K, and the same metallicity as the Sun. Table 4.3 summarizes the stellar parameters. The planet, TOI 179.01, orbits its host star in 4.137438 ± 0.000004 days. It has a radius of $0.24 \pm 0.06 R_J$ and a semi-major axis of 0.048 ± 0.002 AU. More information about the planet can be found in Table 4.4.

Parameter	This Work	Desidera et al. (2023)
Mass $[M_\odot]$	0.85 ± 0.10	0.863 ± 0.020
Radius $[R_\odot]$	0.80 ± 0.048	0.767 ± 0.024
$T_{\rm eff}[K]$	5058 ± 181	5145 ± 50
Metallicity $[Fe/H]dex$	0.0 ± 0.1	0.00 ± 0.08
Log(g)	4.52 ± 0.28	4.54 ± 0.09
Distance $[pc]$	38.56 ± 0.037	

Table 4.3: Stellar parameters for TOI 179. The measures were taken from the TIC catalog.

Parameter	This Work	Desidera et al. (2023)
snrPMa	11.39	
PMaRA$[mas/a]$	-0.407 ± 0.025	
PMaDE$[mas/a]$	-0.032 ± 0.025	
RUWE	0.994	
TESS period$[days]$	4.137438 ± 0.000004	$4.1374354^{+0.0000036}_{-0.0000037}$
Planet radius$[R_J]$	0.24 ± 0.06	$0.231^{+0.009}_{-0.012}$
Semi-major axis$[AU]$	0.048 ± 0.002	0.0480 ± 0.0004

Table 4.4: Parameters for TOI 179.01.

Distance [AU]	Mass[M_J]
3	7.99
5	7.37
10	7.47
30	36.16

Table 4.5: Mass of companion assuming 3,5,10 or 30 au orbit

4.2.2 TOI 200.01 - DS Tuc Ab

The planet TOI 200b has a Confirmed Planet (CP) disposition both in TESS and TFOPWG. The discovery of a transiting planet orbiting around DS Tuc A is confirmed in the paper byBenatti et al. (2019). DS Tuc A B is a physical binary formed by a G6 and a K3 component at a projected separation of 5.4 arcsec (240 au at a distance of 44 pc). In this work, this system was found in the PMa catalog due to the companion in outer orbit. The host star has a mass of $0.94 \pm 0.12 M_{\odot}$, a radius of $0.95 \pm 0.07 R_{\odot}$ and an effective temperature of 5414 ± 161 K. Metallicity of 0.0 ± 0.1dex. Table 4.6 summarizes the stellar parameters. The planet, TOI 200.01, orbits its host star in 8.138224 ± 0.000006 days. It has a radius of $0.58 \pm 0.04 R_J$ and a semi-major axis of 0.077 ± 0.003 AU. More information about the planet can be found in Table 4.7.

Parameter	This Work	Benatti et al. (2019)
Mass [$M_{\odot}$]	0.94 ± 0.12	0.959 ± 0.031
Radius [$R_{\odot}$]	0.95 ± 0.07	0.872 ± 0.027
$T_{\rm eff}[K]$	5414 ± 161	5542 ± 21
Metallicity $[Fe/H]dex$	0.0 ± 0.1	-0.08 ± 0.06
Log(g)	~ 4.438	4.60 ± 0.15
Distance [pc]	44.062 ± 0.07	~ 44

Table 4.6: Stellar parameters for TOI 200A. The measures were taken from the TIC catalog.

Parameter	This Work	Benatti et al. (2019)
snrPMa	4.65	
PMaRA[mas/a]	-0.008 ± 0.025	
PMaDE[mas/a]	0.164 ± 0.025	
RUWE	0.913	
TESS period[$days$]	8.138224 ± 0.000006	8.1387 ± 0.0005
Planet radius[R_J]	0.58 ± 0.04	0.50 ± 0.02
Semi-major axis[AU]	0.077 ± 0.003	0.086 ± 0.003

Table 4.7: Parameters for TOI 200.01.

4.2.3 TOI 4399.01

The planet TOI 4399b has been classified as a Planet Candidate (PC) in TESS disposition and a Confirmed Planet (CP) in TFOPWG. The paper is written by Zhou et al. (2022) announces the confirmation of a Mini-Neptune planet around TOI 4399. The stellar companion was identified in speckle imaging observations of TOI 4399 during the candidate vetting process. In this work, this system was found in the PMa catalog. The separation of the two stars is 506 ± 7 mas with a projected separation of 31 au. The PMa catalog predicts a mass of $30.03 M_J$ at a distance of $30 au$ for the companion in outer orbit. This is not in agreement with the $0.26 \pm 0.04 M_\odot$ found by Zhou et al. (2022) (Table 4.10). This is due to the fact that the true separation of the binary is larger than 30 AU and is not a circular orbit. The host star has a mass of $1.1 \pm 0.14 M_\odot$, a radius of $1.09 \pm 0.05 R_\odot$, an effective temperature of 5985.4 ± 119.7 K, and metallicity 0.0 ± 0.1 dex. Table 4.8 summarizes the stellar parameters. The planet, TOI 4399.01, orbits its host star in 7.7121 ± 0.0011 days. It has a radius of $0.27 \pm 0.11 R_J$ and a semi-major axis of 0.079 ± 0.003 AU. More information about the planet can be found in Table 4.9.

Parameter	This Work	Zhou et al. (2022)
Mass $[M_\odot]$	1.1 ± 0.14	1.01 ± 0.06
Radius $[R_\odot]$	1.09 ± 0.05	0.964 ± 0.029
$T_{\rm eff}[K]$	5985.4 ± 119.7	5428 ± 80
Metallicity $[Fe/H]dex$	0.0 ± 0.1	0.0 ± 0.1
Log(g)	4.4 ± 0.08	
Distance $[pc]$	58.51 ± 0.12	

Table 4.8: Stellar parameters for TOI 4399A. The measures were taken from the TIC catalog.

Parameter	This Work	Zhou et al. (2022)
snrPMa	5.82	
PMaRA$[mas/a]$	0.141 ± 0.029	
PMaDE$[mas/a]$	-0.174 ± 0.025	
RUWE	1.07	
TESS period$[days]$	7.7121 ± 0.0011	7.713057 ± 0.000021
Planet radius$[R_J]$	0.27 ± 0.11	$0.268^{+0.029}_{-0.025}$
Semi-major axis$[AU]$	0.079 ± 0.003	$0.07870^{+0.0056}_{-0.0017}$

Table 4.9: Parameters for TOI 4399.01.

Distance [AU]	Mass$[M_J]$
3	8.96
5	7.14
10	7.48
30	30.03

Table 4.10: Mass of companion assuming 3,5,10 or 30 au orbit

4.2.4 TOI 144.01

The planet TOI 144b in the π Mensae system has been classified as a Confirmed Planet (CP) both in TESS and TFOPWG. The paper written by Damasso et al. (2020) announces the confirmation of a transiting 4 $M_{\oplus}$ planet at ~ 0.07 AU and a sub-stellar companion on a ~ 2100 day eccentric orbit. The external body was first discovered by Jones et al. (2002). Intensive radial velocity monitoring performed with ESPRESSO was used to confirm the precise architecture characterization of the π Mensae planetary system. This system is characterized by highly significant non-coplanarity between π Men b and π Men c ($52.3 \leq i_{rel} \leq 128.8$ deg). In this work, this system was found in the PMa catalog. The semi-major axis of π Man b is 3.28 au (Jones et al., 2002). The PMa catalog predicts a mass of $7.63 M_J$ at a distance of 3 au for the companion in outer orbit. This is not in agreement with the $14.1^{+0.5}_{-0.4} M_{\odot}$ found by Damasso et al. (2020) (Table 4.13). The discrepancy is due to the high eccentricity (~ 0.6) of π Man b orbit. The host star has a mass of $1.1 \pm 0.1 M_{\odot}$, a radius of $1.15 \pm 0.05 R_{\odot}$, an effective temperature of ~ 5950 K, and metallicity of 0.089 ± 0.006 dex. Table 4.11 summarizes the stellar parameters. The planet, TOI 179.01, orbits its host star in 6.26783 ± 0.00002 days. It has a radius of $0.178 \pm 0.007 R_J$ and a semi-major axis of 0.068 ± 0.003 AU. More information about the planet can be found in Table 4.13.

Parameter	This Work	Damasso et al. (2020)
Mass $[M_{\odot}]$	1.1 ± 0.1	1.07 ± 0.04
Radius $[R_{\odot}]$	1.15 ± 0.05	1.17 ± 0.02
$T_{\text{eff}}[K]$	~ 5950	5998 ± 62
Metallicity $[Fe/H]dex$	0.089 ± 0.006	0.09 ± 0.04
Log(g)	~ 4.438	4.43 ± 0.10
Distance $[pc]$	18.27 ± 0.02	

Table 4.11: Stellar parameters for TOI 144. The measures were taken from the TIC catalog.

Parameter	This Work	Damasso et al. (2020)
snrPMa	7.94	
PMaRA$[mas/a]$	0.165 ± 0.047	
PMaDE$[mas/a]$	-0.586 ± 0.06	
RUWE	0.814	
TESS period$[days]$	6.26783 ± 0.00002	6.267852 ± 0.000016
Planet radius$[R_J]$	0.178 ± 0.007	0.185 ± 0.001
Semi-major axis$[AU]$	0.068 ± 0.003	0.067 ± 0.002

Table 4.12: Parameters for TOI 144.01.

Distance [AU]	Mass$[M_J]$
3	7.63
5	6.08
10	6.37
30	25.56

Table 4.13: Mass of companion assuming 3,5,10 or 30 au orbit

4.3 Confirmed Planets

4.3.1 TOI 574.01 - HATS-26 b

HATS-26 b has Known Planet (KP) as disposition both in TESS and TFOPWG. Espinoza et al. (2016) was the first to report the discovery of this planet. The host star has a mass of $1.16 \pm 0.16 M_{\odot}$, a radius of $1.91 \pm 0.10 R_{\odot}$ and an effective temperature of 6071.0 ± 123.1 K. Metallicity is not known. For a summary of the stellar parameters, see table 4.14. This planet was known before the Gaia mission, so the `OrbitalTargetedSearch` pipeline was used and some information was not given, such as the RV semi-amplitude (K). The planet has a radius of $0.70 \pm 0.07 R_J$ and a semi-major axis of 0.4447 ± 0.0007 AU. For further information about the planetary parameters, refer to Table 4.15. The period found by Gaia does not correspond to the period of HATS-26 b and can be associated with a candidate stellar companion that orbits at a distance of 0.688 ± 0.002 AU from HATS-26 and that is not reported in any work in the literature. No additional RV trends or modulations are detected for HATS-26, indicating that the Gaia detections might be spurious (Holl et al., 2023)

Parameter	This Work	Espinoza et al. (2016)
Mass $[M_{\odot}]$	1.16 ± 0.16	$1.299^{+0.113}_{-0.056}$
Radius $[R_{\odot}]$	1.91 ± 0.10	$2.04^{+0.15}_{-0.11}$
$T_{\text{eff}}[K]$	6071.0 ± 123.1	6071 ± 81
Metallicity $[Fe/H]dex$		-0.02 ± 0.05
Log(g)	3.933 ± 0.085	3.936 ± 0.046
Distance $[pc]$	861.8 ± 24.5	907^{+69}_{-49}

Table 4.14: Stellar parameters for TOI 574. The measures were taken from the TIC catalog.

Parameter	This Work	Espinoza et al. (2016)
eccentricity	0.5 ± 0.2	0 (adopted)
Radius$[R_J]$	1.589 ± 0.086	1.75 ± 0.21
Semimajor axis [au]	0.046 ± 0.002	$0.0474^{+0.0013}_{-0.0007}$
Period TESS[days]	3.302391 ± 0.000007	3.302388 ± 0.000008
Period Gaia[days]	193.5 ± 2.9	

Table 4.15: Planet parameters for HATS-26 b.

4.3.2 TOI 5797.01 - WASP-2 b

The planet WASP-2 b has a Known Planet (KP) disposition both in TESS and TFOPWG. Discovery of this planet was first reported by Collier Cameron et al. (2007). The host star has a mass of $0.869 \pm 0.101 M_{\odot}$, a radius of $0.85 \pm 0.04 R_{\odot}$ and an effective temperature of 5147 ± 99 K. Its metallicity is 0.1 ± 0.1 dex. A summary of the stellar parameters can be found in table 4.16. This planet was discovered before the Gaia mission, so the `OrbitalTargetedSearch` pipeline was used. Some information such as the RV semi-amplitude (K) was not given. The planet has a radius of $0.70 \pm 0.07 R_J$ and a semi-major axis of 0.4447 ± 0.0007 AU. For further information about the planetary parameters, refer to Table 4.17. A stellar companion of WASP-2 at a distance of 111 ± 13 AU that orbits WASP-2 in 1.4×10^4 yr was found by Daemgen et al. (2009). This discovery is incompatible with the one found by Gaia (38.0 ± 0.1 days). The period of 38.0 ± 0.1 days is likely due to a fourth unresolved object or an instrumental error (Holl et al., 2023).

Parameter	This Work	Collier Cameron et al. (2007)
Mass $[M_{\odot}]$	0.869 ± 0.101	$0.79^{+0.15}_{-0.04}$
Radius $[R_{\odot}]$	0.85 ± 0.04	0.78 ± 0.06
$T_{\text{eff}}[K]$	5147 ± 99	5200 ± 200
Metallicity $[Fe/H]dex$	0.1 ± 0.1	0.1 ± 0.2
Log(g)	4.51 ± 0.07	4.3 ± 0.3
Distance $[pc]$	153.2 ± 1.6	147 ± 17

Table 4.16: Stellar parameters for WASP-2A. The measures were taken from the TIC catalog.

Planet parameters		
Parameter	This Work	Collier Cameron et al. (2007)
radius $[R_J]$	1.07 ± 0.06	0.95 ± 0.31
semi-major axis $[AU]$	0.031 ± 0.001	0.031 ± 0.001
period TESS$[days]$	2.15216 ± 0.00004	2.152226 ± 0.000004
period Gaia$[days]$	38.0 ± 0.1	

Table 4.17: Parameters for WASP-2 b.

4.3.3 TOI-185.01 - WASP-18 b

The planet WASP-18b has been classified as a Know Planet (KP) both in TESS and TFOPWG disposition. The discovery of a transiting planet around WASP-18 was first reported by Hellier et al. (2009). WASP-18 b orbits its host star in a circular, short-period orbit of 0.9414523 ± 0.0000001 days. The host star has a mass of $1.2 \pm 0.17 M_{\odot}$, a radius of $1.35 \pm 0.07 R_{\odot}$, and an effective temperature of ~ 6400.0 K and a metallicity of 0.1 ± 0.1 dex. For a summary of the stellar parameters, see table 4.18. The planet, likely a brown dwarf, has a radius of $1.382 \pm 0.07 R_J$ and a mass of $10.49 \pm 1.28 M_J$. For more information about the planet, refer to table 4.19.

Parameters	This Work	Hellier et al. (2009)
Mass $[M_{\odot}]$	1.2 ± 0.17	1.25 ± 0.13
Radius $[R_{\odot}]$	1.35 ± 0.07	$1.216^{+0.067}_{-0.054}$
$T_{\text{eff}}[K]$	~ 6400.0	6400 ± 100
Metallicity $[Fe/H]dex$	0.1 ± 0.1	0.00 ± 0.09
Log(g)	~ 4.36583	4.4 ± 0.15
Distance $[pc]$	123.483 ± 0.37	100 ± 10

Table 4.18: Stellar parameters for WASP-18. The measures were taken from the TIC catalog.

Parameter	This Work	Hellier et al. (2009)
mass $[M_J]$	10.49 ± 1.28	10.30 ± 0.69
radius $[R_J]$	1.382 ± 0.07	$1.106^{+0.072}_{-0.054}$
semi-major axis $[AU]$	0.020 ± 0.001	0.0203 ± 0.0007
density$[g/cm^3]$	4.9 ± 0.1	$10.24^{1.03}_{-1.68}$
K = RV semi-amplitude$[m/s]$	1938.0 ± 42.0	1.818 ± 0.008
eccentricity	0.123 ± 0.078	0.0092 ± 0.0028
period TESS$[days]$	0.9414523 ± 0.0000001	$0.94145299 \pm 0.00000087$
period Gaia$[days]$	0.94147 ± 0.00003	

Table 4.19: Planet parameters for WASP 18b.

4.4 Transiting Brown Dwarf

4.4.1 TOI 503.01

The candidate TOI 503.01 has a Confirmed Planet (CP) disposition both in TESS and TFOPWG. The discovery of TOI-503b as a transiting Brown Dwarf (BD) around TOI 503 was first reported by Šubjak et al. (2020). TOI-503b orbits its host star in a circular short-period orbit of 3.6773551 ± 0.000002 days. The host star has a mass of $1.835 \pm 0.280 M_{\odot}$, a radius of $1.68 \pm 0.06 R_{\odot}$, and an effective temperature of 7887.0 ± 218.0 K. Unfortunately, the metallicity is not known. For a summary of the stellar parameters, see table 4.20. The BD has a radius of $1.033 \pm 0.041 R_J$ and a mass of $52.5 \pm 6.9 M_J$. Additional BD information can be found in table 4.21.

Parameter	This Work	Šubjak et al. (2020)
Mass $[M_{\odot}]$	1.84 ± 0.28	$1.80^{+0.06}_{-0.06}$
Radius $[R_{\odot}]$	1.68 ± 0.06	$1.70^{+0.04}_{-0.05}$
$T_{\text{eff}}[K]$	7887.0 ± 218.0	7650^{+140}_{-160}
Metallicity $[Fe/H]dex$		$0.30^{+0.08}_{-0.09}$
Log(g)	4.281 ± 0.476	$4.23^{+0.03}_{-0.03}$
Distance $[pc]$	255.416 ± 3.8885	$257.9^{+3.9}_{-3.8}$

Table 4.20: Stellar parameters for TOI 503. The measures were taken from the TIC catalog.

Parameter	This Work	Šubjak et al. (2020)
mass $[M_J]$	52.5 ± 6.9	53.7 ± 1.2
radius $[R_J]$	1.033 ± 0.041	$1.34^{+0.26}_{-0.15}$
semi-major axis $[AU]$	0.05708 ± 0.00291	0.05727 ± 0.00063
density$[g/m^3]$	59.0 ± 0.3	27^{+13}_{-11}
K = RV semi-amplitude$[m/s]$	4614.0 ± 379.0	4640^{+30}_{-27}
eccentricity	0.062 ± 0.105	0 (adopted)
period TESS$[days]$	3.6773551 ± 0.000002	3.67718 ± 0.00010
period Gaia$[days]$	3.6782 ± 0.001	

Table 4.21: Parameters for TOI 503b.

4.4.2 TOI 2543.01

The candidate TOI 2543b has been classified as a Planet Candidate (PC) in TESS disposition and a Confirmed Planet (CP) in TFOPWG. Psaridi et al. (2022) reported the discovery of a transiting object around a star with a mass of $1.219 \pm 0.174 M_{\odot}$. The star has a radius of $1.87 \pm 0.17 R_{\odot}$, an effective temperature of 6349.8 ± 40.8 K, and a metallicity of -0.446 ± 0.007 dex. The primary stellar parameters can be found in Table 4.22. With a mass of $59.39 \pm 7.75 M_J$ TOI-2543.01 can be considered a BD. This BD orbits its host star in 7.5428 ± 0.00003 days. It has a radius of $0.864 \pm 0.08 R_J$ and a semi-major axis of 0.08041 ± 0.00382 AU. More information about the BD can be found in Table 4.23. It's worth noting that the period found by Gaia and TESS differ by an order of magnitude, which may be due to the fact that Gaia has fewer data points to determine the period accurately and maybe it measured an alias of the transiting object's orbital period as the RV amplitudes are similar.

Parameter	This Work	Psaridi et al. (2022)
Mass $[M_{\odot}]$	1.219 ± 0.174	1.29 ± 0.08
Radius $[R_{\odot}]$	1.87 ± 0.17	1.86 ± 0.15
$T_{\text{eff}}[K]$	6349.8 ± 40.8	6060 ± 82
Metallicity $[Fe/H]dex$	-0.446 ± 0.007	-0.28 ± 0.10
Log(g)	4.11 ± 0.02	4.01 ± 0.08
Distance $[pc]$	426.798 ± 33.976	429.61 ± 33.42

Table 4.22: Stellar parameters for TOI 2543. The measures were taken from the TIC catalog.

Candidate parameters		
Parameter	This Work	Psaridi et al. (2022)
mass $[M_J]$	59.39 ± 7.75	67.62 ± 4.45
radius $[R_J]$	0.864 ± 0.08	0.95 ± 0.09
semi-major axis $[AU]$	0.08041 ± 0.00382	$0.0788^{+0.0079}_{-0.0081}$
Density$[g/cm^3]$	53.8 ± 0.5	$97.53^{+29.35}_{-29.36}$
K = RV semi-amplitude$[m/s]$	5446.0 ± 481.0	6775^{+29}_{-20}
eccentricity	0.147 ± 0.099	$0.009^{+0.003}_{-0.002}$
period TESS$[days]$	7.5428 ± 0.00003	7.54278 ± 0.00003
period Gaia$[days]$	0.79196 ± 0.00004	

Table 4.23: Parameters for TOI 2543.01.

4.5 False Positives

4.5.1 TOI 148.01

The candidate TOI 148.01 has been classified as a Planet Candidate (PC) in TESS disposition and a Confirmed Planet (CP) in TFOPWG. The discovery of a transiting object around TOI 148 was first reported by Grieves et al. (2021). TOI-148b orbits its host star in a circular, short-period orbit of 4.86709 ± 0.00002 days. The host star has a mass of $1.13 \pm 0.15 M_{\odot}$, a radius of $1.15 \pm 0.06 R_{\odot}$, and an effective temperature of 5814.3 ± 793.8 K. TESS did not provide information on the metallicity of the star. For a summary of the stellar parameters, see table 4.24. The candidate, at the boundary between brown dwarfs and very low-mass stars, has a radius of $0.66 \pm 0.04 R_J$ and a mass of $86.72 \pm 14.58 M_J$. For more information about the transiting object, refer to table 4.25.

Parameters	This Work	Grieves et al. (2021)
Mass $[M_{\odot}]$	1.13 ± 0.15	$0.97^{+0.12}_{-0.09}$
Radius $[R_{\odot}]$	1.15 ± 0.06	$1.20^{+0.07}_{-0.07}$
$T_{\text{eff}}[K]$	5814.3 ± 793.8	5990 ± 140
Metallicity $[Fe/H]dex$		-0.24 ± 0.25
Log(g)	4.34 ± 2.0	4.27 ± 0.06
Distance $[pc]$	395.257 ± 9.729	409.668 ± 0.007

Table 4.24: Stellar parameters for TOI 148. The measures were taken from the TIC catalog.

Parameter	This Work	Grieves et al. (2021)
mass $[M_J]$	86.72 ± 14.58	$77.1^{+5.8}_{-4.6}$
radius $[R_J]$	0.66 ± 0.04	$0.81^{+0.05}_{-0.06}$
semi-major axis $[AU]$	0.059 ± 0.002	0.057 ± 0.002
density$[g/cm^3]$	369.4 ± 0.8	183^{+45}_{-32}
K = RV semi-amplitude$[m/s]$	9603.0 ± 1356.0	8950^{+51}_{-52}
eccentricity	0.082 ± 0.133	$0.005^{+0.006}_{-0.004}$
period TESS$[days]$	4.86709 ± 0.00002	4.86710 ± 0.00001
period Gaia$[days]$	4.874 ± 0.003	

Table 4.25: parameters for TOI 148b.

4.5.2 TOI 5394.01

The candidate TOI 5394.01 has a Planet Candidate (PC) disposition both in TESS and TFOPWG. It was found in the TESS catalog, in the PMa catalog and also in the NSS catalog. The star has a radius of $1.07 \pm 0.05 R_{\odot}$, an effective temperature of 5997.0 ± 121.9 K. The primary stellar parameters can be found in Table 4.26. The transiting object, TOI 5394.01, orbits its host star in 15.1935 ± 0.0002 days. It has a $0.86 \pm 0.05 R_J$ radius and a semi-major axis of 0.124 ± 0.005 AU. This object has a mass of $341.05 \pm 28.11 M_J$ and can be classified as a stellar companion. More information about TOI 5394.01 can be found in Table 4.27.

Parameters	This Work
Mass $[M_{\odot}]$	1.1 ± 0.14
Radius $[R_{\odot}]$	1.07 ± 0.05
$T_{\text{eff}}[K]$	5977.0 ± 121.9
Metallicity $[Fe/H]dex$	0.0 ± 0.1
Log(g)	$4,42 \pm 0.08$
Distance $[pc]$	64.28 ± 0.31

Table 4.26: Stellar parameters for 5394. The measures were taken from the TIC catalog.

Candidate parameters	
Parameter	This Work
mass $[M_J]$	341.05 ± 28.11
radius $[R_J]$	0.86 ± 0.05
semi-major axis $[AU]$	0.124 ± 0.005
K = RV semi-amplitude$[m/s]$	27426.6 ± 209.4
eccentricity	0.29 ± 0.29
period TESS$[days]$	15.1935 ± 0.0002
period Gaia$[days]$	15.195 ± 0.001
snrPMa	3.29
PMaRA$[mas/a]$	0.06 ± 0.05
PMaDE$[mas/a]$	-0.193 ± 0.035

Table 4.27: Parameters for TOI 5394.01.

Conclusion

In this work, I have delved into the analysis of the TOIs catalog, the Gaia DR3 NSS catalog, and the PMa catalog, with a particular focus on the objects that have correspondence in one or more of these catalogs. I have analyzed in detail the TOIs that have some interesting characteristics such as an integer period ratio between TESS and Gaia.

After describing the history of the detection of Exoplanets and their general characteristics, I explored various methods to detect these extrasolar planets. I focused my effort on the description of the technique used in this thesis i.e. RV, transit, and Astrometry. Subsequently, I conducted a detailed analysis of the three catalogs, including the NSS Catalogue included in the Gaia DR3 release. The thesis further delves into a comprehensive analysis of TOIs, specifically focusing on the examination of the TOI-NSS and TOI-PMa tables.

Studying the candidates with a Gaia-TESS period ratio equal to 1, 2, or 0.5, I find that 81 objects with TFOP disposition of Planet Candidate or Ambiguous Planet Candidate have a mass above the Brown Dwarf regime, classifying them as False Positives. This represents the 64.12% of the objects with a Gaia-TESS integer period ratio and suggests a correlation between the ratio of Gaia and TESS period and false positive and a potential pattern or characteristic within this subgroup. Three TOIs (5427.01,5882.01 and 6218.01) are instead inside the Brown Dwarf regime and represent an interesting sample for future investigations to improve our knowledge of this kind of planetary system.

Examining the TOI/NSS with astrometric signature I found that 44% of the 84 objects have False Positive flags as TFOP disposition. This suggests that the leftover 47 objects with Planet Candidate or Ambiguous Planet Candidate must be carefully studied as it is highly unlikely to find an exoplanet around one star in a close binary system. Observing them using different filters can be done to discern star mass companions from planetary objects. In different wavelength bands, the depths of the eclipses change, whereas, for planets, this does not happen. In this case, the transit found by TESS is due to a companion in an eclipsing binary or a background transit.

Investigating the TOI/PMa dataset I found that it is an important tool to set low boundary limits on the companion mass, and suggests that the planet found by TESS is a circumprimary object in a binary system. This emphasizes the need to address specific issues such as unresolved stellar companions and considerations related to transit geometry and orbital trends to minimize false positives. The impact of unresolved stellar companions, a notable contributor to false positives in the TOI/PM dataset, underscores the necessity of resolving such issues to elevate the accuracy of planet detection.

It is interesting to note how the percentage of false positive changes in the various tables; in the initial TOI catalog are 1057 over 6836, about 15.46% of the total. In the TOI/NSS dataset, consisting of 322 candidates, 119 are identified as false positives, which accounts for approximately 36.96% of the total dataset. In the TOI/PMa dataset, containing 66 candidates, 15 of them are identified as false positives, representing a percentage of approximately 22.73%. This statistical analysis supports the work done in this thesis emphasizing how the use of Gaia is a powerful tool to highlight false positives but also for addressing possible follow-ups.

It became evident how the integration of Gaia NSS data with TOI proves to be a powerful tool in

detecting false positives, finding objects in the Brown Dwarf regime and uncovering important patterns and characteristics among the identified planets.

In conclusion, this thesis provides valuable insights into the distribution and characteristics of planets and false positives across different datasets. It underscores the importance of rigorous analysis and consideration of specific factors influencing the accuracy of planet detection. A comprehensive understanding of false positive characteristics, coupled with the utilization of advanced tools like Gaia, is imperative for ensuring the success of future missions, like PLATO, and upholding the reliability of planetary data. Further research and refinement of methodologies will continue to be crucial for advancing the field of exoplanetary science.

Table of TOI/NSS

The following table contains all the TOIs that have correspondence in the Non-Single Star catalog. Columns description:

- **TOI**: A unique single numerical identifier of the object of interest in the TESS catalog.
- **TESS**: Disposition flag assigned by TESS. See Table 2.1 for the definition of acronyms
- **TFOP**: Disposition flag assigned by TESS Follow-up Observing Program. See Table 2.1 for the definition of acronyms
- `nss_solution_type`: The NSS solution adopted for the object. See Table 2.2 for the definition.
- **K1**: the Semi-amplitude $[m/s]$ of the center of mass retrieved from NSS catalog
- **Planet Radius**: the radius $[R_J]$ computed by TESS of the transiting object.
- **period G**: the orbital period [day] of the object measured by Gaia
- **period T**: the orbital period [day] of the object measured by TESS
- **Stellar Mass**: the mass of the host star $[M_\odot]$ take from TIC.
- **Distance**: the distance [AU] to the target object.

TOI	TESS	TFOP	nss_solution_type	K1	Planet Radius	period G	Period T	Stellar Mass	Distance
121.01	PC	APC	SB1	8528.6	15.96	14.78109	14.76367	1.14	182.169
148.01	PC	CP	SB1	9603.2	7.43	4.87389	4.86709	1.13	395.257
156.01	EB	FP	SB1	24110.5	10.68	14.15451	14.152	1.21	234.138
158.01	EB	FP	SB1	16800.8	13.36	121.67263	2.51266	1.15	601.367
162.01	PC	APC	SB1	13438.5	15.61	7.76531	7.76469	0.971	274.733
164.01	EB	FP	Acceleration7		8.8		7.31898	1.15	360.131
171.01	PC	PC	Acceleration7		13.58		1.2386	0.88	256.345
171.02	PC	FP	Acceleration7		10.28		1.81358	0.88	256.345
182.01	PC	APC	Orbital		11.62	1117.4594	1.76918		107.399
184.01	EB	FP	SB1	18963.5	24.72	4.81702	4.81707	1.41	247.441
185.01	KP	KP	SB1	1938.3	15.49	0.94147	0.94145	1.2	123.483
217.01	EB	FP	Acceleration7		6.62		3.1386	1.26	142.018
222.01	EB	FP	OrbitalTargetedSearch	9101.6	8.86	33.90357		1.02	84.0311
236.01	EB	FP	SB1	20716.3	23.18	4.535	4.53445	1.29	502.927
254.01	IS	FA	AstroSpectroSB1		3.28	957.9288	20.18654		133.3143
271.01	PC	APC	Acceleration7		2.81		2.47597	1.15	100.245
275.01	PC	APC	AstroSpectroSB1		8.7	175.26456	0.91956	1.0	144.866
276.01	EB	FP	SB1	25290.3	13.88	4.8001	4.80009	1.3	352.383
288.01	PC	PC	OrbitalTargetedSearchValidated		8.99	79.25135	711.7446	1.346	215.387
289.01	PC	PC	OrbitalTargetedSearchValidated	17644.3	16.06	222.79059		1.02	454.65
311.01	PC	APC	Acceleration9		14.81		0.7963	0.63	232.861
312.01	PC	APC	Orbital		10.29	423.16022	3.54138	1.03	506.715
355.01	PC	PC	OrbitalTargetedSearchValidated		4.6	297.81622	1.03734	1.13	313.032
363.01	PC	APC	Acceleration7		12.47		8.22388	0.88	440.102
385.01	EB	FP	AstroSpectroSB1		8.16	440.18134	0.66807		262.782
416.01	EB	FP	SB1	11433.9	18.14	7.0118	7.0114	1.263	131.962
425.01	EB	FP	SB1	10693.1	14.1	3.60469	3.60364	1.47	631.385
445.01	PC	PC	SecondDegreeTrendSB1		12.95		0.76496	1.21	176.617
446.01	EB	APC	SB1	17417.5	22.1	3.50176	3.5018	1.29	674.155
459.01	PC	APC	SB1	52004.2	9.87	4.42917	4.42913	1.36	286.94
472.01	PC	APC	Orbital		24.85	552.60516	0.56826	0.500534	
503.01	CP	CP	SB1	4614.4	11.58	3.67816	3.67736	1.835	255.416
504.01	EB	FP	Orbital		29.28	470.46198	1.67731	1.62	425.719
510.01	PC	APC	Acceleration7		2.83		1.35239	1.07	93.0994
574.01	KP	KP	OrbitalTargetedSearch		17.81	193.53658	3.30239	1.16	861.843
586.01	EB	FP	SB1	19620.5	28.03	22.61198	22.63846	2.42	253.02
592.01	PC	FP	SB1	16603.4	8.38	121.78925	10.4138	1.3	358.441
593.01	EB	FP	SB2	51794.0	37.59	1.00114	13.9086	1.252	382.898
604.01	PC	FP	SB1	23294.5	22.04	194.46683	1.07242		1006.54
609.01	PC	APC	SB2	61785.2	21.41	4.01192	4.97	1.03	144.623
613.01	PC	PC	FirstDegreeTrendSB1		9.22		0.7785		221.016
614.01	PC	FP	OrbitalTargetedSearch		6.77	91.66526	0.88501	0.962	255.901

631.01	EB	FP	SB2	86319.8	5.94	5.19013	2.59507	1.483	233.697
646.01	EB	FP	SB1	18642.3	20.34	13.71695	13.72525	1.15	316.643
665.01	PC	FP	SB1	12334.3	20.71	14.06688	14.06599	1.01	131.018
668.01	EB	APC	SB1	17741.1	21.7	4.37836	4.37873	1.19	344.134
691.01	PC	FP	SB1	36562.6	4.75	33.99614	6.90559	1.06	169.117
701.01	PC	FP	SB1	10133.8	4.21	13.69427	13.69738	1.03	217.621
706.01	PC	PC	AstroSpectroSB1		16.63	59.92132	719.03815	1.02	94.697
710.01	EB	FP	AstroSpectroSB1		18.57	71.93136	216.24583	1.71	157.721
720.01	EB	FP	AstroSpectroSB1		2.39	80.93023	3.16043	1.41	151.634
735.01	PC	FP	AstroSpectroSB1		2.98	788.9195	2.59369	0.92	121.755
746.01	PC	PC	OrbitalTargetedSearch	9311.5	9.67	90.53592	10.9803	0.99	234.418
759.01	PC	APC	SB1	11395.4	12.97	4.21329	4.21357	1.28	516.041
764.01	PC	APC	SB1	22600.7	33.64	5.63079	5.63167	1.43	789.341
768.01	PC	APC	SB1	16732.1	18.71	3.65973	11.52944	1.21	469.997
775.01	PC	FP	Orbital		21.08	802.36334	12.44587	1.45	220.953
803.01	EB	FP	SecondDegreeTrendSB1		10.42		15.30507		403.772
827.01	PC	APC	Acceleration9, SB1	15503.4	13.06	978.0148	1.22824	1.09	336.988
838.01	EB	FP	SB1	35183.2	9.52	7.62315	7.62467	1.72	305.237
844.01	PC	FP	SB1	14562.3	7.16	17.68055	8.90663	1.05	472.297
846.01	PC	FP	SB1	26281.8	12.46	14.20745	14.20489	1.22	446.815
855.01	PC	PC	Acceleration7, SecondDegreeTrendSB1		4.46		1.83012	1.41	294.418
865.01	PC	APC	SB2	106851.7	3.4	1.49117	0.74558	0.95	136.022
877.01	EB	APC	Acceleration9		12.41		6.01494	1.8	452.682
901.01	PC	PC	SB1	49749.0	11.14	3.231	3.23084	1.24	190.467
918.01	PC	FP	Acceleration7		6.35		1.11401	0.99	549.872
924.01	PC	PC	SB1	24069.4	15.68	12.12195	12.12739	1.01	251.24
928.01	EB	FP	Acceleration7		14.12		30.57908	1.1	310.211
933.01	PC	PC	OrbitalTargetedSearch		12.68	49.13271	88.93495	0.98	300.423
946.01	EB	FP	OrbitalTargetedSearch	68657.8	22.99	459.39938	6.12531	0.83	164.458
948.01	PC	APC	SB1	33551.9	10.54	12.71088	12.7009	1.05	370.711
953.01	EB	FP	SB1	16529.4	19.33	2.96835	2.96844	1.19	204.316
996.01	PC	FP	SB1	33698.4	16.05	14.53957	14.5378		379.693
997.01	EB	FP	Acceleration7, FirstDegreeTrendSB1		20.51		8.41349	1.04	113.667
1015.01	PC	PC	FirstDegreeTrendSB1		31.89		1.37373		906.496
1018.01	PC	FP	SB1	35909.1	22.91	4.95921	4.95912	1.07	360.541
1035.01	PC	PC	SB1	9438.5	31.37	11.80113	6.07428	1.09	347.556
1059.01	PC	PC	SB1	21494.2	17.02	9.44988	9.44965	0.88	98.8783
1072.01	EB	FP	SB1	17411.2	25.49	12.85107	12.83797	1.05	703.878
1087.01	PC	FP	SB1	45393.6	14.3	5.71379	9.30992	1.5	416.25
1094.01	PC	APC	AstroSpectroSB1		9.08	299.84628	0.59713	1.81	426.003
1096.01	PC	FP	SB1	55815.3	5.73	6.64382	0.92095	1.36	490.288
1111.01	EB	FP	SB1	46241.0	14.11	11.47501	11.4757	1.64	312.461
1113.01	O	FP	OrbitalTargetedSearch		4.59	1048.569	6.44101	0.531332	23.8853
1115.01	PC	APC	SB1	54062.5	15.89	4.45273	4.45199	1.47	359.215
1119.01	PC	APC	SB1	38762.4	23.97	10.95889	10.95663	1.31	421.518
1120.01	EB	FP	Acceleration7		13.33		1.66226	1.65	386.323
1124.01	PC	APC	Acceleration9, SecondDegreeTrendSB1		14.01		3.51877	1.42	75.7145
1140.01	EB	FP	Acceleration7, SB1	15272.5	15.91	13.743	13.74295	1.122	121.182
1141.01	PC	FP	SB1	28204.4	45.22	16.94776	16.94871	1.08	97.3391
1153.01	PC	APC	SB1	43790.5	9.65	6.03613	6.03608	1.689	147.134
1157.01	PC	FP	SB2	62423.4	35.79	13.07955	13.07275	1.11	432.113
1168.01	PC	FP	SB2	83713.6	17.66	4.27166	2.136	1.199	274.162
1175.01	EB	FP	Acceleration7		5.56		7.50227	1.203	216.517
1187.01	PC	PC	AstroSpectroSB1		3.8	585.7683	2.59424	1.28	221.071
1223.01	PC	FP	AstroSpectroSB1		3.21	155.76173	14.64324	1.3	237.7
1254.01	PC	PC	Acceleration7		6.59		1.01801	0.952	199.039
1270.01	PC	FP	SB1	12083.1	18.49	14.30135	14.30346	0.843	171.138
1309.01	PC	FP	Acceleration7				1.49861	2.21	686.879
1314.01	PC	FP	Orbital		7.79	845.2416	2.63999		285.36
1338.01	CP	CP	SB1	23969.2	7.85	14.6298	95.2	1.02	399.017
1341.01	EB	FP	SB1	37692.1	48.99	6.44757	6.44749	1.407	236.568
1344.01	EB	FP	Acceleration7, SB1	15272.5	13.16	13.743	13.74318		121.182
1345.01	PC	PC	SecondDegreeTrendSB1		16.93		8.47134		788.93
1348.01	PC	FP	Acceleration7		1.84		2.14056	0.706	101.713
1357.01	PC	FP	AstroSpectroSB1		2.62	1249.0232	0.33759	1.683	254.401
1360.01	PC	FP	Acceleration7		5.19		0.70902	2.27	533.615
1367.01	EB	FP	Acceleration7		5.42		2.08811	1.355	195.858
1368.01	PC	FP	Acceleration9, FirstDegreeTrendSB1		2.95		1.25562	1.02	158.181
1371.01	PC	APC	SB1	15942.2	36.26	5.00973	5.00956	1.46	302.295
1372.01	O	FP	Orbital		8.22	315.4255	6.16009	1.034	244.043
1378.01	PC	APC	Acceleration7		42.69		5.77853	2.02	547.399
1392.01	PC	FP	Acceleration7		8.48		2.86876	2.06	594.193
1393.01	PC	FP	SB1	8159.4	4.23	98.13722	0.55903	1.338	248.79
1394.01	PC	FP	AstroSpectroSB1		3.83	963.7028	2.95816	1.234	195.022
1412.01	PC	APC	Acceleration9, FirstDegreeTrendSB1		6.97		4.73198	0.66	81.0643
1413.01	PC	PC	AstroSpectroSB1		6.16	174.30507	6.11821	0.945	115.417
1429.01	PC	FP	Acceleration7		4.84		0.64126	1.058	435.255
1455.01	PC	APC	SB1	15306.0	34.07	3.62345	3.62314	1.378	245.692
1461.01	PC	APC	SB1	20198.2	20.25	3.56774	3.56868	1.12	359.959
1514.01	EB	FP	SB1	14471.8	11.89	64.96555	1.36991	1.736	242.006
1520.01	PC	PC	Acceleration7		6.96		6.14617	1.169	196.55
1522.01	EB	FP	Acceleration9		4.92		2.97986	2.279	303.976
1546.01	PC	PC	Acceleration9		3.03		1.13345	1.201	210.101
1553.01	PC	APC	SB1	29932.9	18.76	5.93844	5.93821	1.47	441.44
1556.01	EB	FP	Acceleration7		9.2		1.44127	1.934	315.386
1567.01	PC	FP	SB1	30281.3	21.06	17.32247		0.71	86.1112
1569.01	PC	APC	SB1	14030.9	14.13	5.95526	1.71614	1.35	755.795
1570.01	PC	FP	Acceleration7		5.63		1.74626	2.06	294.123
1572.01	PC	FP	SB1	29950.6	27.48	17.33133	8.66698	1.32	505.331
1587.01	EB	FP	Acceleration7		8.72		12.5343	1.87	563.997
1591.01	PC	FP	SB1	16762.7	10.43	51.92655		1.736	282.1
1608.01	PC	APC	SB1	11000.6	13.9	2.47284	2.47273	1.148	100.635
1645.01	EB	FP	SB1	18085.1	18.09	2.17218	2.17214	1.189	146.653
1656.01	PC	APC	Orbital	27733.4	20.06	74.20529	1112.7563	1.248	106.477
1671.01	PC	FA	Acceleration7		11.75		8.13664		221.791
1677.01	PC	PC	Acceleration9, SB1	5005.0	4.85	1231.0934	0.64358	1.078	197.14
1684.01	PC	PC	Acceleration7		9.37		1.15499		87.5878
1698.01	PC	PC	SB1	37860.4		8.52111	17.04198		756.791
1709.01	PC	PC	Orbital		18.03	236.9994	7.62884	1.171	268.655
1711.01	PC	FP	SB1	16721.1	7.45	20.54615	10.2558	0.918	112.978
1712.01	PC	FP	SB1	7693.1	20.23	3.56565	3.56628	1.48	574.264
1786.01	PC	FP	SB1	31934.9	20.68	9.57303	9.5727	1.33	248.695
1788.01	PC	FP	SB1	19849.6	10.42	5.34341	5.34326	1.035	191.532

1822.01	PC	APC	SB1	9060.4	14.57	9.60871	9.61366	1.0	312.52
1834.01	PC	APC	SB1	33494.6	16.02	80.858	1.21644	0.993	265.941
1856.01	PC	FP	SB1	14465.8	12.07	98.5329	197.03363	1.02	210.486
1897.01	PC	FP	SB1	12411.9	26.83	48.54992	48.53404	1.084	158.493
1897.02	PC	FP	SB1	12411.9	7.9	48.54992	48.53386	1.084	158.493
1946.01	EB	FP	Acceleration7		21.68		10.84587	1.54	230.033
1951.01	PC	PC	SB1	13100.6	18.4	4.82955	4.8294	1.35	278.462
1952.01	PC	FP	SB1	38658.3	11.32	8.99995	6.89132	1.06	241.981
1974.01	PC	APC	SB1	42067.1	14.78	5.43772	5.43822	0.98	238.426
1991.01	EB	FP	SB1	9571.5	14.89	6.65906	6.65708	1.12	268.254
1993.01	EB	FP	Acceleration9		19.63		3.94169	1.48	290.78
1996.01	PC	FP	SB1	8453.5	20.03	15.44476	7.72433	1.31	422.884
2008.01	PC	FP	OrbitalTargetedSearchValidated	14883.9	13.14	51.56445	723.8345	0.992	139.212
2027.01	PC	FP	Acceleration9		3.55		1.46329	1.176	238.061
2028.01	PC	FP	SB1	20404.8	6.16	27.28205	0.77871	1.83	609.996
2038.01	PC	APC	SB1	12911.2	19.16	3.73216	3.73212	1.36	603.172
2042.01	PC	FP	Acceleration9		7.24		2.41872	1.348	511.22
2065.01	PC	APC	SB1	15600.4	10.44	71.89895		1.02	234.294
2117.01	EB	FP	SB2	67315.5	12.5	6.88804	28.66208	1.227	255.917
2118.01	PC	FP	Acceleration9		4.26		2.34483	1.283	186.825
2157.01	PC	APC	SB1	13627.1	15.04	8.42351	8.4249	1.03	178.43
2159.01	PC	APC	SB1	10468.8	13.59	10.05146	10.05097	1.05	294.398
2218.01	PC	APC	SB1	10723.0	10.19	344.91962	0.34569	1.23	330.15
2315.01	PC	APC	Acceleration7		9.78		1.44082	1.22	290.436
2320.01	PC	FP	AstroSpectroSB1		18.0	165.65475		1.065	167.542
2335.01	PC	APC	SB1	15149.6	6.16	76.99355	1.44921	1.11	439.747
2349.01	PC	APC	SB1	13358.7	22.4	11.56211	11.57385	1.04	528.869
2352.01	PC	PC	Acceleration7		5.37		1.68045	1.014	231.907
2354.01	EB	FP	Acceleration7		9.55		0.51099	1.14	569.651
2360.01	PC	FP	SB1	8544.3	15.18	22.85492	22.84518	1.09	580.188
2366.01	PC	PC	SB1	22477.6	12.93	17.17497	17.18699	1.126	439.569
2400.01	PC	FP	FirstDegreeTrendSB1		5.37		1.0339	1.3	465.461
2413.01	PC	FP	SB1	21863.9	12.43	13.41891	13.41904	0.88	340.766
2442.01	EB	FP	SB1	22111.8	10.23	17.11766	17.12172	1.03	262.475
2444.01	PC	APC	Acceleration7		15.74		1.64739	0.583202	190.748
2469.01	PC	APC	SB1	19224.6	23.4	2.37813	2.37675	1.51	632.183
2482.01	PC	PC	SB1	1314.2	1.58	7.668	14.93156		
2489.01	PC	APC	SB1	17089.2	8.83	1074.244	1.42695	0.91	215.394
2490.01	PC	PC	SB1	6315.1	7.89	4.43988		0.95	267.648
2492.01	PC	APC	SB1	12578.0	17.9	10.09911	10.10114	1.34	421.423
2496.01	PC	PC	Acceleration7		22.96		1.57468	0.571424	196.683
2510.01	EB	FP	Acceleration7		2.7		1.97852	1.24	204.166
2521.01	PC	APC	SB1	7654.2	9.04	4.72321	5.56309	1.023	341.347
2533.01	PC	PC	SB1	7388.5	9.65	6.69241	6.68579	1.17	368.409
2543.01	PC	CP	SB1	5445.7	9.69	0.79196	7.54281	1.219	426.798
2544.01	PC	PC	SB1	29625.0	9.07	21.05714	10.53058	1.12	377.872
2546.01	PC	APC	SB1	38974.7	18.72	13.09276	2.1812	1.16	515.356
2551.01	PC	PC	Acceleration7		7.8		5.43684	1.92	730.421
2598.01	PC	APC	SB1	50019.0	21.05	5.73382	5.73436	0.689	107.256
2606.01	PC	PC	SB1	18377.3	20.54	1.4508	1.45092	1.32	442.105
2614.01	PC	PC	SB1	21510.9	14.97	6.07785	4.8103		315.469
2647.01	PC	PC	Orbital		14.48	269.09015	0.51367	0.9	792.816
2664.01	PC	FP	SB1	46699.3	10.4	3.96011	3.9606	1.06	156.291
2674.01	PC	APC	SB1	29202.4	13.24	26.20439	7.29724	1.3	370.146
2675.01	PC	FP	Orbital		13.22	442.9556	1.47687	1.35	523.999
2708.01	PC	FP	Acceleration7		14.49		2.35402	1.15	825.004
2793.01	PC	PC	Orbital		6.23	598.53015	0.35597	0.98	618.274
2819.01	PC	APC	SB1	50547.6	20.05	4.39132	4.39055	1.17	655.523
2850.01	PC	PC	SB2C	65818.5	7.47	9.43335	6.63292	0.72	106.964
2922.01	PC	PC	Acceleration7		5.14		1.36052	1.08	366.67
2998.01	PC	PC	Orbital		9.92	549.7289	1.52971	1.41	1019.27
3006.01	PC	PC	SB1	50990.7	20.68	8.61119	8.61346	1.38	561.854
3010.01	PC	PC	SB1	18911.0	18.04	9.54298	9.55377	1.05	421.094
3056.01	PC	PC	Acceleration7		23.23		1.80929	1.5	1181.19
3070.01	PC	PC	Orbital		20.24	945.7364	0.65872	1.34	1689.05
3148.01	PC	PC	SB1	22504.4	10.68	4.28108	4.28144		342.833
3155.01	PC	APC	SB1	11736.7	8.96	4.64947	4.64922	0.86	201.727
3191.01	PC	PC	SB1	63511.2	16.91	8.87867	4.43679	1.3	864.432
3241.01	PC	PC	SB1	15931.1	17.5	6.83559	6.83809	1.08	300.417
3243.01	PC	PC	SB1	51982.9	14.75	4.05546	2.05191		
3260.01	PC	PC	SB1	23482.1	9.64	11.45074	11.45201	1.19	599.768
3279.01	PC	PC	Acceleration7		7.77		0.41914	0.99	614.459
3298.01	PC	PC	SB1	41554.7	17.95	3.05342	3.05379	1.15	588.129
3302.01	PC	PC	Acceleration9		10.93		1.55703	0.99	705.625
3357.01	PC	FP	Acceleration7		6.69		2.65358	1.94	607.29
3375.01	PC	FP	Acceleration7		7.4		1.23683	1.15	735.596
3389.01	PC	PC	SB2	56404.7	9.76	1.64171	1.68015	1.2	527.277
3501.01	PC	APC	SB1	13900.4	19.22	15.34617	15.35025	1.099	206.21
3502.01	PC	PC	SB1	23342.4	15.03	3.44688	3.44629	1.87	627.463
3542.01	PC	APC	SB1	13089.0	14.14	4.20558	4.20219	1.42	503.905
3697.01	PC	APC	SB1	8607.7	25.5	63.55906	9.94402	0.898	350.16
3717.01	PC	APC	Orbital		10.49	593.6059	10.11828	1.63	505.231
3756.01	PC	APC	SB1	55273.5	12.63	4.42384	4.42367	1.145	327.13
3792.01	PC	PC	Acceleration9		6.52		0.77291	1.16	640.574
3796.01	PC	FP	SB1	21055.3	9.4	14.99837	14.98574	0.906	216.16
3823.01	PC	APC	Orbital		4.49	454.11975	0.68484	1.28	353.355
3844.01	PC	APC	Acceleration9		13.87		0.89627	1.02	655.503
3880.01	PC	PC	Acceleration7		8.1		2.16148	0.707	300.232
3904.01	PC	APC	SB1	36144.6	7.67	10.15982	10.16148	1.23	379.347
3908.01	PC	APC	Orbital		24.51	248.43124	1.46817	0.95	267.999
3925.01	PC	FP	Orbital		7.4	661.6969	3.03309	1.72	773.332
3979.01	PC	FP	Acceleration7		8.91		2.04166	1.46	871.833
4037.01	PC	FP	Acceleration9		10.55		4.72571	1.16	653.395
4046.01	PC	PC	AstroSpectroSB1		5.41	1306.4896	0.75837	1.194	328.581
4063.01	PC	APC	Orbital		15.85	213.6251	1.63226	0.86	408.646
4143.01	PC	FP	Orbital		13.87	538.76404	9.84822	1.16	1283.53
4146.01	PC	APC	Orbital		13.28	512.24994	0.70116	1.12	464.611
4178.01	EB	FP	SB2C	83407.9	9.79	4.40846	2.20422	1.016	197.507
4226.01	PC	PC	SB1	102797.6	14.7	0.88559	2.9629		867.497
4238.01	PC	PC	Acceleration9		13.86		1.27322	0.82	395.573
4245.01	PC	PC	SB1	16794.5	6.08	5.07358	3.15187	0.99	211.183
4314.01	PC	FA	Acceleration7		3.4		73.58098	1.851	158.797
4331.01	PC	PC	SB1	13756.9	6.62	78.58126	2.90342	1.1	346.327

4338.01	PC	APC	SB1	28258.5	10.2	7.49949	7.49978	0.9	219.732
4346.01	PC	FP	Acceleration9		1.57		3.90771	0.61966	130.457
4369.01	PC	PC	AstroSpectroSB1		3.58	516.8069	13.57686	1.43	311.844
4383.01	PC	PC	SB2	89508.9	16.89	6.08399	3.04213	1.37	335.446
4400.01	PC	PC	SB1	14282.2	19.86	7.06131	7.06731	1.01	534.436
4432.01	PC	PC	Acceleration9		25.35		3.04134	0.631	209.435
4462.01	PC	APC	SB1	9730.8	9.34	4.91455	4.9133	1.08	368.922
4505.01	PC	PC	Acceleration9		17.43		19.47355	1.48	421.749
4555.01	PC	PC	Acceleration7		2.24		522.62726	1.19	96.7153
4614.01	PC	PC	Acceleration9		10.43		13.83389	0.661	101.255
4657.01	PC	PC	SB1	42944.2	9.82	8.11076	8.11295	1.19	433.817
4771.01	PC	APC	SB1	14663.4	12.7	6.48277	6.00495	1.26	498.418
4792.01	PC	APC	SB1	32950.4	10.25	8.44816	8.44817	1.049	243.539
4807.01	PC	PC	SB1	25073.0	8.8	17.68939	17.68686	0.71	153.227
4838.01	PC	PC	SecondDegreeTrendSB1		12.55		0.75998	1.01	515.491
4879.01	PC	PC	Acceleration7		9.72		5.37631	1.35	1071.24
4967.01	PC	PC	Acceleration7		10.33		0.59794	1.05	821.066
4973.01	PC	PC	SB1	23257.3	9.54	7.94833	7.94863	1.03	178.064
4978.01	PC	PC	SB1	27457.8	17.05	2.20144	4.71903	1.28	719.916
5013.01	PC	PC	Acceleration7		13.47		8.98949	1.39	1224.74
5102.01	PC	APC	Orbital		7.92	944.1553	0.4522	0.614948	379.43
5103.01	PC	APC	SB1	59117.7	9.13	4.98999	4.98987	1.21	528.469
5149.01	PC	PC	SB1	8448.8	18.31	27.3883	27.3715	1.073	298.458
5156.01	PC	PC	SB1	13571.4	4.19	22.85312	22.85229	1.059	160.968
5197.01	PC	PC	SB1	31280.5	8.59	20.57286	20.57734	0.85	232.248
5199.01	PC	FP	Orbital		12.44	723.8032	3.91314	0.603055	372.355
5200.01	PC	PC	SB1	28589.0	11.48	17.43558	17.4373	1.34	451.568
5307.01	PC	APC	SB1	65256.4	4.01	5.29846	5.29763	0.63	105.824
5364.01	PC	PC	Acceleration7		12.42		1.44669	1.25	645.231
5372.01	PC	PC	SB1	50552.9	10.18	11.63028	11.62708	1.04	459.882
5379.01	PC	PC	SB1	33530.8	16.68	12.74426	12.74265	1.277	200.226
5383.01	PC	PC	AstroSpectroSB1		1.4	195.86426	2.8115	1.45	102.134
5394.01	PC	PC	SB1	27426.6	9.68	15.19502	15.19351	1.1	64.2806
5399.01	PC	PC	AstroSpectroSB1		3.71	160.04169	4.0626	1.391	320.903
5427.01	PC	PC	SB1	7864.2	14.22	5.2345	5.23742	1.123	363.385
5443.01	PC	PC	Acceleration7		7.63		1.67577	1.52	885.894
5475.01	PC	APC	SB1	49723.0	11.54	10.05227	10.0532	1.36	655.835
5485.01	PC	PC	Acceleration7		5.88		2.58453	1.15	774.157
5544.01	PC	PC	Acceleration9		3.32		4.20507	0.852	113.205
5547.01	PC	PC	SB1	26114.5	14.08	19.63351	19.6305	0.967	193.901
5563.01	PC	PC	Acceleration9, SecondDegreeTrendSB1		8.26			1.035	185.26
5677.01	PC	APC	SB1	31299.9	9.2	3.84803	3.84802	1.169	137.2
5687.01	PC	APC	AstroSpectroSB1		8.57	499.32587	2.92444	0.776	153.891
5702.01	PC	PC	Acceleration7		4.11		3.12913	1.207	222.812
5742.01	EB	FP	SB2C	102939.1	7.03	3.27882	3.96582	1.19	438.137
5746.01	PC	PC	SB1	8364.4	12.63	24.56862	711.7643	0.74	85.5353
5761.01	PC	PC	SB1	35368.4	5.06	19.54594	19.54221	0.89	192.846
5784.01	PC	FP	Acceleration9		5.6		8.68002	1.341	309.386
5797.01	KP	KP	OrbitalTargetedSearch		12.0	38.04406	2.15216	0.869	153.242
5811.01	PC	PC	SB1	5927.4	10.4	915.5919	6.25718		169.494
5860.01	PC	APC	SB1	28068.2	12.94	5.2484	5.24989	1.102	442.817
5882.01	PC	PC	SB1	2379.3	14.19	7.15108	7.14877	1.017	416.104
6053.01	PC	APC	Acceleration7		10.34		2.21183	1.805	359.465
6066.01	PC	PC	Acceleration9, SB1	7958.5	1.93	1143.9843	1.82676	1.253	157.64
6069.01	PC	PC	AstroSpectroSB1		3.95	148.55498	1.62909	1.005	122.51
6077.01	PC	PC	Acceleration9		2.99		2.21111	0.63215	124.484
6096.01	PC	FP	SB1	31244.1	2.56	6.16138	1.31543	1.384	181.94
6106.01	PC	APC	SB1	12834.2	14.84	5.66797	6.42409	0.99	294.59
6111.01	PC	APC	SB1	58050.8	12.17	5.83283	5.83403	1.015	302.326
6117.01	PC	PC	SB1	6618.0	11.57	9.86148	9.86631	1.19	483.576
6133.01	PC	APC	SB1	19284.1	20.76	3.65272	3.65343	1.27	402.816
6142.01	PC	PC	Acceleration7		10.08		4.95648	0.97	518.031
6147.01	PC	PC	Orbital		9.32	307.82367	1.58018	0.716	320.803
6151.01	PC	PC	SB1	5658.9	7.06	2.34169	1.43548	1.11	590.69
6207.01	PC	APC	SB1	12498.6	15.26	9.76641	9.77124	0.91	243.593
6210.01	PC	APC	SB1	12300.1	21.48	1.35547	7.85801	1.29	1093.37
6218.01	PC	PC	SB1	9570.8	12.05	5.15542	5.15702	0.702	159.96
6226.01	PC	PC	Acceleration7		13.8		3.88573	1.14	1027.44
6242.01	PC	FP	SB1	9379.1	11.36	5.6036	5.60203	1.03	328.625
6549.01	PC	PC	SB1	12642.8	19.3	7.57353	6.10791	1.01	575.271
6566.01	PC	PC	SB1	51926.8	10.71	5.2574	7.58378	1.31	793.88
6568.01	PC	PC	SB1	9734.9	18.68	17.43205	17.43681	1.25	366.686
6611.01	PC	PC	SB1	11196.6	12.67	6.56902	6.55687	1.16	534.334
6658.01	PC	PC	AstroSpectroSB1		3.75	895.01495	5.64944		280.1428

Table A.1: List of all TOI with correspondence in the NSS table.

Bibliography

(1997). *The HIPPARCOS and TYCHO catalogues. Astrometric and photometric star catalogues derived from the ESA HIPPARCOS Space Astrometry Mission*, volume 1200 of *ESA Special Publication*.

Baglin, A., Auvergne, M., Boisnard, L., Lam-Trong, T., Barge, P., Catala, C., Deleuil, M., Michel, E., and Weiss, W. (2006). CoRoT: a high precision photometer for stellar ecolution and exoplanet finding. In *36th COSPAR Scientific Assembly*, volume 36, page 3749.

Bakos, G., Noyes, R. W., Kovács, G., Stanek, K. Z., Sasselov, D. D., and Domsa, I. (2004). Wide-Field Millimagnitude Photometry with the HAT: A Tool for Extrasolar Planet Detection. , 116(817):266–277.

Benatti, S., Nardiello, D., Malavolta, L., Desidera, S., Borsato, L., Nascimbeni, V., Damasso, M., D'Orazi, V., Mesa, D., Messina, S., Esposito, M., Bignamini, A., Claudi, R., Covino, E., Lovis, C., and Sabotta, S. (2019). A possibly inflated planet around the bright young star DS Tucanae A. , 630:A81.

Berman, L. (1932). 70 Ophiuchi as a triple system. *Lick Observatory Bulletin*, 443:24–30.

Beuzit, J. L., Vigan, A., Mouillet, D., Dohlen, K., Gratton, R., Boccaletti, A., Sauvage, J. F., Schmid, H. M., Langlois, M., Petit, C., Baruffolo, A., Feldt, M., Milli, J., Wahhaj, Z., Abe, L., Anselmi, U., Antichi, J., Barette, R., Baudrand, J., Baudoz, P., Bazzon, A., Bernardi, P., Blanchard, P., Brast, R., Bruno, P., Buey, T., Carbillet, M., Carle, M., Cascone, E., Chapron, F., Charton, J., Chauvin, G., Claudi, R., Costille, A., De Caprio, V., de Boer, J., Delboulbé, A., Desidera, S., Dominik, C., Downing, M., Dupuis, O., Fabron, C., Fantinel, D., Farisato, G., Feautrier, P., Fedrigo, E., Fusco, T., Gigan, P., Ginski, C., Girard, J., Giro, E., Gisler, D., Gluck, L., Gry, C., Henning, T., Hubin, N., Hugot, E., Incorvaia, S., Jaquet, M., Kasper, M., Lagadec, E., Lagrange, A. M., Le Coroller, H., Le Mignant, D., Le Ruyet, B., Lessio, G., Lizon, J. L., Llored, M., Lundin, L., Madec, F., Magnard, Y., Marteaud, M., Martinez, P., Maurel, D., Ménard, F., Mesa, D., Möller-Nilsson, O., Moulin, T., Moutou, C., Origné, A., Parisot, J., Pavlov, A., Perret, D., Pragt, J., Puget, P., Rabou, P., Ramos, J., Reess, J. M., Rigal, F., Rochat, S., Roelfsema, R., Rousset, G., Roux, A., Saisse, M., Salasnich, B., Santambrogio, E., Scuderi, S., Segransan, D., Sevin, A., Siebenmorgen, R., Soenke, C., Stadler, E., Suarez, M., Tiphène, D., Turatto, M., Udry, S., Vakili, F., Waters, L. B. F. M., Weber, L., Wildi, F., Zins, G., and Zurlo, A. (2019). SPHERE: the exoplanet imager for the Very Large Telescope. , 631:A155.

Bonavita, M., Fontanive, C., Gratton, R., Mužić, K., Desidera, S., Mesa, D., Biller, B., Scholz, A., Sozzetti, A., and Squicciarini, V. (2022). Results from The COPAINS Pilot Survey: four new BDs and a high companion detection rate for accelerating stars. , 513(4):5588–5605.

Borucki, W. J., Koch, D., Basri, G., Batalha, N., Brown, T., Caldwell, D., Caldwell, J., Christensen-Dalsgaard, J., Cochran, W. D., DeVore, E., Dunham, E. W., Dupree, A. K., Gautier, T. N., Geary, J. C., Gilliland, R., Gould, A., Howell, S. B., Jenkins, J. M., Kondo, Y., Latham, D. W., Marcy, G. W., Meibom, S., Kjeldsen, H., Lissauer, J. J., Monet, D. G., Morrison, D., Sasselov, D., Tarter, J., Boss, A., Brownlee, D., Owen, T., Buzasi, D., Charbonneau, D., Doyle, L., Fortney, J., Ford, E. B., Holman, M. J., Seager, S., Steffen, J. H., Welsh, W. F., Rowe, J., Anderson, H., Buchhave, L.,

Ciardi, D., Walkowicz, L., Sherry, W., Horch, E., Isaacson, H., Everett, M. E., Fischer, D., Torres, G., Johnson, J. A., Endl, M., MacQueen, P., Bryson, S. T., Dotson, J., Haas, M., Kolodziejczak, J., Cleve, J. V., Chandrasekaran, H., Twicken, J. D., Quintana, E. V., Clarke, B. D., Allen, C., Li, J., Wu, H., Tenenbaum, P., Verner, E., Bruhweiler, F., Barnes, J., and Prsa, A. (2010). Kepler planet-detection mission: Introduction and first results. *Science*, 327(5968):977–980.

Campbell, B., Walker, G. A. H., and Yang, S. (1988). A Search for Substellar Companions to Solar-type Stars. , 331:902.

Collier Cameron, A., Bouchy, F., Hébrard, G., Maxted, P., Pollacco, D., Pont, F., Skillen, I., Smalley, B., Street, R. A., West, R. G., Wilson, D. M., Aigrain, S., Christian, D. J., Clarkson, W. I., Enoch, B., Evans, A., Fitzsimmons, A., Fleenor, M., Gillon, M., Haswell, C. A., Hebb, L., Hellier, C., Hodgkin, S. T., Horne, K., Irwin, J., Kane, S. R., Keenan, F. P., Loeillet, B., Lister, T. A., Mayor, M., Moutou, C., Norton, A. J., Osborne, J., Parley, N., Queloz, D., Ryans, R., Triaud, A. H. M. J., Udry, S., and Wheatley, P. J. (2007). WASP-1b and WASP-2b: two new transiting exoplanets detected with SuperWASP and SOPHIE. , 375(3):951–957.

Cosentino, R., Lovis, C., Pepe, F., Collier Cameron, A., Latham, D. W., Molinari, E., Udry, S., Bezawada, N., Black, M., Born, A., Buchschacher, N., Charbonneau, D., Figueira, P., Fleury, M., Galli, A., Gallie, A., Gao, X., Ghedina, A., Gonzalez, C., Gonzalez, M., Guerra, J., Henry, D., Horne, K., Hughes, I., Kelly, D., Lodi, M., Lunney, D., Maire, C., Mayor, M., Micela, G., Ordway, M. P., Peacock, J., Phillips, D., Piotto, G., Pollacco, D., Queloz, D., Rice, K., Riverol, C., Riverol, L., San Juan, J., Sasselov, D., Segransan, D., Sozzetti, A., Sosnowska, D., Stobie, B., Szentgyorgyi, A., Vick, A., and Weber, L. (2012). Harps-N: the new planet hunter at TNG. In McLean, I. S., Ramsay, S. K., and Takami, H., editors, *Ground-based and Airborne Instrumentation for Astronomy IV*, volume 8446 of *Society of Photo-Optical Instrumentation Engineers (SPIE) Conference Series*, page 84461V.

Daemgen, S., Hormuth, F., Brandner, W., Bergfors, C., Janson, M., Hippler, S., and Henning, T. (2009). Binarity of transit host stars. Implications for planetary parameters. , 498(2):567–574.

Damasso, M., Sozzetti, A., Lovis, C., Barros, S. C. C., Sousa, S. G., Demangeon, O. D. S., Faria, J. P., Lillo-Box, J., Cristiani, S., Pepe, F., Rebolo, R., Santos, N. C., Zapatero Osorio, M. R., González Hernández, J. I., Amate, M., Pasquini, L., Zerbi, F. M., Adibekyan, V., Abreu, M., Affolter, M., Alibert, Y., Aliverti, M., Allart, R., Allende Prieto, C., Álvarez, D., Alves, D., Avila, G., Baldini, V., Bandy, T., Benz, W., Bianco, A., Borsa, F., Bossini, D., Bourrier, V., Bouchy, F., Broeg, C., Cabral, A., Calderone, G., Cirami, R., Coelho, J., Conconi, P., Coretti, I., Cumani, C., Cupani, G., D'Odorico, V., Deiries, S., Dekker, H., Delabre, B., Di Marcantonio, P., Dumusque, X., Ehrenreich, D., Figueira, P., Fragoso, A., Genolet, L., Genoni, M., Génova Santos, R., Hughes, I., Iwert, O., Kerber, F., Knudstrup, J., Landoni, M., Lavie, B., Lizon, J. L., Lo Curto, G., Maire, C., Martins, C. J. A. P., Mégevand, D., Mehner, A., Micela, G., Modigliani, A., Molaro, P., Monteiro, M. A., Monteiro, M. J. P. F. G., Moschetti, M., Mueller, E., Murphy, M. T., Nunes, N., Oggioni, L., Oliveira, A., Oshagh, M., Pallé, E., Pariani, G., Poretti, E., Rasilla, J. L., Rebordão, J., Redaelli, E. M., Riva, M., Santana Tschudi, S., Santin, P., Santos, P., Ségransan, D., Schmidt, T. M., Segovia, A., Sosnowska, D., Spanò, P., Suárez Mascareño, A., Tabernero, H., Tenegi, F., Udry, S., and Zanutta, A. (2020). A precise architecture characterization of the π Mensae planetary system. , 642:A31.

Desidera, S., Damasso, M., Gratton, R., Benatti, S., Nardiello, D., D'Orazi, V., Lanza, A. F., Locci, D., Marzari, F., Mesa, D., Messina, S., Pillitteri, I., Sozzetti, A., Girard, J., Maggio, A., Micela, G., Malavolta, L., Nascimbeni, V., Pinamonti, M., Squicciarini, V., Alcalá, J., Biazzo, K., Bohn, A., Bonavita, M., Brooks, K., Chauvin, G., Covino, E., Delorme, P., Hagelberg, J., Janson, M., Lagrange, A. M., and Lazzoni, C. (2023). TOI-179: A young system with a transiting compact Neptune-mass planet and a low-mass companion in outer orbit. , 675:A158.

Espinoza, N., Bayliss, D., Hartman, J. D., Bakos, G. Á., Jordán, A., Zhou, G., Mancini, L., Brahm, R., Ciceri, S., Bhatti, W., Csubry, Z., Rabus, M., Penev, K., Bento, J., de Val-Borro, M., Henning,

T., Schmidt, B., Suc, V., Wright, D. J., Tinney, C. G., Tan, T. G., and Noyes, R. (2016). HATS-25b through HATS-30b: A Half-dozen New Inflated Transiting Hot Jupiters from the HATSouth Survey. , 152(4):108.

Evans, D. W., Eyer, L., Busso, G., Riello, M., De Angeli, F., Burgess, P. W., Audard, M., Clementini, G., Garofalo, A., Holl, B., Jevardat de Fombelle, G., Lanzafame, A. C., Lecoeur-Taibi, I., Mowlavi, N., Nienartowicz, K., Palaversa, L., and Rimoldini, L. (2023). Gaia Data Release 3. The Gaia Andromeda Photometric Survey. , 674:A4.

Fulton, B. J., Petigura, E. A., Howard, A. W., Isaacson, H., Marcy, G. W., Cargile, P. A., Hebb, L., Weiss, L. M., Johnson, J. A., Morton, T. D., Sinukoff, E., Crossfield, I. J. M., and Hirsch, L. A. (2017). The California-Kepler Survey. III. A Gap in the Radius Distribution of Small Planets. , 154(3):109.

Gaia Collaboration, Arenou, F., Babusiaux, C., Barstow, M. A., Faigler, S., Jorissen, A., Kervella, P., Mazeh, T., Mowlavi, N., Panuzzo, P., Sahlmann, J., Shahaf, S., Sozzetti, A., Bauchet, N., Damerdji, Y., Gavras, P., Giacobbe, P., Gosset, E., Halbwachs, J. L., Holl, B., Lattanzi, M. G., Leclerc, N., Morel, T., Pourbaix, D., Re Fiorentin, P., Sadowski, G., Ségransan, D., Siopis, C., Teyssier, D., Zwitter, T., Planquart, L., Brown, A. G. A., Vallenari, A., Prusti, T., de Bruijne, J. H. J., Biermann, M., Creevey, O. L., Ducourant, C., Evans, D. W., Eyer, L., Guerra, R., Hutton, A., Jordi, C., Klioner, S. A., Lammers, U. L., Lindegren, L., Luri, X., Mignard, F., Panem, C., Randich, S., Sartoretti, P., Soubiran, C., Tanga, P., Walton, N. A., Bailer-Jones, C. A. L., Bastian, U., Drimmel, R., Jansen, F., Katz, D., van Leeuwen, F., Bakker, J., Cacciari, C., Castañeda, J., De Angeli, F., Fabricius, C., Fouesneau, M., Frémat, Y., Galluccio, L., Guerrier, A., Heiter, U., Masana, E., Messineo, R., Nicolas, C., Nienartowicz, K., Pailler, F., Riclet, F., Roux, W., Seabroke, G. M., Sordo, R., Thévenin, F., Gracia-Abril, G., Portell, J., Altmann, M., Andrae, R., Audard, M., Bellas-Velidis, I., Benson, K., Berthier, J., Blomme, R., Burgess, P. W., Busonero, D., Busso, G., Cánovas, H., Carry, B., Cellino, A., Cheek, N., Clementini, G., Davidson, M., de Teodoro, P., Nuñez Campos, M., Delchambre, L., Dell'Oro, A., Esquej, P., Fernández-Hernández, J., Fraile, E., Garabato, D., García-Lario, P., Haigron, R., Hambly, N. C., Harrison, D. L., Hernández, J., Hestroffer, D., Hodgkin, S. T., Janßen, K., Jevardat de Fombelle, G., Jordan, S., Krone-Martins, A., Lanzafame, A. C., Löffler, W., Marchal, O., Marrese, P. M., Moitinho, A., Muinonen, K., Osborne, P., Pancino, E., Pauwels, T., Recio-Blanco, A., Reylé, C., Riello, M., Rimoldini, L., Roegiers, T., Rybizki, J., Sarro, L. M., Smith, M., Utrilla, E., van Leeuwen, M., Abbas, U., Ábrahám, P., Abreu Aramburu, A., Aerts, C., Aguado, J. J., Ajaj, M., Aldea-Montero, F., Altavilla, G., Álvarez, M. A., Alves, J., Anders, F., Anderson, R. I., Anglada Varela, E., Antoja, T., Baines, D., Baker, S. G., Balaguer-Núñez, L., Balbinot, E., Balog, Z., Barache, C., Barbato, D., Barros, M., Bartolomé, S., Bassilana, J. L., Becciani, U., Bellazzini, M., Berihuete, A., Bernet, M., Bertone, S., Bianchi, L., Binnenfeld, A., Blanco-Cuaresma, S., Blazere, A., Boch, T., Bombrun, A., Bossini, D., Bouquillon, S., Bragaglia, A., Bramante, L., Breedt, E., Bressan, A., Brouillet, N., Brugaletta, E., Bucciarelli, B., Burlacu, A., Butkevich, A. G., Buzzi, R., Caffau, E., Cancelliere, R., Cantat-Gaudin, T., Carballo, R., Carlucci, T., Carnerero, M. I., Carrasco, J. M., Casamiquela, L., Castellani, M., Castro-Ginard, A., Chaoul, L., Charlot, P., Chemin, L., Chiaramida, V., Chiavassa, A., Chornay, N., Comoretto, G., Contursi, G., Cooper, W. J., Cornez, T., Cowell, S., Crifo, F., Cropper, M., Crosta, M., Crowley, C., Dafonte, C., Dapergolas, A., David, P., de Laverny, P., De Luise, F., De March, R., De Ridder, J., de Souza, R., de Torres, A., del Peloso, E. F., del Pozo, E., Delbo, M., Delgado, A., Delisle, J. B., Demouchy, C., Dharmawardena, T. E., Diakite, S., Diener, C., Distefano, E., Dolding, C., Enke, H., Fabre, C., Fabrizio, M., Fedorets, G., Fernique, P., Figueras, F., Fournier, Y., Fouron, C., Fragkoudi, F., Gai, M., Garcia-Gutierrez, A., Garcia-Reinaldos, M., García-Torres, M., Garofalo, A., Gavel, A., Gerlach, E., Geyer, R., Gilmore, G., Girona, S., Giuffrida, G., Gomel, R., Gomez, A., González-Núñez, J., González-Santamaría, I., González-Vidal, J. J., Granvik, M., Guillout, P., Guiraud, J., Gutiérrez-Sánchez, R., Guy, L. P., Hatzidimitriou, D., Hauser, M., Haywood, M., Helmer, A., Helmi, A., Sarmiento, M. H., Hidalgo, S. L., Hilger, T., Hładczuk, N., Hobbs, D., Holland, G., Huckle, H. E., Jardine, K., Jasniewicz, G., Jean-Antoine Piccolo, A., Jiménez-Arranz, Ó., Juaristi Campillo, J., Julbe, F., Karbevska, L., Khanna, S., Kordopatis, G., Korn, A. J., Kóspál,

Á., Kostrzewa-Rutkowska, Z., Kruszyńska, K., Kun, M., Laizeau, P., Lambert, S., Lanza, A. F., Lasne, Y., Le Campion, J. F., Lebreton, Y., Lebzelter, T., Leccia, S., Lecoeur-Taibi, I., Liao, S., Licata, E. L., Lindstrøm, H. E. P., Lister, T. A., Livanou, E., Lobel, A., Lorca, A., Loup, C., Madrero Pardo, P., Magdaleno Romeo, A., Managau, S., Mann, R. G., Manteiga, M., Marchant, J. M., Marconi, M., Marcos, J., Marcos Santos, M. M. S., Marín Pina, D., Marinoni, S., Marocco, F., Marshall, D. J., Martin Polo, L., Martín-Fleitas, J. M., Marton, G., Mary, N., Masip, A., Massari, D., Mastrobuono-Battisti, A., McMillan, P. J., Messina, S., Michalik, D., Millar, N. R., Mints, A., Molina, D., Molinaro, R., Molnár, L., Monari, G., Monguió, M., Montegriffo, P., Montero, A., Mor, R., Mora, A., Morbidelli, R., Morris, D., Muraveva, T., Murphy, C. P., Musella, I., Nagy, Z., Noval, L., Ocaña, F., Ogden, A., Ordenovic, C., Osinde, J. O., Pagani, C., Pagano, I., Palaversa, L., Palicio, P. A., Pallas-Quintela, L., Panahi, A., Payne-Wardenaar, S., Peñalosa Esteller, X., Penttilä, A., Pichon, B., Piersimoni, A. M., Pineau, F. X., Plachy, E., Plum, G., Poggio, E., Prša, A., Pulone, L., Racero, E., Ragaini, S., Rainer, M., Raiteri, C. M., Ramos, P., Ramos-Lerate, M., Regibo, S., Richards, P. J., Rios Diaz, C., Ripepi, V., Riva, A., Rix, H. W., Rixon, G., Robichon, N., Robin, A. C., Robin, C., Roelens, M., Rogues, H. R. O., Rohrbasser, L., Romero-Gómez, M., Rowell, N., Royer, F., Ruz Mieres, D., Rybicki, K. A., Sáez Núñez, A., Sagristà Sellés, A., Salguero, E., Samaras, N., Sanchez Gimenez, V., Sanna, N., Santoveña, R., Sarasso, M., Schultheis, M., Sciacca, E., Segol, M., Segovia, J. C., Semeux, D., Siddiqui, H. I., Siebert, A., Siltala, L., Silvelo, A., Slezak, E., Slezak, I., Smart, R. L., Snaith, O. N., Solano, E., Solitro, F., Souami, D., Souchay, J., Spagna, A., Spina, L., Spoto, F., Steele, I. A., Steidelmüller, H., Stephenson, C. A., Süveges, M., Surdej, J., Szabados, L., Szegedi-Elek, E., Taris, F., Taylor, M. B., Teixeira, R., Tolomei, L., Tonello, N., Torra, F., Torra, J., Torralba Elipe, G., Trabucchi, M., Tsounis, A. T., Turon, C., Ulla, A., Unger, N., Vaillant, M. V., van Dillen, E., van Reeven, W., Vanel, O., Vecchiato, A., Viala, Y., Vicente, D., Voutsinas, S., Weiler, M., Wevers, T., Wyrzykowski, Ł., Yoldas, A., Yvard, P., Zhao, H., Zorec, J., and Zucker, S. (2023a). Gaia Data Release 3. Stellar multiplicity, a teaser for the hidden treasure. , 674:A34.

Gaia Collaboration, Prusti, T., de Bruijne, J. H. J., Brown, A. G. A., Vallenari, A., Babusiaux, C., Bailer-Jones, C. A. L., Bastian, U., Biermann, M., Evans, D. W., Eyer, L., Jansen, F., Jordi, C., Klioner, S. A., Lammers, U., Lindegren, L., Luri, X., Mignard, F., Milligan, D. J., Panem, C., Poinsignon, V., Pourbaix, D., Randich, S., Sarri, G., Sartoretti, P., Siddiqui, H. I., Soubiran, C., Valette, V., van Leeuwen, F., Walton, N. A., Aerts, C., Arenou, F., Cropper, M., Drimmel, R., Høg, E., Katz, D., Lattanzi, M. G., O'Mullane, W., Grebel, E. K., Holland, A. D., Huc, C., Passot, X., Bramante, L., Cacciari, C., Castañeda, J., Chaoul, L., Cheek, N., De Angeli, F., Fabricius, C., Guerra, R., Hernández, J., Jean-Antoine-Piccolo, A., Masana, E., Messineo, R., Mowlavi, N., Nienartowicz, K., Ordóñez-Blanco, D., Panuzzo, P., Portell, J., Richards, P. J., Riello, M., Seabroke, G. M., Tanga, P., Thévenin, F., Torra, J., Els, S. G., Gracia-Abril, G., Comoretto, G., Garcia-Reinaldos, M., Lock, T., Mercier, E., Altmann, M., Andrae, R., Astraatmadja, T. L., Bellas-Velidis, I., Benson, K., Berthier, J., Blomme, R., Busso, G., Carry, B., Cellino, A., Clementini, G., Cowell, S., Creevey, O., Cuypers, J., Davidson, M., De Ridder, J., de Torres, A., Delchambre, L., Dell'Oro, A., Ducourant, C., Frémat, Y., García-Torres, M., Gosset, E., Halbwachs, J. L., Hambly, N. C., Harrison, D. L., Hauser, M., Hestroffer, D., Hodgkin, S. T., Huckle, H. E., Hutton, A., Jasniewicz, G., Jordan, S., Kontizas, M., Korn, A. J., Lanzafame, A. C., Manteiga, M., Moitinho, A., Muinonen, K., Osinde, J., Pancino, E., Pauwels, T., Petit, J. M., Recio-Blanco, A., Robin, A. C., Sarro, L. M., Siopis, C., Smith, M., Smith, K. W., Sozzetti, A., Thuillot, W., van Reeven, W., Viala, Y., Abbas, U., Abreu Aramburu, A., Accart, S., Aguado, J. J., Allan, P. M., Allasia, W., Altavilla, G., Álvarez, M. A., Alves, J., Anderson, R. I., Andrei, A. H., Anglada Varela, E., Antiche, E., Antoja, T., Antón, S., Arcay, B., Atzei, A., Ayache, L., Bach, N., Baker, S. G., Balaguer-Núñez, L., Barache, C., Barata, C., Barbier, A., Barblan, F., Baroni, M., Barrado y Navascués, D., Barros, M., Barstow, M. A., Becciani, U., Bellazzini, M., Bellei, G., Bello García, A., Belokurov, V., Bendjoya, P., Berihuete, A., Bianchi, L., Bienaymé, O., Billebaud, F., Blagorodnova, N., Blanco-Cuaresma, S., Boch, T., Bombrun, A., Borrachero, R., Bouquillon, S., Bourda, G., Bouy, H., Bragaglia, A., Breddels, M. A., Brouillet, N., Brüsemeister, T., Bucciarelli, B., Budnik, F., Burgess, P., Burgon, R., Burlacu, A., Busonero, D., Buzzi, R., Caffau, E., Cambras, J., Campbell, H., Cancelliere, R.,

Cantat-Gaudin, T., Carlucci, T., Carrasco, J. M., Castellani, M., Charlot, P., Charnas, J., Charvet, P., Chassat, F., Chiavassa, A., Clotet, M., Cocozza, G., Collins, R. S., Collins, P., Costigan, G., Crifo, F., Cross, N. J. G., Crosta, M., Crowley, C., Dafonte, C., Damerdji, Y., Dapergolas, A., David, P., David, M., De Cat, P., de Felice, F., de Laverny, P., De Luise, F., De March, R., de Martino, D., de Souza, R., Debosscher, J., del Pozo, E., Delbo, M., Delgado, A., Delgado, H. E., di Marco, F., Di Matteo, P., Diakite, S., Distefano, E., Dolding, C., Dos Anjos, S., Drazinos, P., Durán, J., Dzigan, Y., Ecale, E., Edvardsson, B., Enke, H., Erdmann, M., Escolar, D., Espina, M., Evans, N. W., Eynard Bontemps, G., Fabre, C., Fabrizio, M., Faigler, S., Falcão, A. J., Farràs Casas, M., Faye, F., Federici, L., Fedorets, G., Fernández-Hernández, J., Fernique, P., Fienga, A., Figueras, F., Filippi, F., Findeisen, K., Fonti, A., Fouesneau, M., Fraile, E., Fraser, M., Fuchs, J., Furnell, R., Gai, M., Galleti, S., Galluccio, L., Garabato, D., García-Sedano, F., Garé, P., Garofalo, A., Garralda, N., Gavras, P., Gerssen, J., Geyer, R., Gilmore, G., Girona, S., Giuffrida, G., Gomes, M., González-Marcos, A., González-Núñez, J., González-Vidal, J. J., Granvik, M., Guerrier, A., Guillout, P., Guiraud, J., Gúrpide, A., Gutiérrez-Sánchez, R., Guy, L. P., Haigron, R., Hatzidimitriou, D., Haywood, M., Heiter, U., Helmi, A., Hobbs, D., Hofmann, W., Holl, B., Holland, G., Hunt, J. A. S., Hypki, A., Icardi, V., Irwin, M., Jevardat de Fombelle, G., Jofré, P., Jonker, P. G., Jorissen, A., Julbe, F., Karampelas, A., Kochoska, A., Kohley, R., Kolenberg, K., Kontizas, E., Koposov, S. E., Kordopatis, G., Koubsky, P., Kowalczyk, A., Krone-Martins, A., Kudryashova, M., Kull, I., Bachchan, R. K., Lacoste-Seris, F., Lanza, A. F., Lavigne, J. B., Le Poncin-Lafitte, C., Lebreton, Y., Lebzelter, T., Leccia, S., Leclerc, N., Lecoeur-Taibi, I., Lemaitre, V., Lenhardt, H., Leroux, F., Liao, S., Licata, E., Lindstrøm, H. E. P., Lister, T. A., Livanou, E., Lobel, A., Löffler, W., López, M., Lopez-Lozano, A., Lorenz, D., Loureiro, T., MacDonald, I., Magalhães Fernandes, T., Managau, S., Mann, R. G., Mantelet, G., Marchal, O., Marchant, J. M., Marconi, M., Marie, J., Marinoni, S., Marrese, P. M., Marschalkó, G., Marshall, D. J., Martín-Fleitas, J. M., Martino, M., Mary, N., Matijevič, G., Mazeh, T., McMillan, P. J., Messina, S., Mestre, A., Michalik, D., Millar, N. R., Miranda, B. M. H., Molina, D., Molinaro, R., Molinaro, M., Molnár, L., Moniez, M., Montegriffo, P., Monteiro, D., Mor, R., Mora, A., Morbidelli, R., Morel, T., Morgenthaler, S., Morley, T., Morris, D., Mulone, A. F., Muraveva, T., Musella, I., Narbonne, J., Nelemans, G., Nicastro, L., Noval, L., Ordénovic, C., Ordieres-Meré, J., Osborne, P., Pagani, C., Pagano, I., Pailler, F., Palacin, H., Palaversa, L., Parsons, P., Paulsen, T., Pecoraro, M., Pedrosa, R., Pentikäinen, H., Pereira, J., Pichon, B., Piersimoni, A. M., Pineau, F. X., Plachy, E., Plum, G., Poujoulet, E., Prša, A., Pulone, L., Ragaini, S., Rago, S., Rambaux, N., Ramos-Lerate, M., Ranalli, P., Rauw, G., Read, A., Regibo, S., Renk, F., Reylé, C., Ribeiro, R. A., Rimoldini, L., Ripepi, V., Riva, A., Rixon, G., Roelens, M., Romero-Gómez, M., Rowell, N., Royer, F., Rudolph, A., Ruiz-Dern, L., Sadowski, G., Sagristà Sellés, T., Sahlmann, J., Salgado, J., Salguero, E., Sarasso, M., Savietto, H., Schnorhk, A., Schultheis, M., Sciacca, E., Segol, M., Segovia, J. C., Segransan, D., Serpell, E., Shih, I. C., Smareglia, R., Smart, R. L., Smith, C., Solano, E., Solitro, F., Sordo, R., Soria Nieto, S., Souchay, J., Spagna, A., Spoto, F., Stampa, U., Steele, I. A., Steidelmüller, H., Stephenson, C. A., Stoev, H., Suess, F. F., Süveges, M., Surdej, J., Szabados, L., Szegedi-Elek, E., Tapiador, D., Taris, F., Tauran, G., Taylor, M. B., Teixeira, R., Terrett, D., Tingley, B., Trager, S. C., Turon, C., Ulla, A., Utrilla, E., Valentini, G., van Elteren, A., Van Hemelryck, E., van Leeuwen, M., Varadi, M., Vecchiato, A., Veljanoski, J., Via, T., Vicente, D., Vogt, S., Voss, H., Votruba, V., Voutsinas, S., Walmsley, G., Weiler, M., Weingrill, K., Werner, D., Wevers, T., Whitehead, G., Wyrzykowski, Ł., Yoldas, A., Žerjal, M., Zucker, S., Zurbach, C., Zwitter, T., Alecu, A., Allen, M., Allende Prieto, C., Amorim, A., Anglada-Escudé, G., Arsenijevic, V., Azaz, S., Balm, P., Beck, M., Bernstein, H. H., Bigot, L., Bijaoui, A., Blasco, C., Bonfigli, M., Bono, G., Boudreault, S., Bressan, A., Brown, S., Brunet, P. M., Bunclark, P., Buonanno, R., Butkevich, A. G., Carret, C., Carrion, C., Chemin, L., Chéreau, F., Corcione, L., Darmigny, E., de Boer, K. S., de Teodoro, P., de Zeeuw, P. T., Delle Luche, C., Domingues, C. D., Dubath, P., Fodor, F., Frézouls, B., Fries, A., Fustes, D., Fyfe, D., Gallardo, E., Gallegos, J., Gardiol, D., Gebran, M., Gomboc, A., Gómez, A., Grux, E., Gueguen, A., Heyrovsky, A., Hoar, J., Iannicola, G., Isasi Parache, Y., Janotto, A. M., Joliet, E., Jonckheere, A., Keil, R., Kim, D. W., Klagyivik, P., Klar, J., Knude, J., Kochukhov, O., Kolka, I., Kos, J., Kutka, A., Lainey, V., LeBouquin, D., Liu, C., Loreggia, D.,

Makarov, V. V., Marseille, M. G., Martayan, C., Martinez-Rubi, O., Massart, B., Meynadier, F., Mignot, S., Munari, U., Nguyen, A. T., Nordlander, T., Ocvirk, P., O'Flaherty, K. S., Olias Sanz, A., Ortiz, P., Osorio, J., Oszkiewicz, D., Ouzounis, A., Palmer, M., Park, P., Pasquato, E., Peltzer, C., Peralta, J., Péturaud, F., Pieniluoma, T., Pigozzi, E., Poels, J., Prat, G., Prod'homme, T., Raison, F., Rebordao, J. M., Risquez, D., Rocca-Volmerange, B., Rosen, S., Ruiz-Fuertes, M. I., Russo, F., Sembay, S., Serraller Vizcaino, I., Short, A., Siebert, A., Silva, H., Sinachopoulos, D., Slezak, E., Soffel, M., Sosnowska, D., Straižys, V., ter Linden, M., Terrell, D., Theil, S., Tiede, C., Troisi, L., Tsalmantza, P., Tur, D., Vaccari, M., Vachier, F., Valles, P., Van Hamme, W., Veltz, L., Virtanen, J., Wallut, J. M., Wichmann, R., Wilkinson, M. I., Ziaeepour, H., and Zschocke, S. (2016). The Gaia mission. , 595:A1.

Gaia Collaboration, Vallenari, A., Brown, A. G. A., Prusti, T., de Bruijne, J. H. J., Arenou, F., Babusiaux, C., Biermann, M., Creevey, O. L., Ducourant, C., Evans, D. W., Eyer, L., Guerra, R., Hutton, A., Jordi, C., Klioner, S. A., Lammers, U. L., Lindegren, L., Luri, X., Mignard, F., Panem, C., Pourbaix, D., Randich, S., Sartoretti, P., Soubiran, C., Tanga, P., Walton, N. A., Bailer-Jones, C. A. L., Bastian, U., Drimmel, R., Jansen, F., Katz, D., Lattanzi, M. G., van Leeuwen, F., Bakker, J., Cacciari, C., Castañeda, J., De Angeli, F., Fabricius, C., Fouesneau, M., Frémat, Y., Galluccio, L., Guerrier, A., Heiter, U., Masana, E., Messineo, R., Mowlavi, N., Nicolas, C., Nienartowicz, K., Pailler, F., Panuzzo, P., Riclet, F., Roux, W., Seabroke, G. M., Sordo, R., Thévenin, F., Gracia-Abril, G., Portell, J., Teyssier, D., Altmann, M., Andrae, R., Audard, M., Bellas-Velidis, I., Benson, K., Berthier, J., Blomme, R., Burgess, P. W., Busonero, D., Busso, G., Cánovas, H., Carry, B., Cellino, A., Cheek, N., Clementini, G., Damerdji, Y., Davidson, M., de Teodoro, P., Nuñez Campos, M., Delchambre, L., Dell'Oro, A., Esquej, P., Fernández-Hernández, J., Fraile, E., Garabato, D., García-Lario, P., Gosset, E., Haigron, R., Halbwachs, J. L., Hambly, N. C., Harrison, D. L., Hernández, J., Hestroffer, D., Hodgkin, S. T., Holl, B., Janßen, K., Jevardat de Fombelle, G., Jordan, S., Krone-Martins, A., Lanzafame, A. C., Löffler, W., Marchal, O., Marrese, P. M., Moitinho, A., Muinonen, K., Osborne, P., Pancino, E., Pauwels, T., Recio-Blanco, A., Reylé, C., Riello, M., Rimoldini, L., Roegiers, T., Rybizki, J., Sarro, L. M., Siopis, C., Smith, M., Sozzetti, A., Utrilla, E., van Leeuwen, M., Abbas, U., Ábrahám, P., Abreu Aramburu, A., Aerts, C., Aguado, J. J., Ajaj, M., Aldea-Montero, F., Altavilla, G., Álvarez, M. A., Alves, J., Anders, F., Anderson, R. I., Anglada Varela, E., Antoja, T., Baines, D., Baker, S. G., Balaguer-Núñez, L., Balbinot, E., Balog, Z., Barache, C., Barbato, D., Barros, M., Barstow, M. A., Bartolomé, S., Bassilana, J. L., Bauchet, N., Becciani, U., Bellazzini, M., Berihuete, A., Bernet, M., Bertone, S., Bianchi, L., Binnenfeld, A., Blanco-Cuaresma, S., Blazere, A., Boch, T., Bombrun, A., Bossini, D., Bouquillon, S., Bragaglia, A., Bramante, L., Breedt, E., Bressan, A., Brouillet, N., Brugaletta, E., Bucciarelli, B., Burlacu, A., Butkevich, A. G., Buzzi, R., Caffau, E., Cancelliere, R., Cantat-Gaudin, T., Carballo, R., Carlucci, T., Carnerero, M. I., Carrasco, J. M., Casamiquela, L., Castellani, M., Castro-Ginard, A., Chaoul, L., Charlot, P., Chemin, L., Chiaramida, V., Chiavassa, A., Chornay, N., Comoretto, G., Contursi, G., Cooper, W. J., Cornez, T., Cowell, S., Crifo, F., Cropper, M., Crosta, M., Crowley, C., Dafonte, C., Dapergolas, A., David, M., David, P., de Laverny, P., De Luise, F., De March, R., De Ridder, J., de Souza, R., de Torres, A., del Peloso, E. F., del Pozo, E., Delbo, M., Delgado, A., Delisle, J. B., Demouchy, C., Dharmawardena, T. E., Di Matteo, P., Diakite, S., Diener, C., Distefano, E., Dolding, C., Edvardsson, B., Enke, H., Fabre, C., Fabrizio, M., Faigler, S., Fedorets, G., Fernique, P., Fienga, A., Figueras, F., Fournier, Y., Fouron, C., Fragkoudi, F., Gai, M., Garcia-Gutierrez, A., Garcia-Reinaldos, M., García-Torres, M., Garofalo, A., Gavel, A., Gavras, P., Gerlach, E., Geyer, R., Giacobbe, P., Gilmore, G., Girona, S., Giuffrida, G., Gomel, R., Gomez, A., González-Núñez, J., González-Santamaría, I., González-Vidal, J. J., Granvik, M., Guillout, P., Guiraud, J., Gutiérrez-Sánchez, R., Guy, L. P., Hatzidimitriou, D., Hauser, M., Haywood, M., Helmer, A., Helmi, A., Sarmiento, M. H., Hidalgo, S. L., Hilger, T., Hładczuk, N., Hobbs, D., Holland, G., Huckle, H. E., Jardine, K., Jasniewicz, G., Jean-Antoine Piccolo, A., Jiménez-Arranz, Ó., Jorissen, A., Juaristi Campillo, J., Julbe, F., Karbevska, L., Kervella, P., Khanna, S., Kontizas, M., Kordopatis, G., Korn, A. J., Kóspál, Á., Kostrzewa-Rutkowska, Z., Kruszyńska, K., Kun, M., Laizeau, P., Lambert, S., Lanza, A. F., Lasne, Y., Le Campion, J. F., Lebreton, Y., Lebzelter, T., Leccia, S., Leclerc, N., Lecoeur-Taibi, I., Liao, S., Licata, E. L., Lindstrøm, H. E. P., Lister, T. A.,

Livanou, E., Lobel, A., Lorca, A., Loup, C., Madrero Pardo, P., Magdaleno Romeo, A., Managau, S., Mann, R. G., Manteiga, M., Marchant, J. M., Marconi, M., Marcos, J., Marcos Santos, M. M. S., Marín Pina, D., Marinoni, S., Marocco, F., Marshall, D. J., Martin Polo, L., Martín-Fleitas, J. M., Marton, G., Mary, N., Masip, A., Massari, D., Mastrobuono-Battisti, A., Mazeh, T., McMillan, P. J., Messina, S., Michalik, D., Millar, N. R., Mints, A., Molina, D., Molinaro, R., Molnár, L., Monari, G., Monguió, M., Montegriffo, P., Montero, A., Mor, R., Mora, A., Morbidelli, R., Morel, T., Morris, D., Muraveva, T., Murphy, C. P., Musella, I., Nagy, Z., Noval, L., Ocaña, F., Ogden, A., Ordenovic, C., Osinde, J. O., Pagani, C., Pagano, I., Palaversa, L., Palicio, P. A., Pallas-Quintela, L., Panahi, A., Payne-Wardenaar, S., Peñalosa Esteller, X., Penttilä, A., Pichon, B., Piersimoni, A. M., Pineau, F. X., Plachy, E., Plum, G., Poggio, E., Prša, A., Pulone, L., Racero, E., Ragaini, S., Rainer, M., Raiteri, C. M., Rambaux, N., Ramos, P., Ramos-Lerate, M., Re Fiorentin, P., Regibo, S., Richards, P. J., Rios Diaz, C., Ripepi, V., Riva, A., Rix, H. W., Rixon, G., Robichon, N., Robin, A. C., Robin, C., Roelens, M., Rogues, H. R. O., Rohrbasser, L., Romero-Gómez, M., Rowell, N., Royer, F., Ruz Mieres, D., Rybicki, K. A., Sadowski, G., Sáez Núñez, A., Sagristà Sellés, A., Sahlmann, J., Salguero, E., Samaras, N., Sanchez Gimenez, V., Sanna, N., Santoveña, R., Sarasso, M., Schultheis, M., Sciacca, E., Segol, M., Segovia, J. C., Ségransan, D., Semeux, D., Shahaf, S., Siddiqui, H. I., Siebert, A., Siltala, L., Silvelo, A., Slezak, E., Slezak, I., Smart, R. L., Snaith, O. N., Solano, E., Solitro, F., Souami, D., Souchay, J., Spagna, A., Spina, L., Spoto, F., Steele, I. A., Steidelmüller, H., Stephenson, C. A., Süveges, M., Surdej, J., Szabados, L., Szegedi-Elek, E., Taris, F., Taylor, M. B., Teixeira, R., Tolomei, L., Tonello, N., Torra, F., Torra, J., Torralba Elipe, G., Trabucchi, M., Tsounis, A. T., Turon, C., Ulla, A., Unger, N., Vaillant, M. V., van Dillen, E., van Reeven, W., Vanel, O., Vecchiato, A., Viala, Y., Vicente, D., Voutsinas, S., Weiler, M., Wevers, T., Wyrzykowski, Ł., Yoldas, A., Yvard, P., Zhao, H., Zorec, J., Zucker, S., and Zwitter, T. (2023b). Gaia Data Release 3. Summary of the content and survey properties. , 674:A1.

Gatewood, G. and Eichhorn, H. (1973). An unsuccessful search for a planetary companion of Barnard's star BD +4 3561. , 78:769–776.

Gould, A. and Loeb, A. (1992). Discovering Planetary Systems through Gravitational Microlenses. , 396:104.

Grieves, N., Bouchy, F., Lendl, M., Carmichael, T., Mireles, I., Shporer, A., McLeod, K. K., Collins, K. A., Brahm, R., Stassun, K. G., Gill, S., Bouma, L. G., Guillot, T., Cointepas, M., Dos Santos, L. A., Casewell, S. L., Jenkins, J. M., Henning, T., Nielsen, L. D., Psaridi, A., Udry, S., Ségransan, D., Eastman, J. D., Zhou, G., Abe, L., Agabi, A., Bakos, G., Charbonneau, D., Collins, K. I., Colon, K. D., Crouzet, N., Dransfield, G., Evans, P., Goeke, R. F., Hart, R., Irwin, J. M., Jensen, E. L. N., Jordán, A., Kielkopf, J. F., Latham, D. W., Marie-Sainte, W., Mékarnia, D., Nelson, P., Quinn, S. N., Radford, D. J., Rodriguez, D. R., Rowden, P., Schmider, F.-X., Schwarz, R. P., Smith, J. C., Stockdale, C., Suarez, O., Tan, T.-G., Triaud, A. H. M. J., Waalkes, W., and Wingham, G. (2021). Populating the brown dwarf and stellar boundary: Five stars with transiting companions near the hydrogen-burning mass limit. , 652:A127.

Guerrero, N. M., Seager, S., Huang, C. X., Vanderburg, A., Garcia Soto, A., Mireles, I., Hesse, K., Fong, W., Glidden, A., Shporer, A., Latham, D. W., Collins, K. A., Quinn, S. N., Burt, J., Dragomir, D., Crossfield, I., Vanderspek, R., Fausnaugh, M., Burke, C. J., Ricker, G., Daylan, T., Essack, Z., Günther, M. N., Osborn, H. P., Pepper, J., Rowden, P., Sha, L., Villanueva, Steven, J., Yahalomi, D. A., Yu, L., Ballard, S., Batalha, N. M., Berardo, D., Chontos, A., Dittmann, J. A., Esquerdo, G. A., Mikal-Evans, T., Jayaraman, R., Krishnamurthy, A., Louie, D. R., Mehrle, N., Niraula, P., Rackham, B. V., Rodriguez, J. E., Rowden, S. J. L., Sousa-Silva, C., Watanabe, D., Wong, I., Zhan, Z., Zivanovic, G., Christiansen, J. L., Ciardi, D. R., Swain, M. A., Lund, M. B., Mullally, S. E., Fleming, S. W., Rodriguez, D. R., Boyd, P. T., Quintana, E. V., Barclay, T., Colón, K. D., Rinehart, S. A., Schlieder, J. E., Clampin, M., Jenkins, J. M., Twicken, J. D., Caldwell, D. A., Coughlin, J. L., Henze, C., Lissauer, J. J., Morris, R. L., Rose, M. E., Smith, J. C., Tenenbaum, P., Ting, E. B., Wohler, B., Bakos, G. Á., Bean, J. L., Berta-Thompson, Z. K., Bieryla, A., Bouma, L. G., Buchhave, L. A., Butler, N., Charbonneau, D., Doty, J. P., Ge, J., Holman, M. J., Howard,

A. W., Kaltenegger, L., Kane, S. R., Kjeldsen, H., Kreidberg, L., Lin, D. N. C., Minsky, C., Narita, N., Paegert, M., Pál, A., Palle, E., Sasselov, D. D., Spencer, A., Sozzetti, A., Stassun, K. G., Torres, G., Udry, S., and Winn, J. N. (2021). The TESS Objects of Interest Catalog from the TESS Prime Mission. , 254(2):39.

Heath, M. J. and Doyle, L. R. (2011). Kepler 16: A System of Potential Interest to Astrobiologists. *arXiv e-prints*, page arXiv:1111.0002.

Hellier, C., Anderson, D. R., Collier Cameron, A., Gillon, M., Hebb, L., Maxted, P. F. L., Queloz, D., Smalley, B., Triaud, A. H. M. J., West, R. G., Wilson, D. M., Bentley, S. J., Enoch, B., Horne, K., Irwin, J., Lister, T. A., Mayor, M., Parley, N., Pepe, F., Pollacco, D. L., Segransan, D., Udry, S., and Wheatley, P. J. (2009). An orbital period of 0.94days for the hot-Jupiter planet WASP-18b. , 460(7259):1098–1100.

Holl, B., Sozzetti, A., Sahlmann, J., Giacobbe, P., Ségransan, D., Unger, N., Delisle, J. B., Barbato, D., Lattanzi, M. G., Morbidelli, R., and Sosnowska, D. (2023). Gaia Data Release 3. Astrometric orbit determination with Markov chain Monte Carlo and genetic algorithms: Systems with stellar, sub-stellar, and planetary mass companions. , 674:A10.

Howell, S. B., Sobeck, C., Haas, M., Still, M., Barclay, T., Mullally, F., Troeltzsch, J., Aigrain, S., Bryson, S. T., Caldwell, D., Chaplin, W. J., Cochran, W. D., Huber, D., Marcy, G. W., Miglio, A., Najita, J. R., Smith, M., Twicken, J. D., and Fortney, J. J. (2014). The K2 Mission: Characterization and Early Results. , 126(938):398.

Jacob, W. S. (1855). On certain Anomalies presented by the Binary Star 70 Ophiuchi. , 15:228.

Jones, H. R. A., Paul Butler, R., Tinney, C. G., Marcy, G. W., Penny, A. J., McCarthy, C., Carter, B. D., and Pourbaix, D. (2002). A probable planetary companion to HD 39091 from the Anglo-Australian Planet Search. , 333(4):871–875.

Kervella, P., Arenou, F., Mignard, F., and Thévenin, F. (2019a). Stellar and substellar companions of nearby stars from Gaia DR2. Binarity from proper motion anomaly. , 623:A72.

Kervella, P., Arenou, F., and Thévenin, F. (2022). Stellar and substellar companions from Gaia EDR3. Proper-motion anomaly and resolved common proper-motion pairs. , 657:A7.

Kervella, P., Gallenne, A., Evans, N. R., Szabados, L., Arenou, F., Mérand, A., Nardetto, N., Gieren, W., and Pietrzynski, G. (2019b). Multiplicity of Galactic Cepheids and RR Lyrae stars from Gaia DR2. II. Resolved common proper motion pairs. , 623:A117.

Kostov, V. B., Orosz, J. A., Feinstein, A. D., Welsh, W. F., Cukier, W., Haghighipour, N., Quarles, B., Martin, D. V., Montet, B. T., Torres, G., Triaud, A. H. M. J., Barclay, T., Boyd, P., Briceno, C., Cameron, A. C., Correia, A. C. M., Gilbert, E. A., Gill, S., Gillon, M., Haqq-Misra, J., Hellier, C., Dressing, C., Fabrycky, D. C., Furesz, G., Jenkins, J. M., Kane, S. R., Kopparapu, R., Hodžić, V. K., Latham, D. W., Law, N., Levine, A. M., Li, G., Lintott, C., Lissauer, J. J., Mann, A. W., Mazeh, T., Mardling, R., Maxted, P. F. L., Eisner, N., Pepe, F., Pepper, J., Pollacco, D., Quinn, S. N., Quintana, E. V., Rowe, J. F., Ricker, G., Rose, M. E., Seager, S., Santerne, A., Ségransan, D., Short, D. R., Smith, J. C., Standing, M. R., Tokovinin, A., Trifonov, T., Turner, O., Twicken, J. D., Udry, S., Vanderspek, R., Winn, J. N., Wolf, E. T., Ziegler, C., Ansorge, P., Barnet, F., Bergeron, J., Huten, M., Pappa, G., and van der Straeten, T. (2020). TOI-1338: TESS' First Transiting Circumbinary Planet. , 159(6):253.

Latham, D. W., Mazeh, T., Stefanik, R. P., Mayor, M., and Burki, G. (1989). The unseen companion of HD114762: a probable brown dwarf. , 339(6219):38–40.

Marois, C., Macintosh, B., Barman, T., Zuckerman, B., Song, I., Patience, J., Lafrenière, D., and Doyon, R. (2008). Direct Imaging of Multiple Planets Orbiting the Star HR 8799. *Science*, 322(5906):1348.

Mayor, M., Pepe, F., Queloz, D., Bouchy, F., Rupprecht, G., Lo Curto, G., Avila, G., Benz, W., Bertaux, J. L., Bonfils, X., Dall, T., Dekker, H., Delabre, B., Eckert, W., Fleury, M., Gilliotte, A., Gojak, D., Guzman, J. C., Kohler, D., Lizon, J. L., Longinotti, A., Lovis, C., Megevand, D., Pasquini, L., Reyes, J., Sivan, J. P., Sosnowska, D., Soto, R., Udry, S., van Kesteren, A., Weber, L., and Weilenmann, U. (2003). Setting New Standards with HARPS. *The Messenger*, 114:20–24.

Mayor, M. and Queloz, D. (1995). A Jupiter-mass companion to a solar-type star. , 378(6555):355–359.

Moulton, F. R. (1899). The limits of temporary stability of satellite motion, with an application to the question of the existence of an unseen body in the binary system 70 Ophiuchi. , 20:33–37.

Pepe, F., Cristiani, S., Rebolo, R., Santos, N. C., Dekker, H., Cabral, A., Di Marcantonio, P., Figueira, P., Lo Curto, G., Lovis, C., Mayor, M., Mégevand, D., Molaro, P., Riva, M., Zapatero Osorio, M. R., Amate, M., Manescau, A., Pasquini, L., Zerbi, F. M., Adibekyan, V., Abreu, M., Affolter, M., Alibert, Y., Aliverti, M., Allart, R., Allende Prieto, C., Álvarez, D., Alves, D., Avila, G., Baldini, V., Bandy, T., Barros, S. C. C., Benz, W., Bianco, A., Borsa, F., Bourrier, V., Bouchy, F., Broeg, C., Calderone, G., Cirami, R., Coelho, J., Conconi, P., Coretti, I., Cumani, C., Cupani, G., D'Odorico, V., Damasso, M., Deiries, S., Delabre, B., Demangeon, O. D. S., Dumusque, X., Ehrenreich, D., Faria, J. P., Fragoso, A., Genolet, L., Genoni, M., Génova Santos, R., González Hernández, J. I., Hughes, I., Iwert, O., Kerber, F., Knudstrup, J., Landoni, M., Lavie, B., Lillo-Box, J., Lizon, J. L., Maire, C., Martins, C. J. A. P., Mehner, A., Micela, G., Modigliani, A., Monteiro, M. A., Monteiro, M. J. P. F. G., Moschetti, M., Murphy, M. T., Nunes, N., Oggioni, L., Oliveira, A., Oshagh, M., Pallé, E., Pariani, G., Poretti, E., Rasilla, J. L., Rebordão, J., Redaelli, E. M., Santana Tschudi, S., Santin, P., Santos, P., Ségransan, D., Schmidt, T. M., Segovia, A., Sosnowska, D., Sozzetti, A., Sousa, S. G., Spanò, P., Suárez Mascareño, A., Tabernero, H., Tenegi, F., Udry, S., and Zanutta, A. (2021). ESPRESSO at VLT. On-sky performance and first results. , 645:A96.

Pepper, J., Gould, A., and Depoy, D. L. (2003). Using All-Sky Surveys to Find Planetary Transits. , 53:213–228.

Perryman, M. (2011). *The Exoplanet Handbook*.

Perryman, M. (2018). *The Exoplanet Handbook*.

Pollacco, D. L., Skillen, I., Collier Cameron, A., Christian, D. J., Hellier, C., Irwin, J., Lister, T. A., Street, R. A., West, R. G., Anderson, D. R., Clarkson, W. I., Deeg, H., Enoch, B., Evans, A., Fitzsimmons, A., Haswell, C. A., Hodgkin, S., Horne, K., Kane, S. R., Keenan, F. P., Maxted, P. F. L., Norton, A. J., Osborne, J., Parley, N. R., Ryans, R. S. I., Smalley, B., Wheatley, P. J., and Wilson, D. M. (2006). The WASP Project and the SuperWASP Cameras. , 118(848):1407–1418.

Psaridi, A., Bouchy, F., Lendl, M., Grieves, N., Stassun, K. G., Carmichael, T., Gill, S., Peña Rojas, P. A., Gan, T., Shporer, A., Bieryla, A., Brahm, R., Christiansen, J. L., Crossfield, I. J. M., Galland, F., Hooton, M. J., Jenkins, J. M., Jenkins, J. S., Latham, D. W., Lund, M. B., Rodriguez, J. E., Ting, E. B., Udry, S., Ulmer-Moll, S., Wittenmyer, R. A., Zhang, Y., Zhou, G., Addison, B., Cointepas, M., Collins, K. A., Collins, K. I., Deline, A., Dressing, C. D., Evans, P., Giacalone, S., Heitzmann, A., Mireles, I., Mounzer, D., Otegi, J., Radford, D. J., Rudat, A., Schlieder, J. E., Schwarz, R. P., Srdoc, G., Stockdale, C., Suarez, O., Wright, D. J., and Zhao, Y. (2022). Three new brown dwarfs and a massive hot Jupiter revealed by TESS around early-type stars. , 664:A94.

Rauer, H., Catala, C., Aerts, C., Appourchaux, T., Benz, W., Brandeker, A., Christensen-Dalsgaard, J., Deleuil, M., Gizon, L., Goupil, M. J., Güdel, M., Janot-Pacheco, E., Mas-Hesse, M., Pagano, I., Piotto, G., Pollacco, D., Santos, Ċ., Smith, A., Suárez, J. C., Szabó, R., Udry, S., Adibekyan, V., Alibert, Y., Almenara, J. M., Amaro-Seoane, P., Eiff, M. A.-v., Asplund, M., Antonello, E., Barnes, S., Baudin, F., Belkacem, K., Bergemann, M., Bihain, G., Birch, A. C., Bonfils, X., Boisse, I., Bonomo, A. S., Borsa, F., Brandão, I. M., Brocato, E., Brun, S., Burleigh, M., Burston, R., Cabrera, J., Cassisi, S., Chaplin, W., Charpinet, S., Chiappini, C., Church, R. P., Csizmadia, S., Cunha, M., Damasso, M., Davies, M. B., Deeg, H. J., Díaz, R. F., Dreizler, S., Dreyer, C., Eggenberger, P.,

Ehrenreich, D., Eigmüller, P., Erikson, A., Farmer, R., Feltzing, S., de Oliveira Fialho, F., Figueira, P., Forveille, T., Fridlund, M., García, R. A., Giommi, P., Giuffrida, G., Godolt, M., Gomes da Silva, J., Granzer, T., Grenfell, J. L., Grotsch-Noels, A., Günther, E., Haswell, C. A., Hatzes, A. P., Hébrard, G., Hekker, S., Helled, R., Heng, K., Jenkins, J. M., Johansen, A., Khodachenko, M. L., Kislyakova, K. G., Kley, W., Kolb, U., Krivova, N., Kupka, F., Lammer, H., Lanza, A. F., Lebreton, Y., Magrin, D., Marcos-Arenal, P., Marrese, P. M., Marques, J. P., Martins, J., Mathis, S., Mathur, S., Messina, S., Miglio, A., Montalban, J., Montalto, M., Monteiro, M. J. P. F. G., Moradi, H., Moravveji, E., Mordasini, C., Morel, T., Mortier, A., Nascimbeni, V., Nelson, R. P., Nielsen, M. B., Noack, L., Norton, A. J., Ofir, A., Oshagh, M., Ouazzani, R. M., Pápics, P., Parro, V. C., Petit, P., Plez, B., Poretti, E., Quirrenbach, A., Ragazzoni, R., Raimondo, G., Rainer, M., Reese, D. R., Redmer, R., Reffert, S., Rojas-Ayala, B., Roxburgh, I. W., Salmon, S., Santerne, A., Schneider, J., Schou, J., Schuh, S., Schunker, H., Silva-Valio, A., Silvotti, R., Skillen, I., Snellen, I., Sohl, F., Sousa, S. G., Sozzetti, A., Stello, D., Strassmeier, K. G., Švanda, M., Szabó, G. M., Tkachenko, A., Valencia, D., Van Grootel, V., Vauclair, S. D., Ventura, P., Wagner, F. W., Walton, N. A., Weingrill, J., Werner, S. C., Wheatley, P. J., and Zwintz, K. (2014). The PLATO 2.0 mission. *Experimental Astronomy*, 38(1-2):249–330.

Reuyl, D. and Holmberg, E. (1943). On the Existence of a Third Component in the System 70 Ophiuchi. , 97:41.

Richardson, L. J., Deming, D., Horning, K., Seager, S., and Harrington, J. (2007). A spectrum of an extrasolar planet. , 445(7130):892–895.

Ricker, G. R. (2015). The Transiting Exoplanet Survey Satellite (TESS): Discovering New Earths and Super-Earths in the Solar Neighborhood. In *AAS/Division for Extreme Solar Systems Abstracts*, volume 47 of *AAS/Division for Extreme Solar Systems Abstracts*, page 503.01.

Sahu, K. C., Casertano, S., Bond, H. E., Valenti, J., Ed Smith, T., Minniti, D., Zoccali, M., Livio, M., Panagia, N., Piskunov, N., Brown, T. M., Brown, T., Renzini, A., Rich, R. M., Clarkson, W., and Lubow, S. (2006). Transiting extrasolar planetary candidates in the Galactic bulge. , 443(7111):534–540.

See, T. J. J. (1896). Researches on the orbit of 70 Ophiuchi, and on a periodic perturbation in the motion of the system arising from the action of an unseen body. , 16:17–23.

Stassun, K. G., Oelkers, R. J., Pepper, J., Paegert, M., De Lee, N., Torres, G., Latham, D. W., Charpinet, S., Dressing, C. D., Huber, D., Kane, S. R., Lépine, S., Mann, A., Muirhead, P. S., Rojas-Ayala, B., Silvotti, R., Fleming, S. W., Levine, A., and Plavchan, P. (2018). The TESS Input Catalog and Candidate Target List. , 156(3):102.

Struve, O. (1952). Proposal for a project of high-precision stellar radial velocity work. *The Observatory*, 72:199–200.

van de Kamp, P. (1969). Alternate dynamical analysis of Barnard's star. , 74:757–759.

Vogt, S. S., Allen, S. L., Bigelow, B. C., Bresee, L., Brown, B., Cantrall, T., Conrad, A., Couture, M., Delaney, C., Epps, H. W., Hilyard, D., Hilyard, D. F., Horn, E., Jern, N., Kanto, D., Keane, M. J., Kibrick, R. I., Lewis, J. W., Osborne, J., Pardeilhan, G. H., Pfister, T., Ricketts, T., Robinson, L. B., Stover, R. J., Tucker, D., Ward, J., and Wei, M. Z. (1994). HIRES: the high-resolution echelle spectrometer on the Keck 10-m Telescope. In Crawford, D. L. and Craine, E. R., editors, *Instrumentation in Astronomy VIII*, volume 2198 of *Society of Photo-Optical Instrumentation Engineers (SPIE) Conference Series*, page 362.

Šubjak, J., Sharma, R., Carmichael, T. W., Johnson, M. C., Gonzales, E. J., Matthews, E., Boffin, H. M. J., Brahm, R., Chaturvedi, P., Chakraborty, A., Ciardi, D. R., Collins, K. A., Esposito, M., Fridlund, M., Gan, T., Gandolfi, D., García, R. A., Guenther, E., Hatzes, A., Latham, D. W., Mathis, S., Mathur, S., Persson, C. M., Relles, H. M., Schlieder, J. E., Barclay, T., Dressing, C. D., Crossfield, I., Howard, A. W., Rodler, F., Zhou, G., Quinn, S. N., Esquerdo, G. A., Calkins, M. L.,

Berlind, P., Stassun, K. G., Blažek, M., Skarka, M., Špoková, M., Žák, J., Albrecht, S., Sobrino, R. A., Beck, P., Cabrera, J., Carleo, I., Cochran, W. D., Csizmadia, S., Dai, F., Deeg, H. J., de Leon, J. P., Eigmüller, P., Endl, M., Erikson, A., Fukui, A., Georgieva, I., González-Cuesta, L., Grziwa, S., Hidalgo, D., Hirano, T., Hjorth, M., Knudstrup, E., Korth, J., Lam, K. W. F., Livingston, J. H., Lund, M. N., Luque, R., Montanes Rodríguez, P., Murgas, F., Narita, N., Nespral, D., Niraula, P., Nowak, G., Pallé, E., Pätzold, M., Prieto-Arranz, J., Rauer, H., Redfield, S., Ribas, I., Smith, A. M. S., Van Eylen, V., and Kabáth, P. (2020). TOI-503: The First Known Brown-dwarf Am-star Binary from the TESS Mission. , 159(4):151.

Wolszczan, A. and Frail, D. A. (1992). A planetary system around the millisecond pulsar PSR1257 + 12. , 355(6356):145–147.

Zapatero Osorio, M. R., Béjar, V. J. S., Martín, E. L., Rebolo, R., Barrado y Navascués, D., Bailer-Jones, C. A. L., and Mundt, R. (2000). Discovery of Young, Isolated Planetary Mass Objects in the σ Orionis Star Cluster. *Science*, 290(5489):103–107.

Zhou, G., Wirth, C. P., Huang, C. X., Venner, A., Franson, K., Quinn, S. N., Bouma, L. G., Kraus, A. L., Mann, A. W., Newton, E. R., Dragomir, D., Heitzmann, A., Lowson, N., Douglas, S. T., Battley, M., Gillen, E., Triaud, A., Latham, D. W., Howell, S. B., Hartman, J. D., Tofflemire, B. M., Wittenmyer, R. A., Bowler, B. P., Horner, J., Kane, S. R., Kielkopf, J., Plavchan, P., Wright, D. J., Addison, B. C., Mengel, M. W., Okumura, J., Ricker, G., Vanderspek, R., Seager, S., Jenkins, J. M., Winn, J. N., Daylan, T., Fausnaugh, M., and Kunimoto, M. (2022). A Mini-Neptune from TESS and CHEOPS Around the 120 Myr Old AB Dor Member HIP 94235. , 163(6):289.